INVESTIGATION OF SYNGAS OXY-COMBUSTION IN A GAS TURBINE MODEL COMBUSTOR

BY

MANSUR ALIYU

A Thesis Presented to the

DEANSHIP OF GRADUATE STUDIES

KING FAHD UNIVERSITY OF PETROLEUM & MINERALS

DHAHRAN, SAUDI ARABIA

In Partial Fulfillment of the
Requirements for the Degree of

MASTER OF SCIENCE

In

MECHANICAL ENGINEERING

MAY 2016

KING FAHD UNIVERSITY OF PETROLEUM & MINERALS

DHAHRAN- 31261, SAUDI ARABIA

DEANSHIP OF GRADUATE STUDIES

This thesis, written by **Mansur Aliyu** under the direction of his thesis advisor and approved by his thesis committee, has been presented and accepted by the Dean of Graduate Studies, in partial fulfillment of the requirements for the degree of **MASTER OF SCIENCE IN MECHANICAL ENGINEERING**

Dr. Syed A. M. Said
(Advisor)

Dr. Zuhair Gasem
Department Chairman

Dr. Mohammed A. M. Habib
(Member)

Dr. Salam A. Zummo
Dean of Graduate Studies

Dr. Hassan M. Badr
(Member)

29/5/16

Date

Dedicated to

My parents, siblings, wife, immediate and extended family including those that Allah took their lives during my program. May Allah forgive them and have mercy on their souls.

And also, to my friends and well-wishers.

ACKNOWLEDGMENTS

All praise, adorations, and thanks are due to Allah alone, the Lord of all that exist for His exposed and concealed bounties since the time my soul was created. I actually appreciate His immeasurable mercy by saying Alhamdulillah for not only making my program a successful one but making it done at the appropriate time despite the challenges. After that, I would like to appreciate the physical, spiritual and financial support of my parents up to the level I currently find myself, sincerely speaking I am really indebted to them.

I would like to express my sincere appreciation to my thesis advisor, Dr. Syed Ahmad Muhammad Said for his patience, support both physically and financially, and encouragement throughout my MS program. I certainly believe that Allah really used him through his personality and position to make my research work a successful one within the required period of time. In almost the same regards, I would like to appreciate my other two professors, I mean my committee members; Dr. Mohamed Abdel-Aziz Mostafa Habib and Dr. Hassan Mohamed Badr for their time and immense contributions in my research most especially during the clarification of my thesis objectives. My appreciation would not be completed in this aspect if I failed to mention Dr. Medhat Nemitallah. I really acknowledged his unquantified contributions in my research, thank you so much Dr. Medhat.

I would like to appreciate the love and care of the old man (Mr. Karam) for taking most of his time to put me through the experimental setup and responded to my problems without hesitation during the period I spent with him in the laboratory. I would like to appreciate the constructive criticisms and voluntary service rendered by Mr. Ibrahim Balarabe Mansir, Mr. Shakirudeen Salaudeen Alade, Mr. Sherif Seif Eldin and Mr. Shabeeb Alkhaldi during

the experimental stage of my research, and also, the assistance rendered by Mr. Shakirudeen Salaudeen Alade, Mr. Haixia Li and Dr. Rached Ben Mansour in numerical study of my research are highly appreciated. I would like to appreciate the contribution of Mr. Romeo for providing me with the swirler within the required period despite his tight schedules. I would also like to appreciate the entire staff of Carbon Capture and Sequestration including Dr. Ahmed Abdelhafez, Dr. Basem and also the combustion group including Dr. Sanusi, Mr. Zubairu, and others.

I sincerely appreciate the support of my siblings, niece, nephew and the entire family of Babanagari Aliyu at all time for their prayers, love and care. Alhamdulillah, I am honored to be part of you.

I so much appreciate the patience displayed by my wife during the period of my study, I think the only thing I could say is that she's more than a wife. I would also like to appreciate the support of my in-laws through their prayers and advice during the period of my study.

I would like to acknowledge the support of the entire staff of Automobile Engineering Department, Abubakar Tafawa Balewa University (ATBU) Bauchi, Nigeria, starting from Prof. Habou Dandakuta (HOD) and the entire management of ATBU through their constant update. I so much appreciate the prayers and valuable advice of friends and well-wishers here in KFUPM and other places around the world.

Finally, I so much appreciate the opportunity given to me by Kingdom of Saudi Arabia to undertake my MS program in one of the great university in the world (i.e. KFUPM) through the Deanship of Graduate Study and Mechanical Engineering Department.

I say to you all, Jazaakumullahu Khairan!

TABLE OF CONTENTS

LIST OF TABLES

LIST OF FIGURES

LIST OF ABBREVIATIONS

GHGs	:	Greenhouse Gases
CCS	:	Carbon (CO_2) Capture and Storage
IGCC	:	Integrated Gasification Combined Cycle
DO	:	Discrete Ordinate
WSGGM	:	Weighted Sum of Gray Gases Model
RTE	:	Radiative Transfer Equation
LES	:	Large Eddy Simulation
JL	:	Jones and Lindstedt
WD	:	Westbrook and Dryer
CFD	:	Computational Fluid Dynamics
RNG	:	Renormalization Group
RSM	:	Reynolds Stress Model
LES	:	Large Eddy Simulation
EDC	:	Eddy Dissipation Concept
KRR	:	Kinetic Rate of Reaction
DR	:	Digital Readout
GRI	:	Gas Research Institute
SIMPLE	:	Semi Implicit Method for Pressure Linked Equation
ISAT	:	In Situ Adaptive Tabulation

ABSTRACT

Full Name : Mansur Aliyu

Thesis Title : Investigation of Syngas Oxy-Combustion in a Gas Turbine Model Combustor

Major Field : Mechanical Engineering

Date of Degree : May 2016

In this study, an experimental and numerical investigations on atmospheric gas turbine model combustor is presented. The study considers the oxy-combustion process of turbulent diffusion flames for hydrogen-enriched-methane (i.e. H_2-enriched-CH_4 as syngas fuel). The combustion characteristics of the flames and the effect of swirl angle are investigated over a range of operating conditions. The effects of equivalence ratio, fuel composition, and oxidizer mixture composition on flame stability, flame structure, and temperature distributions are studied. The study was conducted for a range of equivalence ratio of 0.55, 0.65 and 0.75, a range of fuel composition of 100%CH_4/0%H_2 to 50%CH_4/50%H_2 and oxidizer mixture (O_2 plus CO_2) composition range from 0% up to the value of blow-off. Different swirl degrees are considered with different swirl vane angles including 30^o, 45^o and 55^o corresponding to swirl numbers ranging from 0.44 to 1.10. The numerical study is achieved using ANSYS Fluent. The models considered for turbulence, radiation, and species transport modeling are k-ε (standard), discrete ordinate (DO), and eddy-dissipation-concept (EDC) respectively. The reaction mechanism, which comprises modified Jones and Lindstedt reaction mechanism for oxy-combustion of CH_4 and Marinov reaction mechanism for H_2, is imported into ANSYS Fluent through CHEMKIN mechanism import. Pressure discretization is achieved using standard while other partial

discretizations were achieved using the second-order upwind method. A SIMPLE scheme is used to handle pressure-velocity coupling and the solutions are considered to be converged when the residuals for the equations were less than 10^{-3} for momentum equations and 10^{-6} for others. The results show that flame blow-off occurred at very low oxygen levels in the oxidizer mixture (20%O_2 or even less) and at hydrogen enrichment level of 50% which indicates wide stability limits when hydrogen is used for fuel enrichment. Among the experimentally considered values of swirl degree, the swirler with 30^o swirl degree showed the lowest level of flame stability, highest flame length, and highest temperature. On the other hand, the swirler with 55^o swirl degree exhibited the highest level of stability with moderate flame length and temperature. The numerical results obtained are in good agreement with the experimental result. The numerical results show that oxy-fuel combustion of H_2-enriched-CH_4 is not achievable at 0.95 equivalence ratio and above due to stability issue. The stability is highly enhanced by the formation of inner recirculation zone and, better performance of gas turbine combustor can be achieved by a swirler with swirl vane angle of 65^o.

ملخص الرسالة

الإسم بالكامل: منصور عليو

عنوان الرسالة: دراسة احتراق غاز اصطناعى بالأوكسجين فى نموذج مفاعل توربين غازى

التخصص: الهندسة الميكانيكية

تاريخ الدرجة العلمية: مايو 2016

في هذه الدراسة، تم إجراء دراسة تجريبية وعددية على نموذج مفاعل توربين غازى تحت الضغط الجوى. تم دراسة عملية الحرق بالأوكسجين للهب انتشارى لوقود الميثان المخصب بالهيدروجين (وقود غاز الميثان المخصب بالهيدروجين لتكوين غاز إصطناعى). تم إجراء دراسة إستقصائية لدراسة خصائص اللهب ودراسة تأثير السريان الدوامى خلال مدى من ظروف التشغيل. تم دراسة آثار نسبة التكافؤ، استهلاك الوقود، وتكوين الخليط المؤكسد على استقرار للهب، وهيكل اللهب، وتوزيعات درجة الحرارة. وقد أجريت الدراسة على مجموعة من نسب التكافؤ 0.55، 0.65 وو 0.75ومجموعة من تكوين الوقود بنسبة $100\%CH_4/0\%H_2$ إلى $50\%CH_4/50\%H_2$ وخليط مؤكسد (خليط من الأوكسجين وثانى أكسيد الكربون) من 0.0% حتى حدود إنطفاء اللهب. تم إعتبار درجات مختلفة لمولد الدوامات ذات زوايا ريشة مختلفة بما في ذلك 30^o، 45^o و 55^o والمقابلة لأرقام دوامة تتراوح بين 0.44 و 1.10. تم اجراء الدراسة العددية باستخدام برنامج ANSYS-Fluent. النماذج المستخدمة لدراسة الاضطرابات، والإشعاع، وتوزيع العناصر هى k-ε (القياسي)، و discrete ordinate (تنسيق منفصلة)، و eddy-dissipation-concept (مفهوم تبديد الدوامة) على التوالي. تم استخدام آلية للتفاعلات تضم تفاعلات جونز ويندستيد المعدلة لحالات حرق الميثان بالأوكسجين و آلية تفاعل الهيدروجين لمارينوف وتم دمج تلك التفاعلات مع برنامج ANSYS عن طريق الإدخال فى صورة CHEMKIN. تم اعتبار الحل العددى متقارب عندما تكون بقايا حسابات المعادلات أقل من 10^{-3}لمعادلات الزخم و 10^{-6}للمعادلات الآخري. وأظهرت النتائج أن انطفاء اللهب حدث عند مستويات منخفضة جداً من الاوكسجين (20% أو أقل) عند مستوى تخصيب للهيدروجين حوالى 50٪ مما يشير إلى حدود استقرار واسعة عند استخدام الهيدروجين لتخصيب الوقود. من بين القيم المعتبرة تجريبياً من درجة الدوامة، أظهر مولد الدوامات ذات درجة ميل للريشة 30^o أدنى مستوى من استقرار اللهب، وأعلى طول لهب، وأعلى درجة حرارة .من ناحية أخرى، فإن مولد

الدوامات ذات درجة ميل للريشة 55^{o} أظهر أعلى مستوى من الاستقرار مع طول لهب ودرجة حرارة معتدلين. أظهرت النتائج الرقمية التي تم الحصول عليها اتفاق جيد مع النتائج المعملية .أظهرت النتائج العددية ما يلى: حرق الميثان المخصب بالهيدروجين بالأوكسجين غير قابل للتحقيق عند مستوى 0.95 نسبة تكافؤ بسبب عدم استقرار اللهب، تم تعزيز الاستقرار بشكل كبير نتيجة تشكل منطقة إعادة تدوير داخلية، وكذلك تم تحقيق أداء أفضل لمفاعل التوربين الغازى من خلال استخدام مولد دوامات ذات درجة ميل للريشة 65^{o}.

CHAPTER 1

INTRODUCTION

Fossil fuels have been in use for several decades to meet a reasonable fraction of the global energy demand. The usage of these fuels for power generation, transportation, and other industrial applications may actually continue for more decades to come due to their abundant availability, energy density, low cost and existing dependable technology for their production. But, the most unfortunate situation about the consumption of such fuels is that their major by-product terrorizes the human's environment (i.e. atmosphere). The consumption of fossil fuels give rise to a number of greenhouse gasses (GHGs) particularly CO_2 (which act as an opaque to heat just as the way the glass in an opaque in a greenhouse) in the atmosphere, thereby, increasing the earth temperature (a phenomenon regards as global warming). Also, it is no longer a news that 30% (approximately) of CO_2 emitting to the atmosphere on an annual basis are as a result of fossil fuel based power generation plants [1]. So, due to the adverse effect of CO_2 on human's environment, several international organizations have proposed a way to regulate its increase in the atmosphere while still maintaining the standard of living. Part of their resolutions were presented in [2] which required parallel implementation, they include; increase energy efficiency, converting to less carbon-concentrated fuels for energy sources, and carbon storage. Adhering to these consensuses most especially the last two, it will be meaningful to say that utilization of low-carbon fuel such as synthetic gas (syngas) or hydrogen-enriched-hydrocarbons

with a means of carbon capturing and storage (e.g. oxy-fuel combustion technique) in power generation is actually a way to salvage the depleting atmosphere.

In order to minimize global warming and also to realize pollution free environment as explained above, renewable sources of energy need to be considered. Syngas is a renewable form of energy. It is a mixture of hydrogen, carbon oxides (CO & CO_2), and gaseous hydrocarbons such as methane in various compositions with a heating value which ranges between 5-20 MJ/Kg [3], [4]. Syngas can be produced from numerous numbers of sources which include: hydrocarbon (methane) steam reforming and gasification of biomass [4], [5], [6] and its composition depends on the fuel source. This potential clean fuel (i.e. syngas) is being consumed in power generating gas turbines in the integrated gasification combined cycle (IGCC) [4], [7]. An oxy-fuel combustion technique utilizes pure oxygen and part of recycled exhaust gas as an oxidizer during the combustion process. It would be observed in the sections to come that oxy-combustion of syngas would surely signify an advance step towards environmental goals.

1.1 Problem Statement

The study focused on experimental and numerical investigation of oxy-combustion of syngas in a gas turbine combustor model. Such study is inevitable for addressing environmental pollutions and global warming. It aims at solving the problem associated with emission control, temperature distribution and flame stability in a gas turbine combustor. The experimental investigation is carried out using the existing setup available in the Heat Engine Laboratory at the Mechanical Engineering Department, King Fahd University of Petroleum and Minerals while the numerical investigation is achieved using ANSY Fluent R15.0 software.

1.2 Objectives

The main objective of this study is to determine experimentally and numerically the effect of different operating parameters on the characteristics of oxy-combustion of syngas in a gas turbine combustor model. The specific objectives include:

- The influence of CO_2 circulation on combustion instability;
- The effect of swirl number on some combustion parameters such as temperature distribution for a constant equivalence ratio.
- Numerical prediction of the flow and thermal fields.

CHAPTER 2

LITERATURE REVIEW

2.1 Carbon Capture and Storage

Carbon dioxide (CO_2) capture and storage (CCS) is gaining a lot of recent attention as one of the effective methods of reducing the emission of greenhouse gasses and hence minimizing global warming [8], [9]. This method involves a wide range of skills that are being established to allow the CO_2 emissions resulting from the combustion of fossil fuel to be collected and transported (either by pipelines or industrial tanks) to a safer storage location usually geological formation, rather than emitting it into the atmosphere [10], [11]. The most popular processes through which CO_2 capture is being achieved include; post-combustion capture, pre-combustion capture or integrated gasification combined cycle (IGCC) [12] and oxy-fuel combustion. Wall [12] compared the characteristic of these processes as shown in Table 1. In the post-combustion capturing process, CO_2 is separated from the flue gasses through chemical absorption systems by cleaning the flue gasses in the aqueous solution of amine. This capturing process consumes a lot of energy due to a large amount of energy attributed to the amine solutions regeneration which makes the process expensive [13]. The pre-combustion process is somehow contradicting in the sense that CO_2 is not at all available for capturing prior to the combustion process [10]. In this process a gasification of the concern fuel needs to be done, in which the fuel will be partly combusted in the presence of oxygen (and/or steam) at an elevated temperature and pressure to yield a mixture of H_2 and CO (i.e. syngas), further reaction of these products

with steam would then produce CO_2 and H_2. The CO_2 can then be separated from H_2 with any applicable separation methods such as membranes technique. The problem associated with this method is the initial gasification process which is expensive as well [13].

Table 1: Comparison of major characteristics of carbon capture and storage techniques [12].

Technique	**Suitable for Modified Existing Pulverized Fuel Plant**	**Applicable for Partial CO_2 Capturing**	**Requires the Supply of O_2**	**Requires CO_2 to be Captured Before the Compression Process**	**Produces H_2 as an Alternative Fuel**
Pre-Combustion Capture	Yes	Yes	No	Yes	No
Post-Combustion Capture	No	Yes, but doubtful	Yes	Yes	Yes
Oxy-fuel Combustion	Yes	No	Yes	No	No

Oxy-combustion process involves burning fuel in the presence of pure O_2 and recycled exhaust gas to produce a mixture of CO_2 and water vapor. The water vapor can then be separated from the mixture by condensation (heat recovery) process leaving the flue gas with CO_2 which can then be captured for further storage [14]. This process is more simplified as compared to the other two processes but the cost of separation of O_2 from air and exhaust gas recirculation may suffer the economic benefit of the process [11]. The steps involved in these three methods are explained in Figure 1.

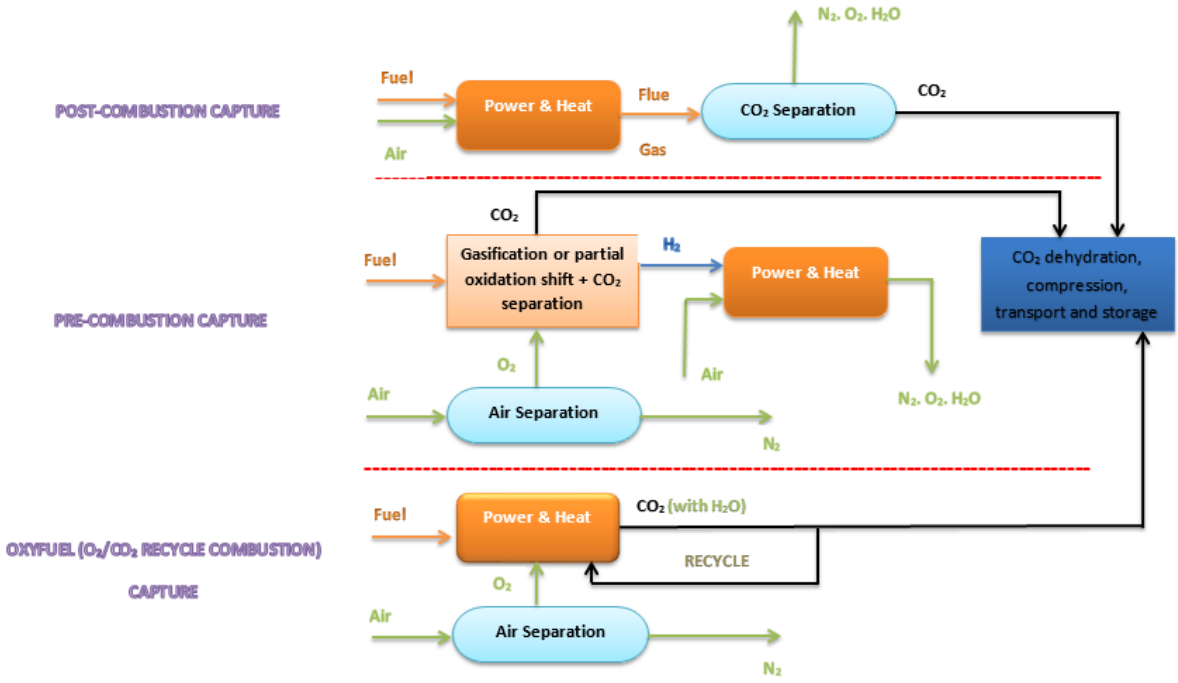

Figure 1: Three major techniques involved in CO_2 capturing [14].

2.2 Oxy-fuel Combustion

Oxy-fuel combustion techniques use pure oxygen as an oxidizer and, in most cases, recycled exhaust gas in order to lower the temperature of the flame [15]. This combustion process can either occur as pre-mixed combustion in which there will be a mixture of fuel and oxidizer prior to the combustion chamber, non-premixed combustion where there is no interaction between the fuel and the oxidizer prior to the combustion chamber, or partially-premixed in which both previous situations will be encountered. Oxy-fuel combustion technology received several attentions in recent years due to the fact that it gives rise towards zero-emission of NO_x and CO_2 [16]. Since the combustion process takes place in the absence of nitrogen, the combustion products will comprise of mainly CO_2 and H_2O and some other impurities in a very low

concentration such as argon and oxygen. Thus, CO_2 can then be separated by condensing H_2O in the flare gas [5], [16], [17]. Oxy-fuel combustion has been applied to different power generation processes ranging from coal combustion to syngas combustion. Although, this technology may be simple and perhaps a favorable method among the proposed CO_2 capturing methods but, oxy-fuel combustion technology [18] also introduce some undesirable effect such as instability and blow-off or it may not even be economically visible at some certain value of equivalence ratio [19], some of which were explained in some sections to follow.

2.3 Syngas Combustion

Syngas combustion is determined mainly by carbon monoxide (CO) and hydrogen (H_2) contents which are mostly categorized by high (laminar) flame velocities, high variety of temperature flammability bounds, and a low explosion delay time which has many advantages when it comes to pollutants emission [20] and which generally enhanced the great danger of flashback phenomenon [21]. Due to this peculiarity of the syngas fuels, combustion of syngas is largely carried out in diffusion flames that is extremely thinned (with diluent such as N_2 or steam) [21], [22]. Sarli et al. [23] experimentally and numerically (using CHEMKIN) quantified the effect of CO/H_2 ratio, equivalence ratio, oxygen-enrichment factor and CO_2 concentration on the laminar flame velocity of CO_2/syngas mixtures. They reported that the effect of the CO_2 was majorly thermal, and at low laminar flame velocity, it was found to be both kinetic and thermal. Shabanian et al. [24] investigated mild combustion burner which was fed with the mixture of $CO_2/H_2/H_2O$ and H_2 experimentally and numerically. The method of discrete ordinate (DO) alongside with Weighted-Sum-of-Gray-Gases-Model (WSGGM) was used in solving radiative transfer equation (RTE) and velocity-pressure coupling was

handled by SIMPLE algorithm. They reported that both kinetic mechanisms and turbulence model were the significant factors in the mild combustion system simulation. They further stated that k-ω-transition and standard-k-ε failed to predict the CO values obtained from an experiment at the exit plane. Salzano et al. [5] Studied the effect of fuel composition (CO/H_2 ratio), equivalence ratio, O_2-enrichment factor and CO_2 concentration on the laminar flame velocity and explosion behavior of the mixtures of $CO/H_2/O_2/CO_2/N_2$. They reported that pressure time history showed anomalous behavior at extremely O_2-enriched mixtures. Kutne et al. [25] characterized the behavior of H_2 rich syngas fuels combustion at an elevated pressure in a stabilized swirl flames. They reported a stable flame with no form of thermo-acoustic fluctuations at any level of operating conditions. They also reported that irrespective of equivalence ratio and fuel composition influence on the structure of the flame, the overall shape of the flame is identical for all investigated flames. Fan et al. [26] conducted an experiment to investigate the basic features of syngas (mainly CO, CH_4, and H_2) combustion with the analysis and measurement of flue gas composition and flame temperature. They reported that increase in the component of H_2 enhances both the temperature profile and stability of the flame. Zhang et al. [27] investigated the detailed interaction of flame turbulence and flame front structure of the oxy-fuel combustion of syngas model by extremely diluting CO_2 with a mixture of $CO/H_2/O_2$ and, compared it with CH_4/air and $CO/H_2/CO_2$/air flames. They reported that the turbulence flame velocity of syngas-O_2 (i.e. CHO) flame is higher as compared to the other mixtures and that the surface flame density for $CO_2/CO/H_2/O_2$ is more than CH_4/air flames. Dam et al. [28] analyzed the stabilities of oxy-combustion $CH_4{-}O_2{-}CO_2$ and $CO/H_2{-}O_2{-}CO_2$ burning in the presence of steam. After investigated wide range of operating parameters that affect the stability of the flame, they reported that without exhaust gasses recirculation, $CH_4{-}O_2$

flames were not stabilized even when low firing inputs were considered due to the mixture's high adiabatic flame temperature. Kishore et al. [29] computed the laminar flame velocity and also investigated the flame stability of a producer gas (i.e. H_2, CO, CH_4, N_2, and CO_2). They reported that: out of the reaction mechanisms considered, sensibly precise predictions were obtained by using mechanism of Warnatz with C1 chemistry for all the fuels at temperature of 300K and pressure of 1 bar, H_2 improved the flame speed but lowered the equivalence ratio when the burning velocity got to the peak and, the extent to which burning velocity is increased is been restricted by the CH_4 presence. Also in the area of numerical modeling, Davis et al. [30] proposed H_2–CO kinetic model that included kinetic, species transport, and thermodynamics updates which were pertinent to extreme temperature of CO and H_2 oxidation. They reported that the model showed a good performance when compared with the major H_2/CO combustion data with some discrepancies which were resolved through optimization. Lee et al. [31] examined N_2, CO_2 and steam dilution effect on the combustion performance of H_2/CO syngas and their investigation showed that there was a decrease in NO_x emissions as the percentage of diluents increased, efficiency of combustion is satisfactorily good and that neither combustion instability nor flashback was observed in all the tested conditions. Although, the characteristics of syngas combustion may be varied in accordance with the percentage of hydrogen to carbon monoxide but the syngas did not yield combustion throbbing unlike methane [32].

2.4 H_2-Enriched-CH_4

Relating the amount of CO_2 produced from combustion of hydrocarbon fuels with C/H ratio of the fuels, it could be said that CH_4 will produce the smallest amount of CO_2. Nevertheless, CH_4 possess a number of disadvantages which limited its ability to

improve system performance and overall thermal efficiency of the engine. Some of these disadvantages include low flame speed and poor ability of lean burn [33], [34]. In order to get rid of these situations so that the thermal efficiency of the engine can be improved while still keeping the CO_2 emission, even more, smaller than it may be achieved in the case of CH_4, a fuel such as a hydrogen with high flame speed and a good ability of lean burn will be required. Hydrogen can be highly categorized as a clean fuel which produces clean energy (since it's free of carbon and carbon dioxide respectively) with a high rate of burning. Considering the said properties of H_2, it may be logical enough to assume that enriching CH_4 with H_2 will actually produce the least emission combustion with high efficiency by increasing the rate of the combustion process and improving the ability of lean burn of the engine [35]. Several studies have been conducted in the area of H_2-enriched-CH_4 and the results showed an increase in flame speed of the resulting fuel mixture. Huang et al. [33] presented a summary paper on H_2-enriched-hydrocarbons fuel combustion and the applicability of such in engines. They reported that H_2 enrichment can actually shorten the duration of combustion, increase the flame speed and extend the limits of flammability. They also reported that when natural gas is enriched with H_2 with flue gas combination, low emission and temperature combustion with greater thermal efficiency will be realized. These were also reported by Hu et al. [36]. Miao et al. [37] showed that the flammability limits (both lower and upper) of CH_4 can be extended through the addition of H_2 and which may actually improve its lean burn ability. Hu et al. [38] reported that for CH_4-H_2 fuel blend, three regimes exist according to the fraction of H_2 present in the fuel blend. These regimes are CH_4-dominated combustion, transition, and CH_4-inhibited H_2 combustion regime, for H_2 fractions of less than 60%, in the range of 60% to 80%, and greater than 80% respectively. In both the first and the third regimes, there was a linear increase in

laminar burning velocity as the H_2 fraction in the fuel blends is increased whereas, an exponential increase was observed in the regime of transition as the fraction of H_2 in the fuel blends is increased. Considering the optimum value of H_2 fraction that may be considered for enrichment, Wang et al. [39] recommended that for natural gas-H_2 fuel blends, the volumetric fraction of H_2 should be approximately 20% so as to enable concession between emissions (e.g. NO_x) and performance. Although, this value may not necessarily be applicable in the case of oxy-fuel combustion.

2.5 Combustion (Flame) Instabilities

Instability in combustion is characterized by thermo-acoustic (usually referred to as combustion noise) [40], lift-off and blow-off. The sources/causes of instabilities have been attributed to a number of factors. Combustion instability is an oscillatory fluid motion which takes place due to the coupling of the unsteady fluid mechanics and the combustion process (i.e. flame) [41], [42]. The dynamic heat released from the combustion process supplied the energy for the oscillating fluid motion [41], [43]. For the syngas combustor, turbulent flame normally undergoes an intrinsic flame instability particularly in a premixed mode as a result of the presence of a large amount of hydrogen as well as the significant inconsistency of hydrogen fraction [44]. For the composition of H_2/CO/CH_4 syngas at various variation of each component gas, Lee et al. [45] showed that the driving mechanisms for combustion instability include the periodic alternation in the flame attachment/detachment as well as vortex in combination with timelessness flames at the outer recirculation region owing to the high reactivity of hydrogen. They also indicated that the location and intensity of combustion instability driving/damped are affected by the fuel composition and that the fundamental sources of a high instability mode and sensible mode shift are relatively

due to the brief span of mixing and extremely fuel-dependence flame length. Another combustion characteristic that affects the instability are the flame speed and oxidizer flow rate (due to the presence of diluent), which affect the frequency as well as instability amplitude. It has been experienced that whenever O_2 and CO_2 are premixed and supplied together as an oxidizer to the flame there is always occurrence of flame instability and burnout [46]. Heil et al. [47] reported that when mole fraction of oxygen in the CO_2/O_2 stream was set to 21% there appeared lifted dark flames and poor burnout. In a premixed combustion system instability occurs as a result of fluctuations in the rate at which heat is released due to highly enriched hydrogen flame which will eventually induce extremely high flame speed [48]. A study by Kadowaki [49] demonstrated that the comparatively large amount of heat loss due to radiation to the surroundings from the surface of the flame is one of the sources of fine wrinkles structure that promotes the diffusive—thermal and hydrodynamic instability. On this context, Jinhua et al. [50] showed that radiation heat loss associated with syngas oxy-fuel flame is stronger as compared to any other hydrocarbons—air and syngas-air flame as a result of the presence of large amount of CO_2 in the flame.

2.5.1 Blow-off

Blow-off may be defined as an instant where the flame has been separated from the combustion base and was substantially blown-off the combustor which leads to the flame extinction. This phenomenon is normally detected through identification of the above events in the flame images [20]. Blow-off limits are very important in the operation of gas turbine which is affected by several characteristics which include; geometric swirl number, kinetic rate of reaction, fuel type, and combustion process (either premixed, partially premixed or diffusion) [51]. Several ways in which

correlation (using Well Stirred Reactor ideas) is developed that give a clear description of a blow-off appearance for different types of fuel have been extensively analyzed through a significant number of past investigations [52]–[56]. Most of these investigations essentially headed to the identical kind of relationship which relate the limits of blow-off to Damkohler number, Da (i.e. ratio of characteristics mixing time to a characteristics chemical time) [20]. Da may also be represented as the ratio of a residence time to chemical kinetic time, η_{res}/η_{min} [57]. It is widely recognized that blow-off occurs once the chemical kinetic time surpasses residence time [20], [58].

2.6 Swirl Stabilized Flame

Swirl combustors are widely employed in gas turbines including several other practices of combustion owing to the fact that it increases fuel and oxidizer mixing with an increase in flame stability and improved limits of blow-off [59]. In order to stabilize the flame in a gas turbine combustor, it has been realized that a swirling flow in an abrupt expansion formation needs to be utilized. The research on the effect of swirler geometry and vane angle configuration on gas turbine performance are still ongoing. Palies et al. [60] compared the responses of swirling flames yielded to acoustic velocity instabilities when the rotation of flow is achieved either by axial or radial swirler. It was observed that the feedback and flame dynamics are essentially alike for both swirlers' geometries and also, the value of swirl number clearly sways the response obtained. Huang and Yang [61] conducted a broad review of the developments made in the area of combustion instability in systems of the gas turbine combustor. They reported that the essential parameter describing the flow dynamics and flame is the swirl number. Wan et al. [62] highlighted the mechanisms surrounding the flame

stabilization in a premixed system of CH_4/air flame in a cavity to be; the formation of recirculation zone and low velocity zone in the cavities, preferential diffusion effect, as well as the preheating effect of upstream inner walls. Huang and Yang [63] examined the inlet swirl effect on dynamics of combustion and flow development in a lean-premixed swirl stabilized combustor by utilizing the approach of large eddy simulation joined with level-set flamelet library. They reported that surface area reduction of the flame is as a result of turbulence intensity increase and flame speed which were ascribed to larger swirl number. Abdulsada et al. [59] examined the blow-off limits and the ability of the combustor in a state of premixed to change fuels while still sustaining same thermal load for several H_2 based fuel mixtures substitutes in certain configurations. They reported that both configurations and fuel compositions enhanced the blow-off limits. Kulsheimer and Buchner [64] examined the impact of mass flow rate cyclic excitation on the descriptions of flame in a swirl burners with diverse swirl strengths as well as the dynamical behavior of premixed lean swirl flames. They reported that swirl premixed flames were controlled by an influence which hinders the strong entrainment of the ambient channel in contrast with the equivalent quasi-steady-state swirl flames. Ditaranto and Hals [17] experimentally investigated the oxy-fuel combustion instabilities in a sudden expansion formation. They reported that in order to obtain combustion with characteristics similar to that of the air, oxygen content should be more than 30%. From the study conducted by Linck et al. [65], it was observed that the flame structure depends strongly on the characteristics of the fuel spray and the recirculation region. They also reported 70^o as an upper limit of practicable swirl vane angle. Fanaca et al. [66] examined the flow field of both annular and single burner combustor. They reported that the single burner geometry was

identified by swirling wall jet flow patterns while for the annular combustor, a free swirling jet flow patterns were observed.

2.7 H_2 Effect on Flame Stabilities

Many previous investigations have shown how H_2 (as a component of syngas) strongly influenced the stability range of practical flame. Specifically, the following investigations [20], [53], [54], [67] revealed that the range of stability is displaced towards the leaner circumstances as the percentage of CO or H_2 is increased. As a matter of fact, so many studies [21], [68], [69] used the addition of hydrogen in lean premixed burners to avoid blow-off. Schefer [70] examined the effect of H_2 addition on the flame stability in a fuel lean conditions. Extensions of burner lean stability limits were noted when the H_2 percentage in the CH_4/air mixture was somewhere around 20%. Allison et al. [71] suggested that in order to reduce the thermo-acoustic instabilities by decreasing the acoustic amplitude, H_2 content of the fuel needs to be increased. From Zhang et al. [57] point of view, flame stabilization can be achieved at low adiabatic flame temperatures, lower equivalence ratios (lean) and laminar flame speeds with an increase in H_2 percentage. Noble et al. [54] and Zhang et al. [55] investigated the fuel compositions effects on the lean blowout features of syngas mixtures. They reported that percentage of H_2 in the fuel controls the mixture blowout features. Lieuwen et al. [52] also reported that the major parameter that controls the dynamic stability and blowout is a the percentage of H_2 in the fuel (syngas) composition. Alavandi and Agrawal [72] investigated the combustion of H_2-syngas/CH_4 fuel mixture in a lean premixed condition to show fuel suppleness of a two-section porous burner. They reported that there was a decrease in temperature close to the lean blow-off limit due to

the presence of H_2/CO in the fuel mixture especially when they are at higher percentages.

2.8 Oxidizer Mixture Effect on Flame Stabilities

It has been clearly understood from section 2.5 that flame instabilities are experienced when CO_2 and O_2 were premixed and supplied to the flame as an oxidizer [16]. Amato et al. [73] conducted an investigation that leads to the characterization of the stability limits of a stabilized swirl combustor. They reported that running a CO_2 diluted system considerably diminishes operability limits due to the slower kinetics of such system comparative to air. It was categorically stated that for CO_2 diluted system; blowout will occur when the temperature of the flame is around 300 K hotter than that of the air diluted system at a specified nozzle outlet velocity. Liu et al. [74] presented in brief the chemical effect of CO_2 on burning velocity of premixed CH_4 and H_2 flames when N_2 is been replaced by CO_2 in air. They reported that CO_2 chemical effect reduced the burning velocity of the fuel mixture significantly and that this chemical effect increases with the concentration of CO_2 in the new mixture. De Persis et al. [75] examined the effects of CO_2 dilution and O_2 enrichment on laminar flames speed of CH_4. They reported an increase in the CO_2 content of the flue gasses and a decreased in adiabatic temperature which may be due to the CO_2 dilution. Seepana and Jayanti [76] examined likelihoods of retrofitting and flame extinction of an oxy-fuel combustion in a horizontally-fired co-axial stabilized swirl burner. They reported that steady operation of oxy-fuel flames can only be accomplished at a concentration of O_2 less than 30% by volume if the temperature at the peak of the flame is reduced. Fujimori and Yamada [77] suggested the strategies required for achieving stability in oxy-fuel combustion to include: increasing the O_2 concentration to an appropriate level in the combustion gas,

to direct O_2 injection into the base of the burner and to improve burner aerodynamics. Kutne et al. [78] performed a methodical parametric study during an experiment under partly premixed swirl stabilized state to explain the oxy-fuel flames behavior for several parameters. They reported that in order to achieve a stable flame, the O_2 fraction in CO_2 must exceed 21%. Xie et al. [79] examined the effects of CO_2 excessive dilution on flame instability, flame radiation and combustion chemical reaction of $CH_4/CO_2/O_2$ mixtures. They reported that CO_2 suppressed the instability in the flame by the joint effect of thermal-diffusive and hydrodynamic instabilities.

2.9 Numerical Studies

In addition to what has been presented in the previous sections, other notable numerical investigations in the area of syngas combustion and gas turbine combustor are presented as follows. Ghenai [80] conducted an investigation on syngas combustion in a gas turbine can type combustor to study the influence of the changeability in the fuel configuration and heating value on the performances of combustion and emissions using P-1 and k-ε model to model radiation and turbulent flow respectively. The fuels considered in the combustor were varied from CH_4 to syngas. Five syngas fuel mixtures with H_2 to CO capacity ratio varied from 0.63 to 2.63 were considered. All the five syngas tested displayed a lesser gas temperature as compared with the temperature obtained when CH_4 was considered. The reduction in temperature of the gas was attributed to the lower calorific value and the combustible and non-combustible components of the syngas fuel. Torre et al. [81] investigated the diluents (CO_2), firing input, and the percentage of H_2 effect on premixed oxy-syngas combustions to carry out analysis on the overall radiation of syngas oxy-combustion. They reported that the radiative heat emit factor associated with syngas flames dropped at high hydrogen

concentrations and higher firing inputs while it increased at lesser concentrations. Increase in the heat emit factor was also observed when both equivalence ratio and recirculation percentage of diluents (CO_2) were increased. Keramida et al. [82] investigated the heat transfer due to radiation in an industrial natural-gas furnace configuration using two different radiation models. Eddy dissipation, *k-ε* and discrete transfer model were used in calculating heat release, turbulence dissipation, and kinetic energy, and radiative transfer equation respectively. They reported that the effect of thermal radiation on flame temperature forecasted was very important and to have a healthier conformity between experimental data and numerical estimates, radiative heat transfer needs to be included in the combustion analysis. Both models performed very similarly and showed better agreement with the experimental data. Safer et al. [83] numerically examined the O_2 enhancement impact on the emissions and structure of syngas flame in opposite flow arrangement using GRI 3.0 mechanism to modeled oxidation chemistry of syngas. They reported that addition of O_2 increased the flame temperature, the radiative heat transfer, and NO_x formation. Silva et al. [84] performed a simulation for the non-premixed combustion process in an axis-symmetrical cylindrical combustion chamber using 2-step global reaction mechanism. The Zonal method was used to model the thermal radiation and the dependence of the wavelength of the gas properties was solved using WSGGM while the *k-ε* model was used to describe the turbulent model. They reported that the model predicted the concentration and temperature distribution that were very close to experimental data most especially up to 1.1 m from the inlet section. Tabatabaei and Soroudi [85] investigated the effect of variations in syngas compositions on combustion characteristics of syngas under gas turbine operating conditions. Four different reaction mechanisms were considered and they reported that for both 50% CO - 50% H_2 and 95% CO - 5% H_2 fuel mixture

compositions, GRI 3.0 are worse for laminar flame speed at NTP conditions. Davis et al and San Diego mechanisms show better results for diluted mixtures (with N_2 and CO_2). Arrieta and Amell [86] examined the effect of the fuel composition, the thermal power input and ratio of air-to-fuel on the pollutant emissions and flame stability in the combustion of an equal molar of syngas and methane mixture in a ceramic stabilized surface combustion burner. They reported an increase in CO emissions of 9-107% and reduction in NO_x emission of about 31-56% and that the ratio of air-to-fuel and thermal input have a significant effect on the flame structure, the efficiency of radiation and the pollutant emissions. Kumaresh and Kim [87] investigated the characteristics of combustion and emission in a combustion chamber made of a can using P-1 and 3-D k-ε model to model radiation and turbulent flow respectively. Their motive was to decrease the NO_x emission and to come up with an operative angle of swirler by varying the secondary holes for cooling the combustion products. They reported that 60^o axial swirl angle gave less NO emission because the exit temperature of the combustor is less as compared to what was obtained from 30^o and 45^o swirl angle geometry. Krieger et al. [88] conducted an investigation on Oxy-fuel combustion for gas turbine application using Reynolds Stress Model (RSM) to handle turbulent. They reported that the propane/oxy-fuel flame ($O_2/CO_2 = 1$) is similar to the baseline case (propane air) but with much higher temperature level in the central core of the combustor leading to a poor gas turbine combustor pattern factor, while oxy-syngas flames showed deep reactions in the primary zone before the first dilution hole resulting to a very good gas turbine combustor pattern factor. They also stated that operating oxy-fuel combustion near stoichiometric condition can only be considered in a situation where instabilities in combustion are of lesser interest

2.10 Reaction Kinetics

Reaction kinetics deals with the rates of chemical processes. Several reaction kinetics have been developed in syngas combustion with air [89] but with little or no one in the area of syngas oxy-combustion. For the case of the H_2-enriched-CH_4 reaction mechanism, the method involves includes the combination of CH_4 reaction mechanism with that of H_2 with the former being the base mechanism. Ilbas et al. [90] numerically investigated the non-premixed turbulent H_2 and H_2-hydrocarbon flames where they combined two-step general reaction mechanism for hydrocarbons oxidation with global reaction mechanism for H_2 combustion. De and Acharya [91], [92] did a similar thing in which 2-step chemistry for CH_4 combustion was combined with 1-step H_2 reaction mechanism proposed by Marinov et al. [93] in studies where Large Eddy Simulation (LES) was used. For the case of oxy-fuel combustion, Frassoldati et al. [94] presented kinetic schemes that were simplified for oxy-fuel combustion where Jones and Lindstedt mechanism (JL) for CH_4 was modified through some optimization. Also, Andersen et al. [95] presented a refined 2-step Westbrook and Dryer (WD) mechanism, 2-global multistep schemes and 4-step JL mechanism, for the purpose of oxy-fuel combustions. So, in order to obtain a reaction mechanism for oxy-combustion of H_2-enriched-CH_4, any of the oxy-fuel combustion mechanism can be combined with Marinov single-step reaction mechanism for H_2.

From the literature review presented, it could be observed that fewer investigations have been conducted in the area of syngas oxy-combustion. In fact, to the best of my knowledge, there is no single study that combined the effect of the fuel composition, oxidizer mixture and swirl vane angle on syngas oxy-combustion for gas turbine application.

CHAPTER 3

EXPERIMENTAL SETUP AND NUMERICAL MODELING

3.1 Experimental Investigation

3.1.1 Experimental Setup

The effect of swirl vane angle on the features of oxy-combustion of H_2-enriched-CH_4 flame was experimentally investigated. Figure 2 shows a schematic of the experimental setup that was considered for this study. The O_2 and CO_2 were premixed (so as to reduce the flame temperature) before being introduced as an oxidizer into the combustor. The mixing was carried out in a mixing chamber built up of a cylinder of 0.150 m diameter, an inner throat of 0.050 m diameter and length of 0.300 m. The mixing chamber contains two inlets and one outlet as shown in Figure 2. The O_2 and CO_2 mixture (i.e. oxidizer) flow through a vertical pipe (0.0508 m internal diameter and 1.2 m height) that contains at its center a small tube carrying fuel as shown in Figure 2. The fuel which consists of a mixture of H_2 and CH_4 was supplied through the center tube of 0.00635 m diameter to the combustor bay and a bluff body with slits on its surface is attached to the end of the tube to form exit nozzles allowing the fuel channel to produce the needed flow rate. Figure 3 shows the sectional view of the combustor. All the gasses were supplied from pressurized gas cylinders and the flows were regulated via valves and pressure regulators. To determine the flow rates, a flow rotameter was utilized in each flow line and mass flow controllers were utilized to control the mass flow rates.

The controllers were connected to computers for data input and post-processing. The mass flow controller is of the D-type supplied by Bronkhorest High-Tech with the model number of F-202AI-M20-AAD-55-V, F-201CI-10K-AGD-22-V, F-202AI-M20-AGD-55-V and F-201CI-10K-AGD-22-V for O_2, CH_4, CO_2, and H_2 respectively and the uncertainty of full scale is ±0.5%. The temperatures of the exhaust gas were measured at the outlet plane and along the axis of the combustor with R-type thermocouple which has a capability of measuring temperature up to the range of 1200 ^oC with ±0.6 ^oC uncertainty. The thermocouple probe was connected to digital readout so as to record the average temperature over one minute at the required locations. Similarly, measurements of the local temperature were repeated and mean values were determined at every location. The thermocouple probe was positioned at the top of the reactor as shown in Figure 2 and a mechanism was used to move the probe both axially and radially within the combustor. A high-speed camera with a speed of 80 frames per second was utilized for flame visualization for the comparison of different flame structures. The camera was positioned at the same level as the combustor.

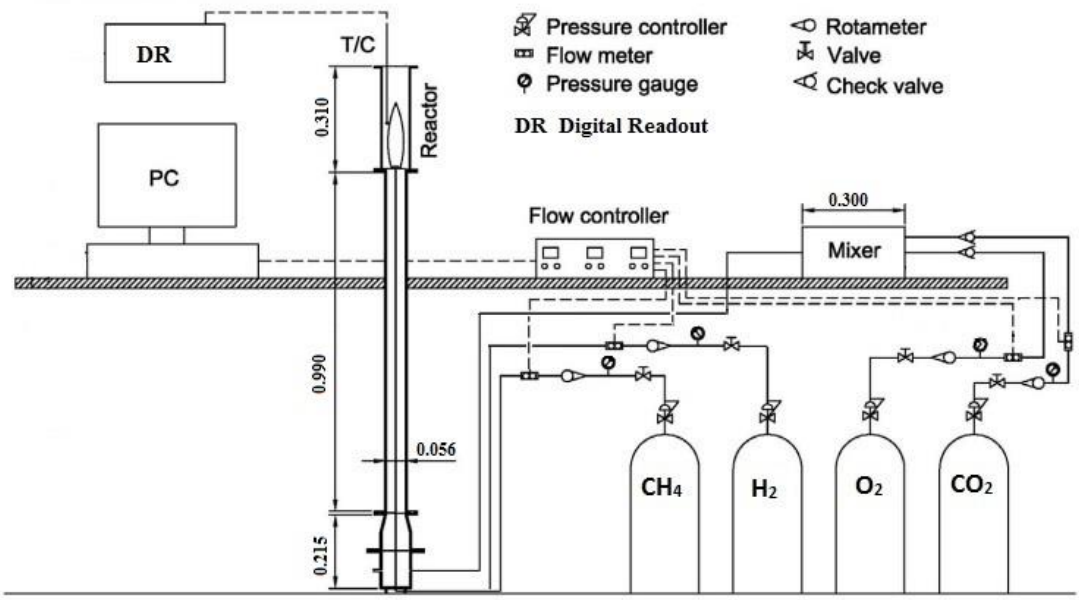

Figure 2: The Schematic diagram showing experimental setup (all dimensions are in meters).

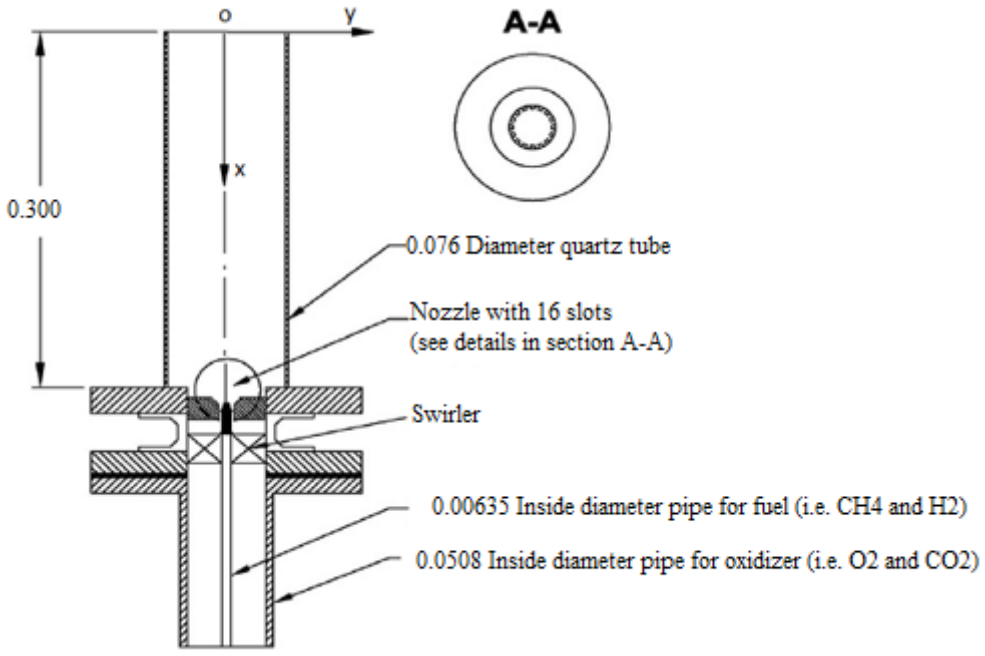

Figure 3: The sectional view of the modeled gas turbine combustor (all dimensions are in meters).

3.1.2 Operating Conditions

The present study includes determination of blow-off limits, analysis of flame structures, and measurement of flame temperature in the vicinity of the exit plane in both axial and radial directions for ranges of equivalence ratio (Φ), fuel composition and oxidizer mixture composition. The equivalence ratios considered were 0.55, 0.65, and 0.75 and the swirl effects were examined at fixed equivalence ratio of 0.65 over ranges of fuel composition and oxidizer mixture composition. Three swirlers with different swirl vane angles including 30^o, 45^o, and 55^o were considered in the present study. The equivalence ratio was computed using the method adopted by Habib et al. [9] which was based on the fuel-air ratio. The energy level of the combustor was kept constant at $4MW/m^3$ throughout the experiments irrespective of the fuel composition so as to establish a basis for comparison. The fuel composition (CH_4 plus H_2) was varied from 100% CH_4 (i.e. 0% H_2) to 50% CH_4 (i.e. 50% H_2). The O_2 percentage in the oxidizer mixture (O_2 plus CO_2) was varied from 100% (i.e. 0% CO_2) to the value of blow-off. From the flow rate of O_2 obtained at a given equivalence ratio, the total flow rate of the oxidizer mixture was calculated based on the required percentage of O_2 [9]. The swirl number (S) for each of the considered swirlers was calculated based on the following equation:

$$S = {}^{2}/_{3}\left[\frac{1-(d_h/d_o)^3}{1-(d_h/d_o)^2}\right]\tan\theta \qquad (3.1)$$

Where d_h, d_o and θ are hub diameter, outside diameter, and swirl vane angle of the swirler respectively. The calculated values of the swirl number for the considered three swirlers ranged from 0.44 to 1.1.

3.2 Numerical Modeling

This section discussed the model adopted and the procedure followed towards the realization of numerical study. As it will be discussed in the solution technique, both Gambit and ANSYS Fluent R15.0 software were utilized in achieving the set objectives.

3.2.1 Conservation Equations

The conservation of mass, momentum, and energy, transport and radiative transfer equations were solved numerically for the equations that are elliptical in nature using the finite volume approach of the CFD so as to predict the pattern of flow and thermal features of the reacting medium within a gas turbine combustor model. The governing equation which generalized all the conservation and species transport equations is given in equation (3.2) [96], [97].

$$\frac{\partial}{\partial x_j}\left(\bar{\rho}\,\bar{U}_j\phi_r + \bar{\rho}\,\bar{u}_j\varphi_r\right) = \frac{\partial}{\partial x_j}\left[\Gamma_{\varphi_r}\frac{\partial \phi_r}{\partial x_j}\right] + \rho\bar{S}_{\phi_r} \tag{3.2}$$

Where ϕ_r and φ_r are the averaged and fluctuating values of the Reynolds's reliant variable and u_j is the constituent of velocity along the x_j direction, ρ denote the fluid density, $\Gamma\varphi_r$ is the coefficient of diffusion and $S_{\phi r}$ represent the source term. The filtered continuity, momentum, and energy equations are given in equation (3.3), (3.4), and (3.5) respectively [98].

$$\frac{\partial}{\partial x_j}\left(\rho\bar{u}_j\right) = 0 \tag{3.3}$$

$$\frac{\partial}{\partial x_j}\left(\rho\bar{u}_i\bar{u}_j\right) + \frac{\partial \bar{p}}{\partial x_i} = \frac{\partial \sigma_{ij}}{\partial x_j} - \frac{\partial \tau_{ij}}{\partial x_i} \tag{3.4}$$

$$\frac{\partial \rho \bar{u}_i \bar{h}_s}{\partial x_i} - \bar{u}_j \frac{\partial \bar{p}}{\partial x_i} - \frac{\partial}{\partial x_i}\left(\lambda \frac{\partial \bar{T}}{\partial x_i}\right) = -\frac{\partial}{\partial x_i}\left[\rho\left(\overline{u_i h_s} - \bar{u}_i \bar{h}_s\right)\right] \quad (3.5)$$

Where:

σ_{ij} is a stress tensor given by;

$$\sigma_{ij}(\text{stress tensor}) \equiv \left[\mu\left(\frac{\partial \bar{u}_i}{\partial x_j} + \frac{\partial \bar{u}_j}{\partial x_i}\right)\right] - \frac{2}{3}\mu \frac{\partial \bar{u}_l}{\partial x_l}\delta_{ij}$$

τ_{ij} is the subgrid-scale stress given by;

$$\tau_{ij} \equiv \rho\overline{u_i u_j} - \rho \bar{u}_i \bar{u}_j$$

The term inside the square bracket in equation (5) is Subgrid enthalpy flux given by;

$$\rho\left(\overline{u_i h_s} - \bar{u}_i \bar{h}_s\right) = -\frac{\mu_{SGS} C_P}{Pr_{SGS}} \frac{\partial T}{\partial x_j}$$

λ and h_s are the thermal conductivity and sensible enthalpy respectively.

μ_{SGS} is a subgrid viscosity, and

Pr_{SGS} is a subgrid Prandtl number = 0.85.

3.2.2 Turbulence Model

From the conservative equations presented above, it could be realized that the flow encounter in a diffusion flame is been dominated by a turbulent flow which enhances mixing, the rate of energy dissipation and heat transfer rate. Several models have been in existence through which such flow could be modeled in ANSYS Fluent. Out of these models, k-ε turbulence models were considered for this study. These turbulence models consist of two transport equations one in *k* and one in *ε* which are separately solve to obtain both turbulence length and time scale. The three types of k-ε turbulence model include; Standard, RNG, and Realizable, and the major difference among these models lie in; method employed in calculating the turbulence viscosity, destruction and generation term in the equation of ε, and turbulent Prandtl numbers governing the turbulent diffusion of k and ε. The choice of these models depends on the application

as neither of them is universally accepted but one may be preferred over other. As it could be seen in the following transport equations, all the three models are similar in *k*-equations with modifications in their *ε*-equations. Details about these models could be found in [98] including the model constants. The transport equations for these models after some truncations were given below.

Transport equations for the standard k- ε model:

$$\frac{\partial}{\partial x_i}(\rho k u_i) = \frac{\partial}{\partial x_j}\left[\left(\mu + \frac{\mu_t}{\sigma_k}\right)\frac{\partial k}{\partial x_i}\right] + G_k - \rho\varepsilon \tag{3.6}$$

$$\frac{\partial}{\partial x_i}(\rho \varepsilon u_i) = \frac{\partial}{\partial x_j}\left[\left(\mu + \frac{\mu_t}{\sigma_\varepsilon}\right)\frac{\partial \varepsilon}{\partial x_j}\right] + C_{1\varepsilon}\frac{\varepsilon}{k}G_k - C_{2\varepsilon}\rho\frac{\varepsilon^2}{k} \tag{3.7}$$

Where turbulence viscosity μ_t, can be computed from;

$$\mu_t = \rho C_\mu \frac{k^2}{\varepsilon}$$

C_μ is a constant in this case and G_k denote turbulence kinetic energy generation.

Transport equations for the RNG k- ε model:

$$\frac{\partial}{\partial x_i}(\rho k u_i) = \frac{\partial}{\partial x_j}\left(a_k \mu_{eff}\frac{\partial k}{\partial x_i}\right) + G_k - \rho\varepsilon \tag{3.8}$$

$$\frac{\partial}{\partial x_i}(\rho \varepsilon u_i) = \frac{\partial}{\partial x_j}\left(a_\varepsilon \mu_{eff}\frac{\partial \varepsilon}{\partial x_j}\right) + C_{1\varepsilon}\frac{\varepsilon}{k}G_k - C_{2\varepsilon}\rho\frac{\varepsilon^2}{k} - R_\varepsilon \tag{3.9}$$

Turbulence viscosity μ_t, is computed the same way as that of standard *k-ε* at high Reynolds number but with slight difference in the value of C_μ .

Transport equations for the realizable k- ε model:

$$\frac{\partial}{\partial x_i}(\rho k u_i) = \frac{\partial}{\partial x_j}\left[\left(\mu + \frac{\mu_t}{\sigma_k}\right)\frac{\partial k}{\partial x_i}\right] + G_k - \rho\varepsilon \tag{3.10}$$

$$\frac{\partial}{\partial x_j}\left(\rho\varepsilon u_j\right) = \frac{\partial}{\partial x_j}\left[\left(\mu + \frac{\mu_t}{\sigma_k}\right)\frac{\partial \varepsilon}{\partial x_j}\right] - \rho C_2 \frac{\varepsilon^2}{k+\sqrt{v\varepsilon}} \quad (3.11)$$

Where $C_1 = \max\left[0.43, \frac{\eta}{\eta+5}\right], \eta = S\frac{k}{\varepsilon}, S = \sqrt{2S_{ij}S_{ij}}$

Turbulence viscosity μ_t, is computed the same way as that of standard *k-ε* but C_μ is given as;

$$C_\mu = \frac{1}{(A_0 + A_s)\frac{kU^*}{\varepsilon}}$$

Out of these three models presented, the standard was used because RNG is only good for swirling flow with swirl number less than 0.5 [98] and realizable is not appropriate in modeling recirculation zone [99], [100].

3.2.3 Radiation Model

The major mode of heat transfer from the combustor to the surrounding is radiation heat transfer, and as a result, the radiative transfer equation (RTE) for emitting, scattering & absorbing medium, was solved using Discrete Ordinate (DO) radiation model which transform the RTE into equation of transport for intensity of radiation in the spatial coordinates. The RTE equation in the direction $\vec{S}$ is given in equation (3.12) while the field equation of the RTE in the same direction as a result of a DO model is given in equation (3.13) [98].

$$\frac{dI(\vec{r},\vec{s})}{ds} + (a + \sigma_s)I(\vec{r},\vec{s}) = \frac{an^2(\sigma T^4)}{\pi} + \frac{\sigma_s}{4\pi}\int_0^{4\pi} I\,(\vec{r},\vec{s}')\phi(\vec{s}.\vec{s}')d\Omega' \quad (3.12)$$

$$\nabla.\left(I(\bar{r},\bar{s})\bar{s}\right) + (a + \sigma_s)I(\bar{r},\bar{s}) = \; an^2\frac{\sigma T^4}{\pi} + \frac{\sigma_s}{4\pi}\int_0^{4\pi} I(\bar{r},\overline{s'})\;\phi(\bar{s},\overline{s'})\,d\Omega' \quad (3.13)$$

WSGGM of domain based was used to cater for the radiation influence of the gas mixture and the total emissivity was calculated using equation (3.14) [101].

$$\varepsilon = \sum_{i=1}^{i=I} a_{\varepsilon,i}(T)\left[1 - e^{-k_i PL}\right] \quad (3.14)$$

Where $a_{\varepsilon,i}$ is the weighting factors of the emissivity for the grey gas i, which depend on the temperature of the gas T, P represent the summation of partial pressures of all the absorbing gases, k_i and L are coefficient of absorption and gas layer thickness respectively.

3.2.4 Species Transport Model

In order to account for the chemical interaction of the reacting or participating species in the combustion process, the conservation equation for the convection-diffusion equation needs to be solved. This equation for the i species is given as;

$$\frac{\partial}{\partial x_i}(\rho \bar{U}_ı m_i) = -\frac{\partial}{\partial x_i} J_i + R_i \quad (3.15)$$

Where;

J_i represents the species i diffusion flux, which result from the concentration gradients and for turbulent flows it is given as[98];

$$\bar{J}_i = -\left(\rho D_{i,m} + \frac{\mu_t}{S_{c_t}}\right)\nabla m_i - D_{T,i}\frac{\nabla T}{T}$$

Where;

S_{c_t} is the turbulent number $=\frac{\mu_t}{\rho D_t}$

$D_{i,m}$ and $D_{T,i}$ are mass and thermal diffusion respectively.

R_i represents the mass rate of production or exhaustion by chemical reaction of the species i, which was computed by using Eddy-Dissipation-Concept (EDC) model.

$$R_i = \frac{\rho(\xi^*)^2}{\tau^*[1-(\xi^*)^3]}(Y^*_i - Y_i)$$

ξ^* is the length fraction given by [102];

$\xi^* = C_\xi \left(\frac{v\varepsilon}{k^2}\right)^{\frac{1}{4}}$, and

τ^* is the time scale given by;

$\tau^* = C_\tau \left(\frac{v}{\varepsilon}\right)^{\frac{1}{2}}$ which is numerically integrated using ISAT algorithm [98].

3.2.5 Combustion Chemistry

The simplified oxy-fuel combustion mechanism for CH_4 proposed by Frassoldati et al. [94] (Table 2) was combined with 1-step H_2 reaction mechanism proposed by Marinov [93] (Table 3) and considered for this study.

Table 2: Modified JL reaction mechanism for oxy-combustion of CH_4 [94]**.**

Reaction	**Order**	Pre-Exponential Factor (A)	**Temperature Exponent (n)**	**Activation Energy (E_a)**
$CH_4 + 0.5O_2 => CO + 2\ H_2$	$[CH_4]^{0.5}$ $[O_2]^{1.30}$	3.06E+10	0.0	30000
$CH_4 + H_2O => CO + 3\ H_2$	$[CH_4]^{1.0}$ $[H_2O]^{1.0}$	3.84E+09	0.0	30000
$CO + H_2O <=> CO_2 + H_2$	$[CO]^{1.0}$ $[H_2O]^{1.0}$	2.01E+09	0.0	20000
$H_2 + 0.5O_2 <=> H_2O$	$[H_2]^{0.3}$ $[O_2]^{1.55}$	8.03E+16	-1.0	40000
$O_2 <=> 2O$	$[O_2]^{1.0}$	1.5E+09	0.0	113000
$H_2O <=> H + OH$	$[H_2O]^{1.0}$	2.3E+22	-3.0	120000

Table 3: Marinov reaction mechanism for H_2 [93]**.**

Reaction	**Order**	**Pre-Exponential Factor (A)**	**Temperature Exponent (n)**	**Activation Energy (E_a)**
$H_2 + 0.5O_2 => H_2O$	$[H_2]^{1.0}\ [O_2]^{0.5}$	1.8E+16	0.0	35002

Units of reaction parameters are; cal, mol, l, s.

3.2.6 Model Description, Boundary Conditions, and Solution Technique

The model combustor showed in Figure 3 is developed by considering its half with appropriate consideration for the exit boundary condition as shown in Figure 4. Computational domain was developed by discretizing the geometry (i.e. half section) into 77,170 (after conducting grid dependency test) non-uniform, non-equally distributed structural grid meshes using Gambit, Figure 5. The boundary conditions were set by considering both the fuel (a mixture of CH_4 and H_2) and oxidizer (a mixture of CO_2 and O_2) inlets as the velocity inlets and the exit of the combustor as the pressure outlet. The wall of the combustor is divided into two; bottom and side wall due to differences in their materials (i.e. steel and quartz respectively). The centerline of the combustor is considered as an axis. The mesh is then exported to ANSYS Fluent R15.0 where 2-D axisymmetric with gravity in the negative x-direction is activated to obtain a steady state solution.

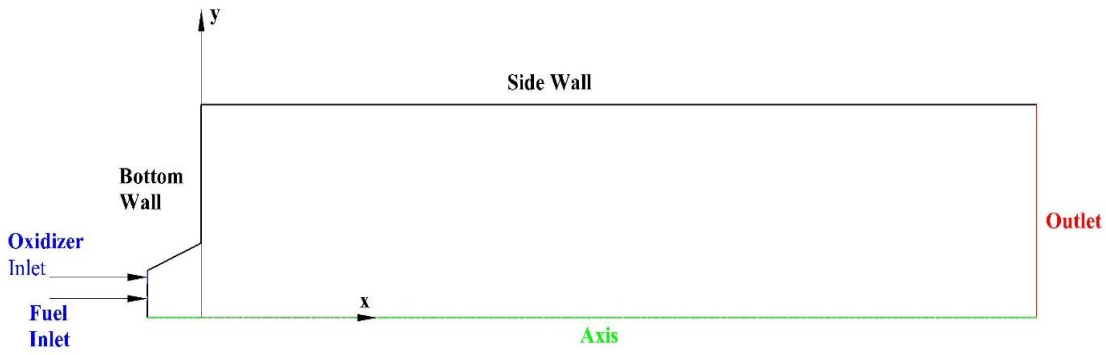

Figure 4: Schematic diagram showing 2-D axisymmetric of the combustor.

The modified JL reaction mechanism for CH_4 that is combined with Marinov 1-step H_2 mechanism and transport data files were imported through CHEMKIN mechanism import into the ANSYS-Fluent R15.0. In each of the cases considered, the fuel and oxidizer velocity (taking swirler distribution into consideration) with their respective

mass fractions were accurately specified. The mixed thermal boundary condition is specified for the two types of wall and the radiation heat transfer through the side wall is modeled as semi-transparent with a diffuse fraction of 0.9. The outlet of the combustor is modeled as pressure outlet with zero gauge pressure and backflow total temperature of 300 K, which means that the combustor is expected to discharge to the environment at atmospheric conditions. The pressure-velocity coupling is handled using SIMPLE scheme. All the partial differential equations described in the previous sections were discretized, apart from pressure discretization that is done using standard, all other spatial discretizations were achieved using the second order upwind method. The criterion for convergence was set to be 10^{-3} for momentum equations and 10^{-6} for others.

Figure 5: Structural grid mesh.

CHAPTER 4

EXPERIMENTAL INVESTIGATIONS: RESULTS AND DISCUSSION

4.1 Oxy-Combustion Characteristics of Syngas

In this section, the combustion characteristics of syngas in terms of flame structure, stability and temperature field are investigated. The presented results in this section were based on measurements for a swirl vane angle of 45^{o} and over different ranges of operating conditions. It should be noted that all the experimental measurements were carried out with respect to the axis shown in Figure 3.

4.1.1 Flame Stability and Structure

Figure 6 shows how H_2 concentration in the inlet fuel affects the flame stability in terms of the percentage of O_2 at the blow-off conditions. The results are presented for three different equivalence ratios including 0.55, 0.65 and 0.75. The blow-off point was obtained by reducing O_2 volumetric concentration in the oxidizer at a fixed equivalence ratio until the flame blows off. For every equivalence ratio, the region above the blow-off limit signifies the stable region. As it could be seen from Figure 6, an increase in H_2 percentage in the fuel composition results in an improvement in the flame stability which allows for flame operation at lower concentrations of O_2 in the oxidizer mixture [57]. At low equivalence ratio, the flame blows off at higher oxygen concentrations. This situation is due to the increase in the inlet flow velocity while decreasing the

equivalence ratio due to the associated increase in the oxidizer flow rate. Since CO_2 has higher molecular weight as compared to O_2, the replacement of O_2 by CO_2 results in the higher mass flow rate of the oxidizer which subsequently increase the Reynolds number (R_e) of the oxidizer and, as a result, the flame blows off at higher CO_2 concentrations. Also, the introduction of diluent (i.e. CO_2) provides the extinguishing effect by suppressing the elementary rate of chemical reactions accountable for flame propagation which resulted in flame speed reduction. On the other hand, increasing the equivalence ratio resulted in a reduction of the oxidizer flow rate and, accordingly, reduction in inlet velocity of the oxidizer. This situation may justify the operation of the flame at lower O_2 concentrations at higher equivalence ratios. As a matter of fact, H_2 has excellent combustion characteristics in terms of its high diffusivity and high flame speed. Increasing H_2 concentrations in the fuel resulted in a wider range of stable flame operation as presented in Figure 6.

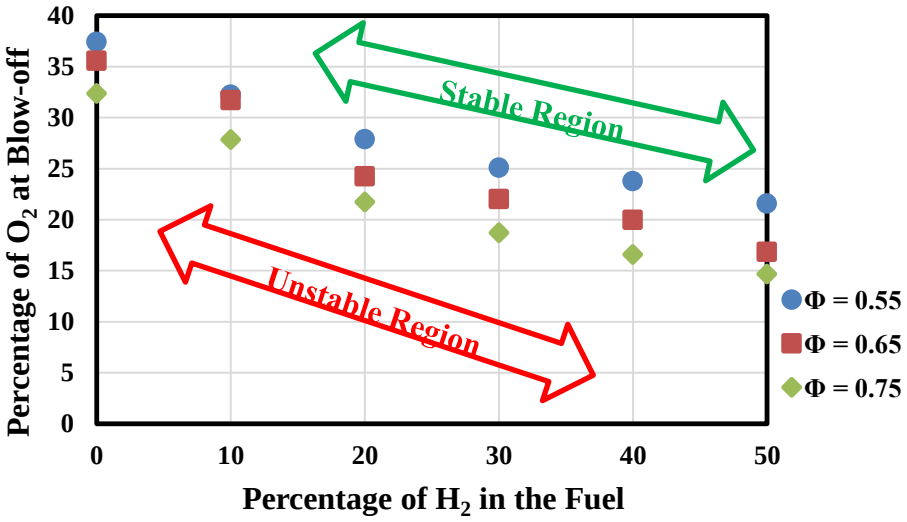

Figure 6: Effect of H_2 concentration on flame stability limits at different equivalence ratios.

At 50% H_2 enrichment, the percentages of O_2 and the Reynolds number of the oxidizer at blow-off were 21.60%, 16.85%, and 14.69% and, 81181, 89268 and 89289 for

equivalence ratios of 0.55, 0.65, and 0.75, respectively. This indicates that H_2 enrichment at equivalence ratios close to stoichiometric conditions under oxy-combustion conditions is an achievable concept with a wide range of stable flame operation.

The effect of oxidizer mixture composition on the flame structure in terms of flame length and appearance is presented in Figure 7 at fixed fuel composition of 80%CH_4/20%H_2 and for three different equivalence ratios. There is an increase in Reynolds number when the percentage of CO_2 in the oxidizer mixture is increased as a result of CO_2 high molecular weight. On the other hand, increasing the percentage of O_2 in the oxidizer mixture results in a reduction in the Reynolds number and increase in the flame speed. As a result, the flame is stabilized effectively at low Reynolds numbers of the oxidizer (say 10224 at 0.75 equivalence ratio) and high oxygen concentrations (i.e. 100%) as shown in Figure 7.

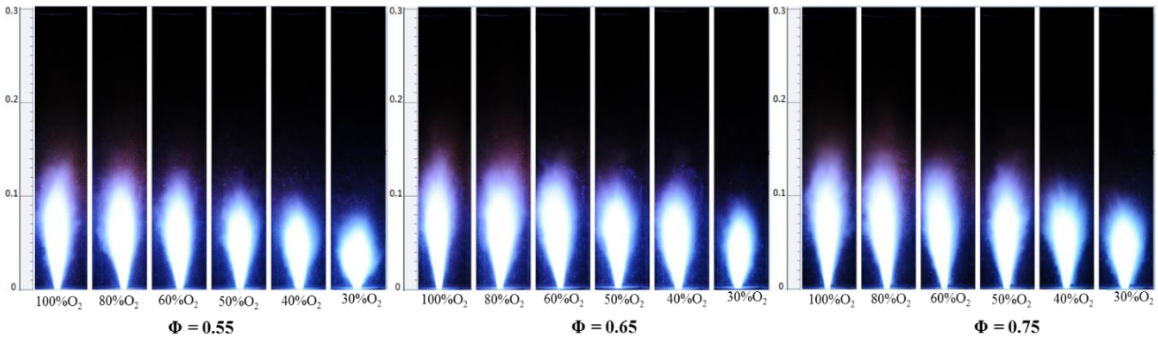

Figure 7: Effect of oxidizer mixture composition on the flame structure at 80%CH_4/20%H_2 fuel compositions for different equivalence ratios.

Increasing CO_2 concentrations results in higher oxidizer volume flow rate at a given equivalence ratio, as a result, effective flow swirl occurs and enhanced mixing is obtained resulting in a shorter length of the flame as shown in Figure 7. At high percentages of O_2, the oxidizer volume flow rate is low and the mixing rate is low which

results in elongated flame at all equivalence ratios. As the percentage of CO_2 is increased, combustion noise and transition in combustion dynamics were noticed as the flame continued to become bigger but with a shortage in length until blow-off point was reached for all equivalence ratios. Increasing the equivalence ratio means a low amount of oxygen is available in the flame zone which results in extended flame length as shown in Figure 7 and Figure 8. Figure 8 presents the influence of H_2 enrichment on flame appearance at fixed oxidizer composition of $50\%CO_2/50\%O_2$ for three different equivalence ratios. Due to its high diffusivity, increasing H_2 concentration in the fuel results in extended flame length. Also, due to its high combustibility features, H_2 enhancement resulted in more stable flame as presented in Figure 8 [78].

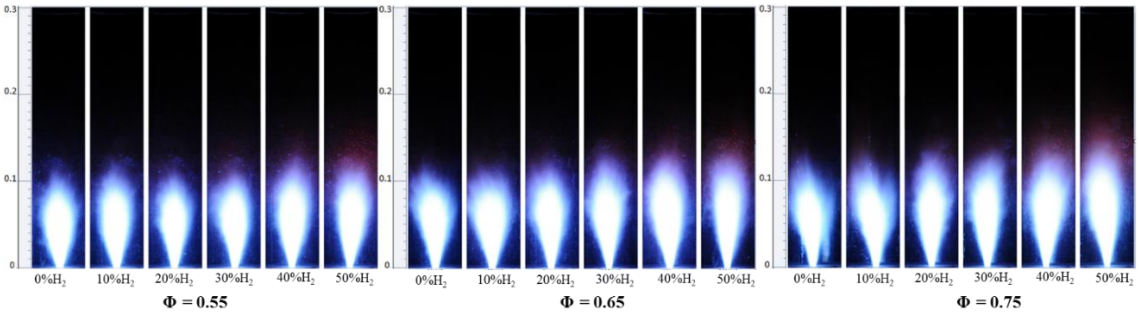

Figure 8: Effect of fuel composition on the flame structure at $50\%CO_2/50\%O_2$ oxidizer mixtures for different equivalence ratios.

4.1.2 Temperature Distributions

The axial (along the center of the combustor) and radial (at the exit plane) temperature distributions measured under various operating conditions are shown in Figure 9, Figure 10, and Figure 11. Figure 9 represents axial and radial temperature distributions at different equivalence ratios for fixed fuel and oxidizer mixture compositions. The distributions show that there was an increase in temperature as the equivalence ratio is increased with almost a regular pattern for all equivalence ratios under consideration. This situation is attributed to the reduction in the available excess oxidizer flow rate,

which cools down the flame, as the operating conditions are changed toward stoichiometric operation.

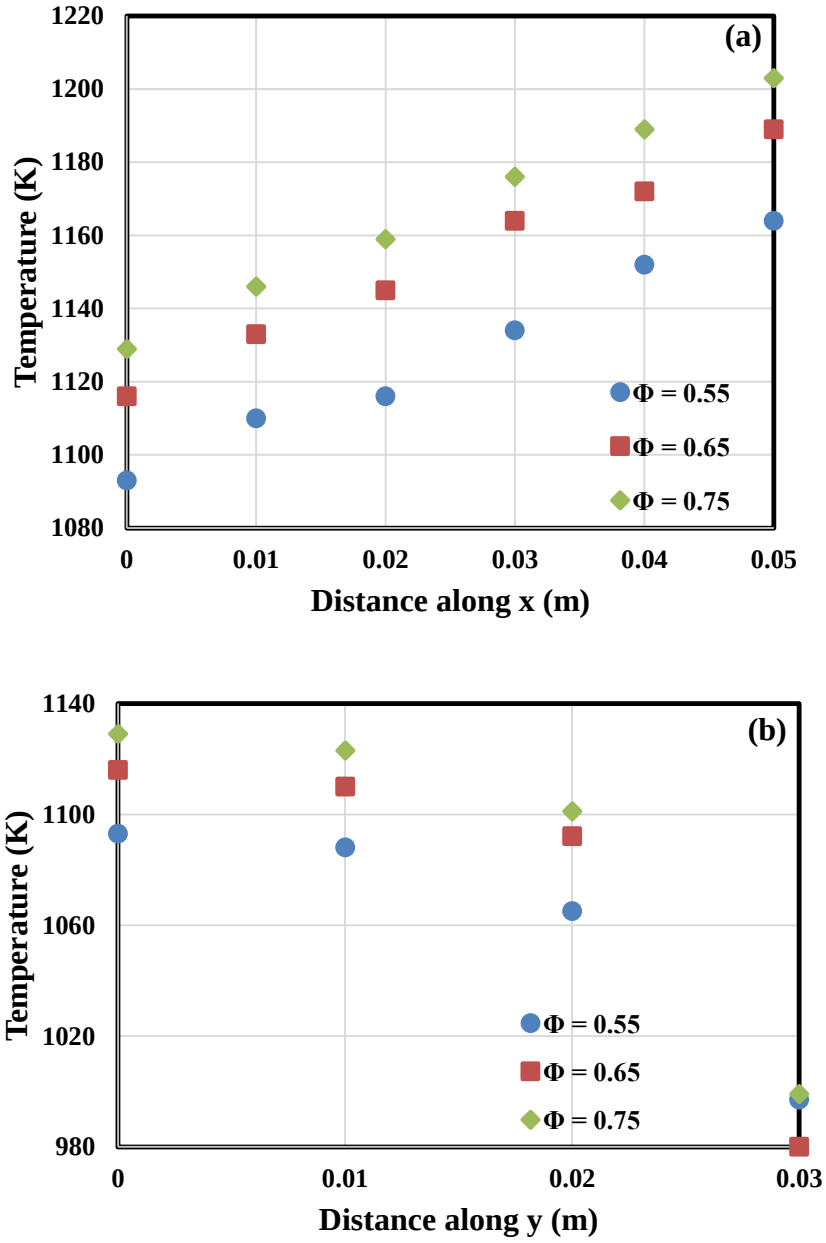

Figure 9: Effect of equivalence ratio on axial (a) and radial (at the exit plane) (b) temperature distributions at fixed fuel and oxidizer mixture compositions of 80%CH_4/20%H_2 and 50%O_2/50%CO_2, respectively.

At all equivalence ratios, the axial temperature is increased from the exit section toward the flame core as presented in Figure 9-a. Due to the heat transfer through the walls of

the combustor, the temperature is reduced from the center towards the walls of the combustor as shown in Figure 9-b for all values of equivalence ratio.

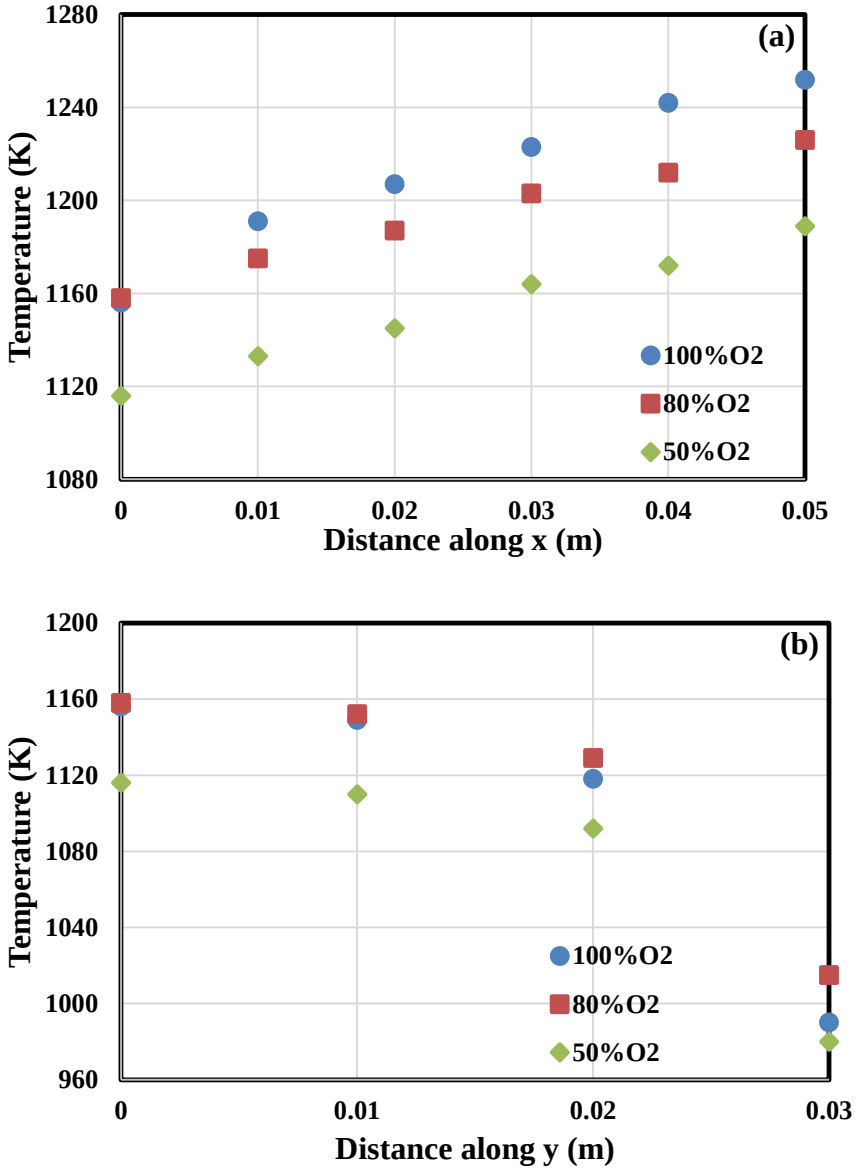

Figure 10: Effect of oxidizer mixtures composition on axial (a) and radial (at the exit plane) (b) temperature distributions at fixed fuel composition of 80%CH_4/20%H_2 and at an equivalence ratio of 0.65.

The effect of oxidizer mixture composition on axial and radial distributions of temperature is shown in Figure 10 for fixed fuel composition and at an equivalence ratio of 0.65. Figure 10 indicates that the higher the percentage of O_2 (corresponding to the lower CO_2 percentage) in the oxidizer mixture the higher the temperature. As the

fraction of CO_2 in the oxidizer is increased, the flame radiation becomes stronger [79], which subsequently influence the combustion and wall temperatures of the combustor. One of the major reasons behind this phenomenon is attributed to the higher heat capacity of the CO_2. Figure 11 explains the effect of fuel composition (H_2 enrichment) on axial and radial temperature distributions at an equivalence ratio of 0.65 and at fixed oxidizer mixture composition. The axial temperature increased at all H_2 enrichment levels towards the flame core in the axial direction as shown in Figure 11-a. Small increase in the temperature is encountered at H_2 enrichment level of 10% while a significant change in temperature is encountered at H_2 enrichment level of 20%. In the case of radial distributions, Figure 11-b indicates a uniform temperature distribution from the center of the combustor to a radial position of 0.02 m. Then, a sharp decrease in temperature is observed towards the wall of the combustor due to heat losses through the walls. Also, the effect of H_2 enrichment level of 10% is small on the temperature and the temperature is even reduced when approaching the wall. This situation is due to the fact that the energy level of the combustor is kept constant for all the cases. At low enrichment levels of H_2 (10%H_2); the amount of H_2 added to balance the CH_4 in order to keep the energy level constant is actually unable to maintain the temperature of the system. At higher H_2 enrichment levels (20%H_2); the temperature inside the combustor is increased as shown in Figure 11.

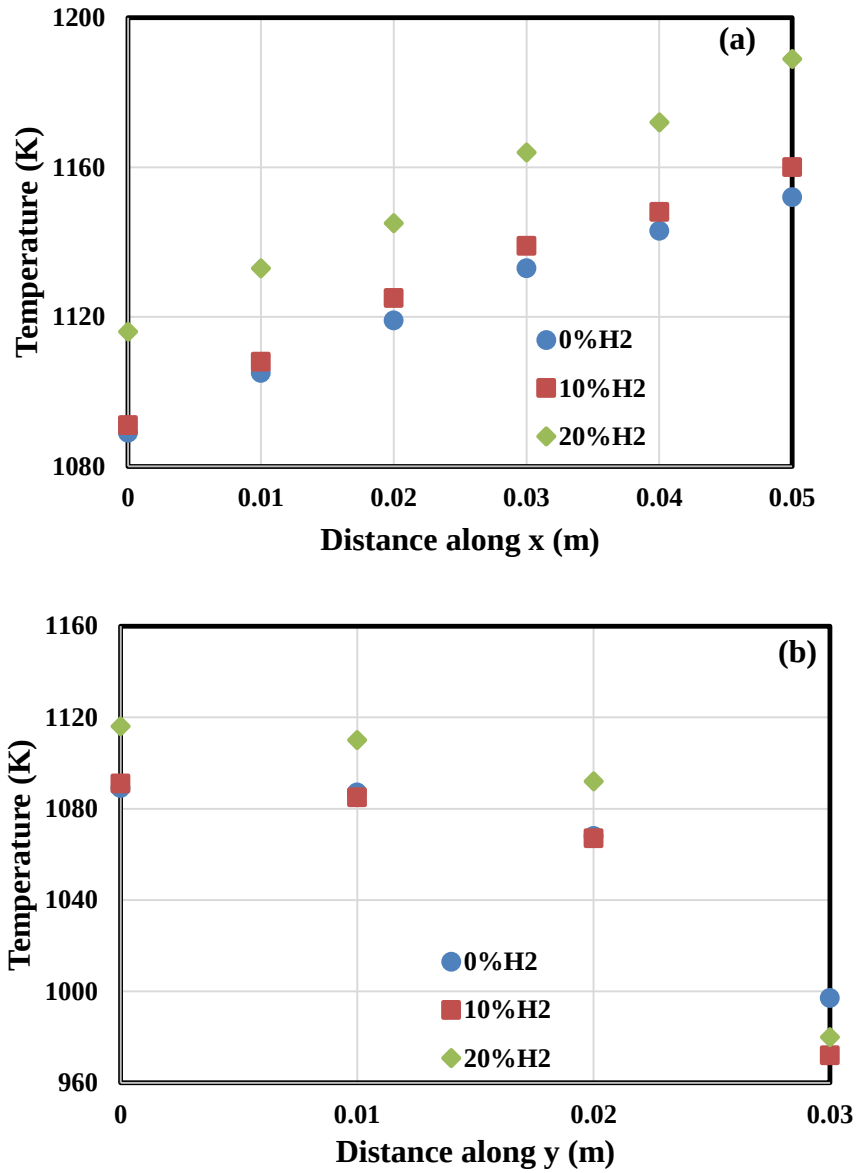

Figure 11: Effect of fuel composition on axial (a) and radial (at the exit plane) (b) temperature distributions at fixed oxidizer mixture composition of 50%O_2/50%CO_2 and at an equivalence ratio of 0.65.

4.2 Oxy-Combustion Characteristics of Syngas for 30º and 55º Swirl Vane Angle

4.2.1 Flame Stability and Structure for 30º Swirl Vane Angle

For the case of 30º swirl vane angle, the swirl number obtained using equation (1) was 0.44. Similar procedure was followed in the results' analysis. The dependency of equivalence ratio, oxidizer mixtures, and fuel composition on the flame stability and structure were investigated. An increase in surface area of the flame for 30º swirl vane angle is observed as compared to the results obtained when 45º swirl vane angle is considered.

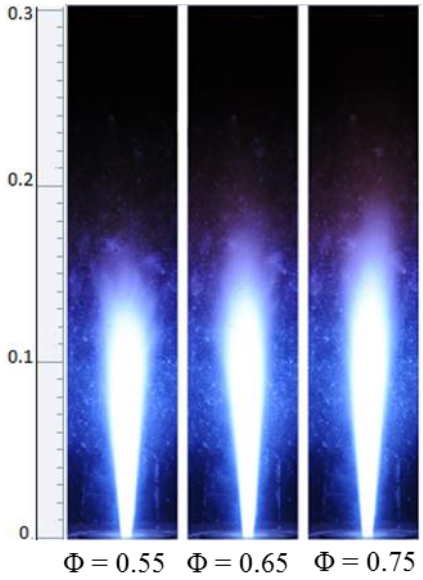

Figure 12: Effect of equivalence ratio on the flame structure at 80%CH_4/20%H_2 fuel compositions and 50%CO_2/50%O_2 oxidizer mixtures for 30º swirl vane angle.

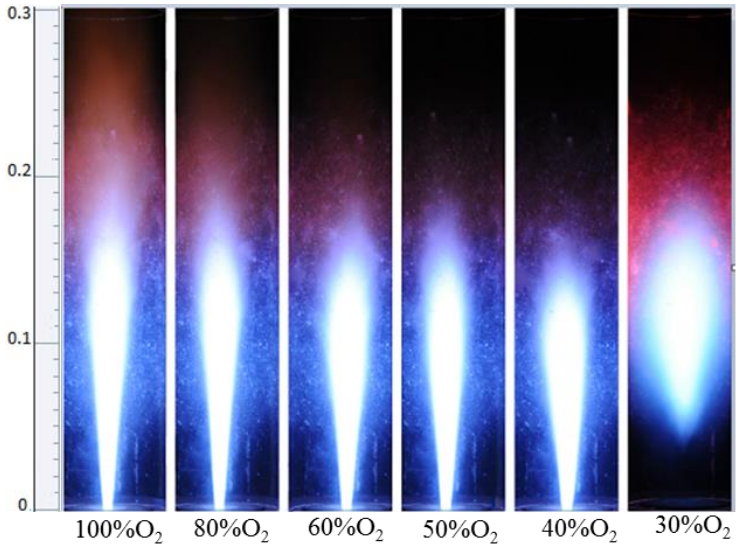

Figure 13: Effect of oxidizer mixtures on the flame structure at 0.65 equivalence ratio and 80%CH_4/20%H_2 fuel compositions for 30^o swirl vane angle.

This increase in flame surface area is attributed to low turbulent intensity and flame speed associated with lower swirl number [63]. The effect of variation in equivalence ratio and H_2 concentration in the fuel compositions are shown in Figure 12 and Figure 14 respectively. The figures indicate the little effect on the physical structure of the flame compared to the case of 45^o swirl vane angle. Figure 13 rather shows the effect of oxidizer mixtures on the flame structure. As the concentration of O_2 in the mixture decreases through the addition of CO_2 the flame length gradually became shorter until lifted flame is observed at a point where the concentration of O_2 was around 30%. The gradual reduction in the flame length can also be attributed to the low turbulence intensities associated with the swirler and lifted flame is caused due to; a large amount of the axial flow and large reduction in flame speed which lead to the disappearance in shear layer that exist between the fuel and oxidizer mixture. This should be expected because the majority of the flow were being supplied as axial due to the low swirl number and at a very point in time (i.e. at higher Reynolds number) the flame got lifted. The lifted flame is highly characterized by a combustion noise.

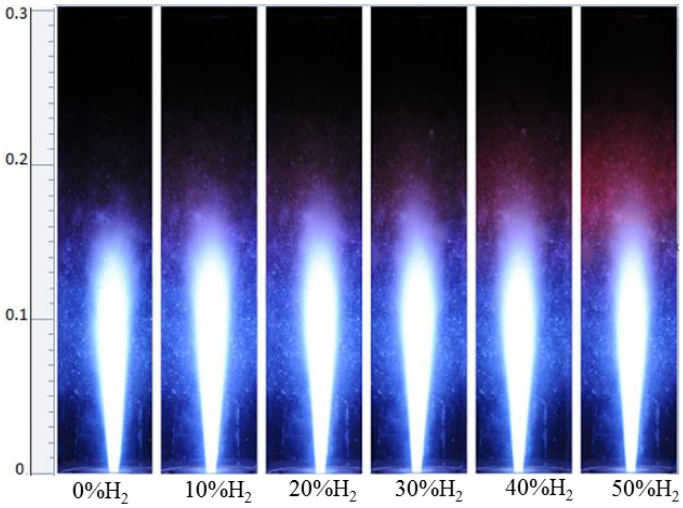

Figure 14: Effect of H_2 concentrations on the flame structure at 0.65 equivalence ratio and 50%CO_2/50%O_2 oxidizer mixtures for 30º swirl vane angle.

4.2.2 Temperature Distributions for 30º Swirl Vane Angle

Similar to the previous case (i.e. 45º swirl vane angle), the axial and radial temperature distributions at various operating parameters were presented.

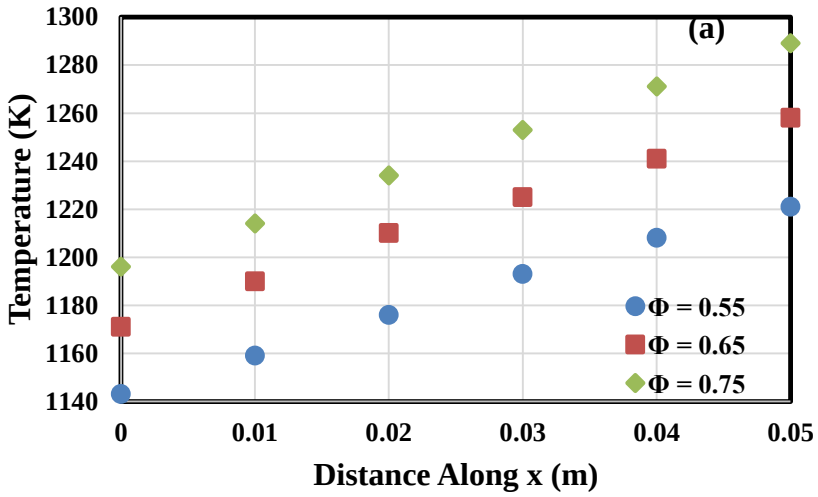

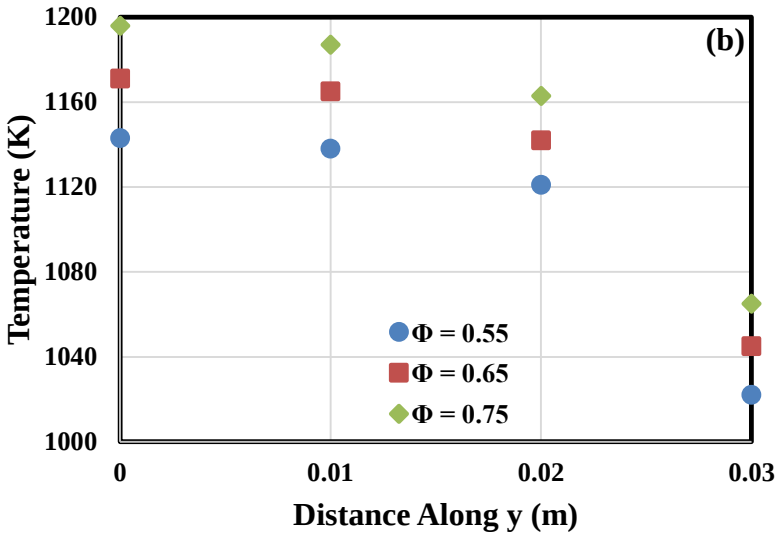

Figure 15: Effect of equivalence ratio on both axial (a) and radial (at the exit plane) (b) temperature distributions at fixed fuel and oxidizer mixture compositions of 80%CH_4/20%H_2 and 50%O_2/50%CO_2, respectively for 30° swirl vane angle.

From Figure 15 it could be noticed that the higher the equivalence ratio the higher the temperature due to the less amount of oxidizer as the equivalence ratio is increased. As the flame is approached axially (i.e. Figure 15-a) from the exhaust position, there is an increase in temperature while a sharp decrease in temperature is observed towards the wall (i.e. Figure 15-b) due to the reason that was previously explained. Figure 16 and Figure 17 show the effect of oxidizer mixture and H_2 concentration on the temperature distributions respectively. As the percentage of O_2 in the oxidizer mixtures is decreased, there is a decrease in the temperature of the combustion product at every section of the combustor due to the high heat capacity of the CO_2.

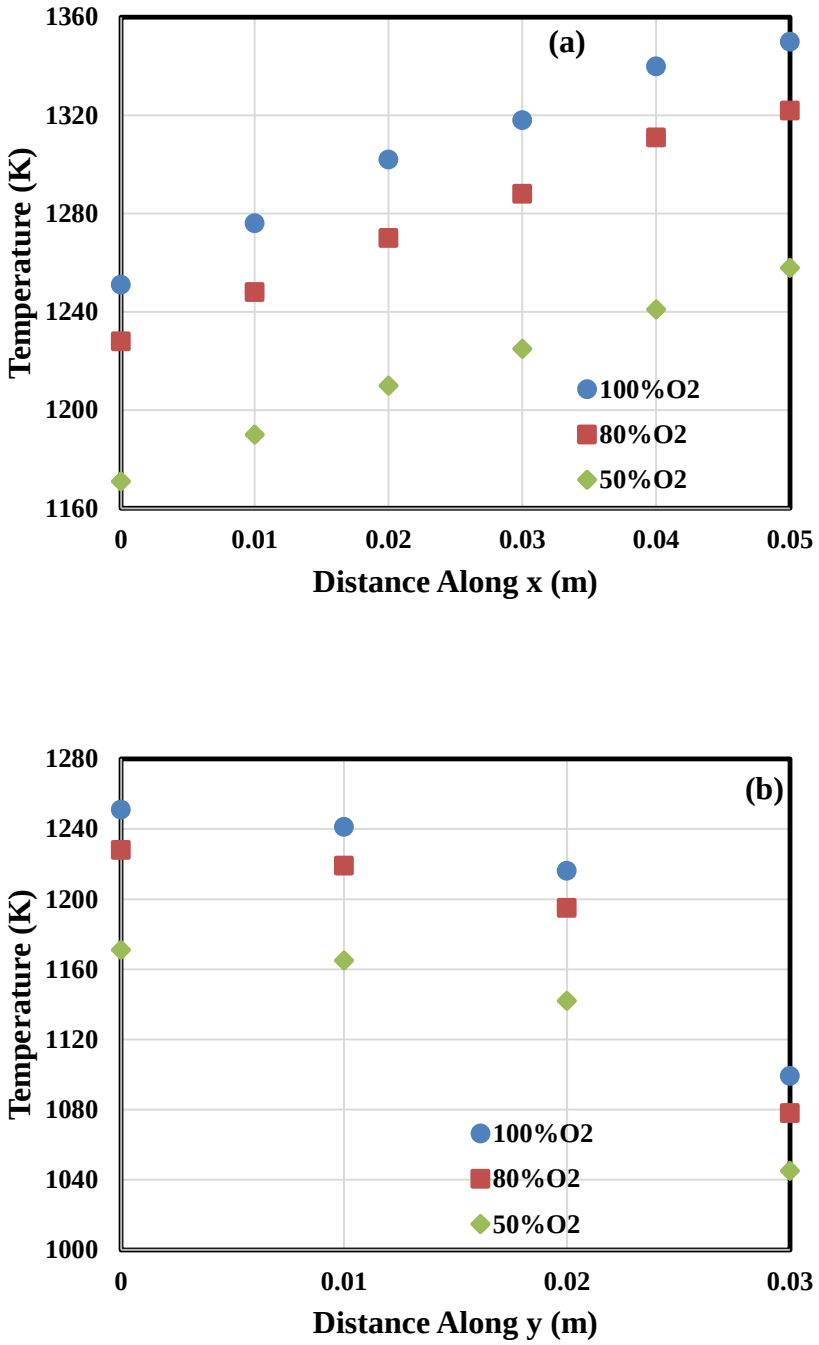

Figure 16: Effect of oxidizer mixtures composition on axial (a) and radial (at the exit plane) (b) temperature distributions at fixed fuel composition of 80%CH_4/20%H_2 and at an equivalence ratio of 0.65 for 30° swirl vane angle.

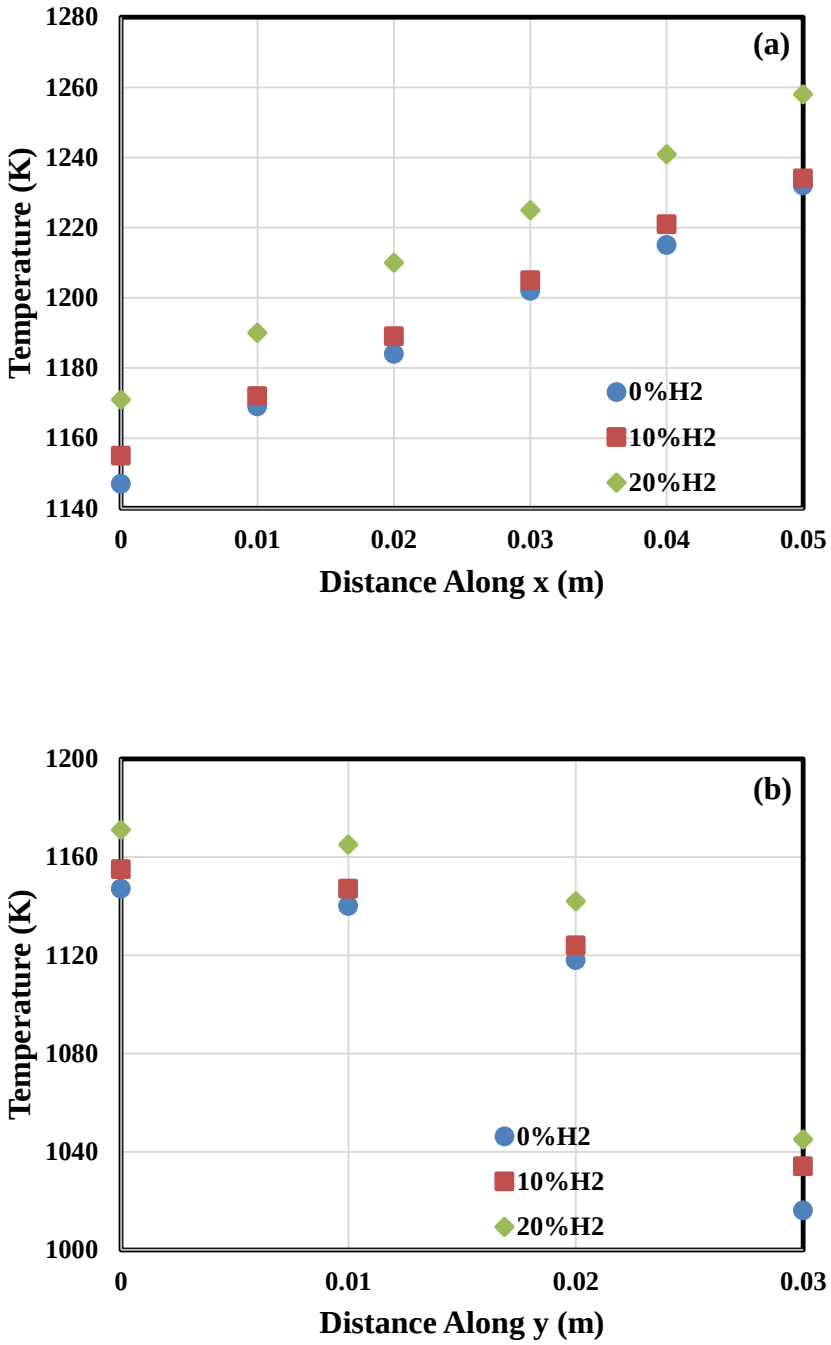

Figure 17: Effect of fuel composition on axial (a) and radial (at the exit plane) (b) temperature distributions at fixed oxidizer mixture composition of 50%O_2/50%CO_2 and at an equivalence ratio of 0.65 for 30° swirl vane angle.

Unlike the previous case (i.e. 45° swirl vane angle), Figure 17-b shows that increase in H_2 concentrations actually increased the temperature at every percentage of H_2 though

the trend and the values were very similar or almost the same for 0% H_2 and 10% H_2 but 10% H_2 not in any situation below 0% H_2 as it was observed for 45^o swirl vane angle. Looking carefully through Figure 15 to Figure 17, an orderliness could be noticed which is due to less mixing rate of the species present in the reactor as a result of low turbulence intensities.

4.2.3 Flame Stability and Structure for 55^o Swirl Vane Angle

Similar to the previous cases, the equivalence ratio, fuel compositions, and oxidizer mixture effects were investigated on the flame stability and structure. The swirl number estimated in this case was 1.10. The combustion dynamics were very similar to the previous cases, Figure 18 and Figure 20 show the effect of equivalence ratio and H_2 concentration on the flame structures respectively. It could also be noticed that these parameters do not really impact the physical structure of the flame. Coming to the oxidizer mixtures effect, it could be seen from Figure 19 that the flame surface area and flame speed happened to be decreasing with a decrease in the O_2 percentage of the mixtures. Unlike 30^o swirl vane angle, the flame continued to get shorter until blowout is reached, no lifted flame is observed and for the given operating parameters the blowoff occur when O_2 concentration is around 21.9% in the oxidizer mixtures. The flame is characterized with a lot of wobbling due to the high turbulence intensities.

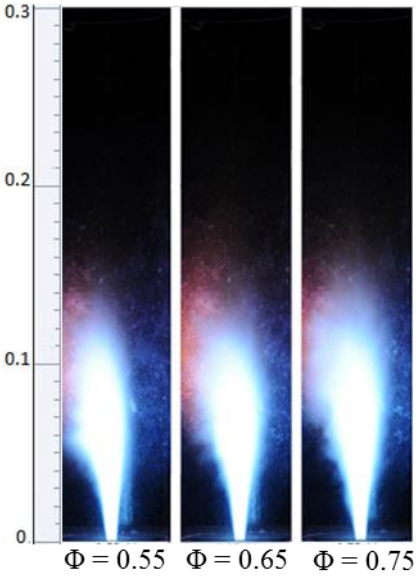

Figure 18: Effect of equivalence ratio on the flame structure at 80%CH_4/20%H_2 fuel compositions and 50%CO_2/50%O_2 oxidizer mixtures for 55º swirl vane angle.

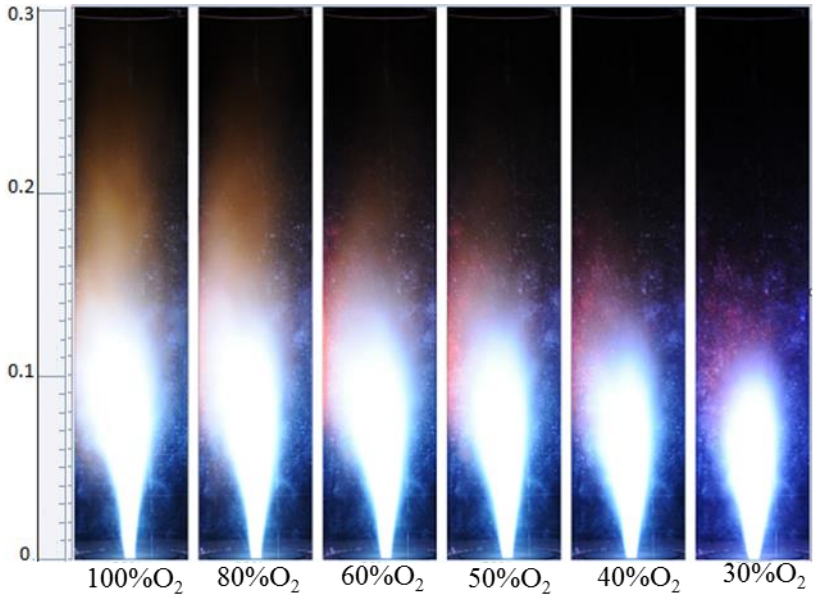

Figure 19: Effect of oxidizer mixtures on the flame structure at 0.65 equivalence ratio and 80%CH_4/20%H_2 fuel compositions for 55º swirl vane angle.

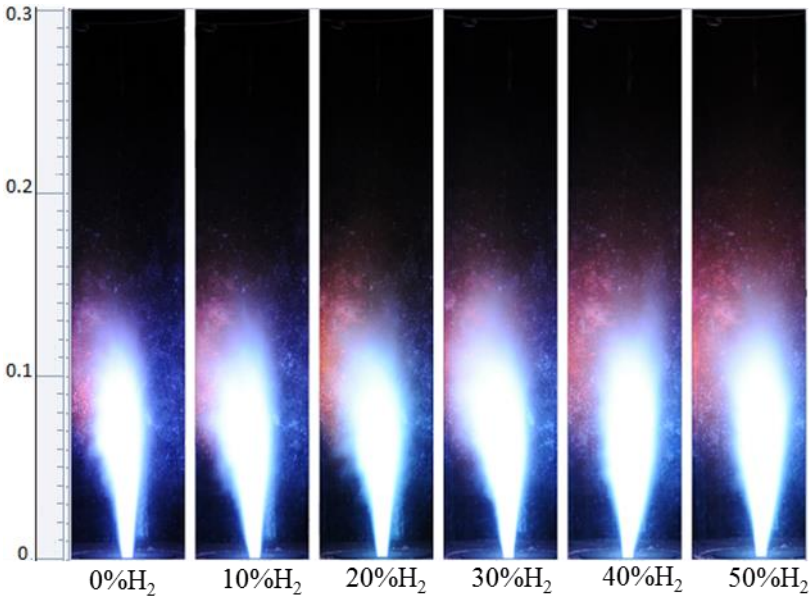

Figure 20: Effect of H_2 concentrations on the flame structure at 0.65 equivalence ratio and 50%CO_2/50%O_2 oxidizer mixtures for 55º swirl vane angle.

4.2.4 Temperature Distributions for 55º Swirl Vane Angle

Effects of equivalence ratio, oxidizer mixtures and fuel compositions on temperature distribution for swirl number of 1.10 were presented in Figure 21, Figure 22 and Figure 23 respectively. The distributions followed almost the same trend with the previous cases with a little discrepancy in radial temperature distributions of 0.65 equivalence ratio in Figure 21 as the wall is approached, and for oxidizer mixture, the behavior of 100% and 80% O_2 were almost overlapped. These situations were due to a high level of turbulence intensities which brought about the high rate of mixing of fresh oxidizer with burned gasses along the radial direction of the combustor. Other than those situations, all other things remained as expected and analyses were quite similar with the previous cases.

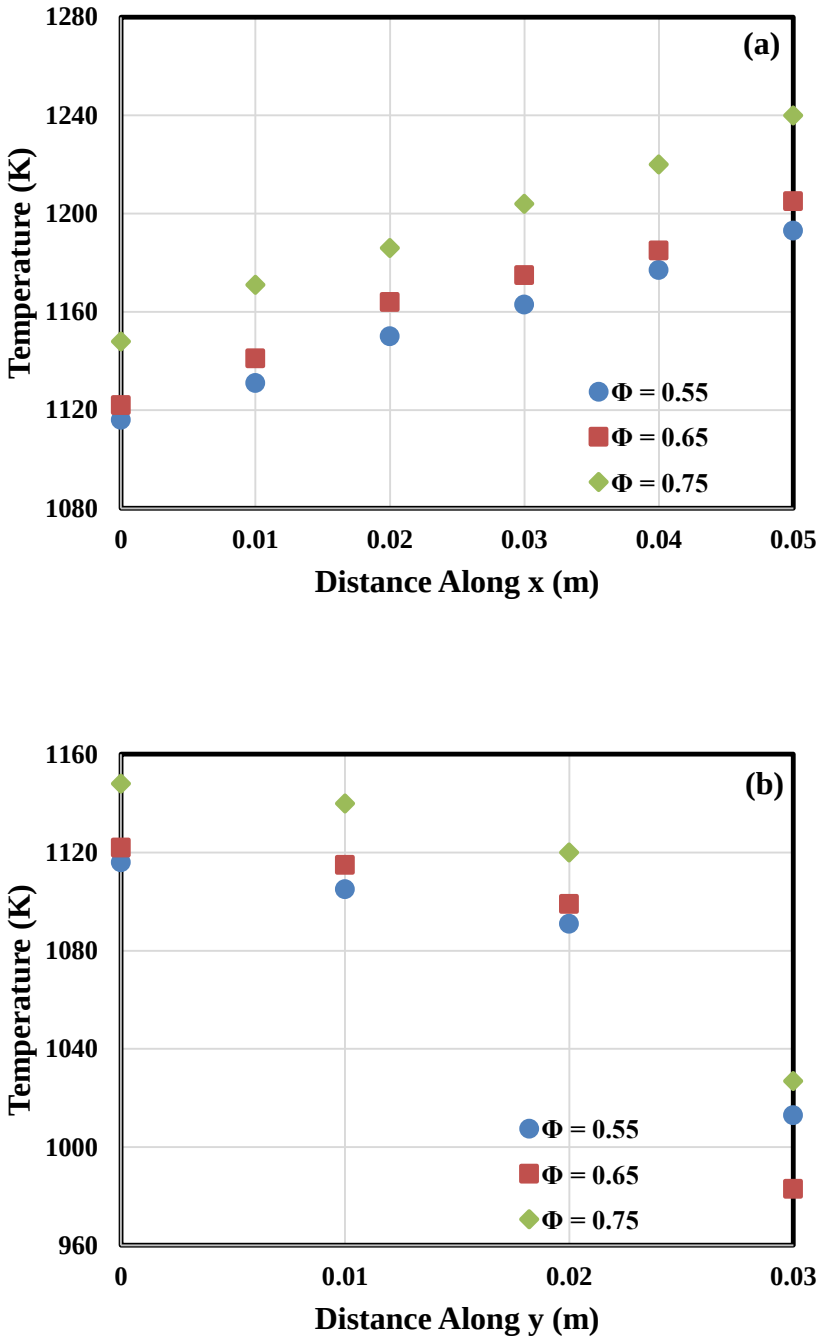

Figure 21: Effect of equivalence ratio on both axial (a) and radial (at the exit plane) (b) temperature distributions at fixed fuel and oxidizer mixture compositions of 80%CH_4/20%H_2 and 50%O_2/50%CO_2, respectively for 55° swirl vane angle.

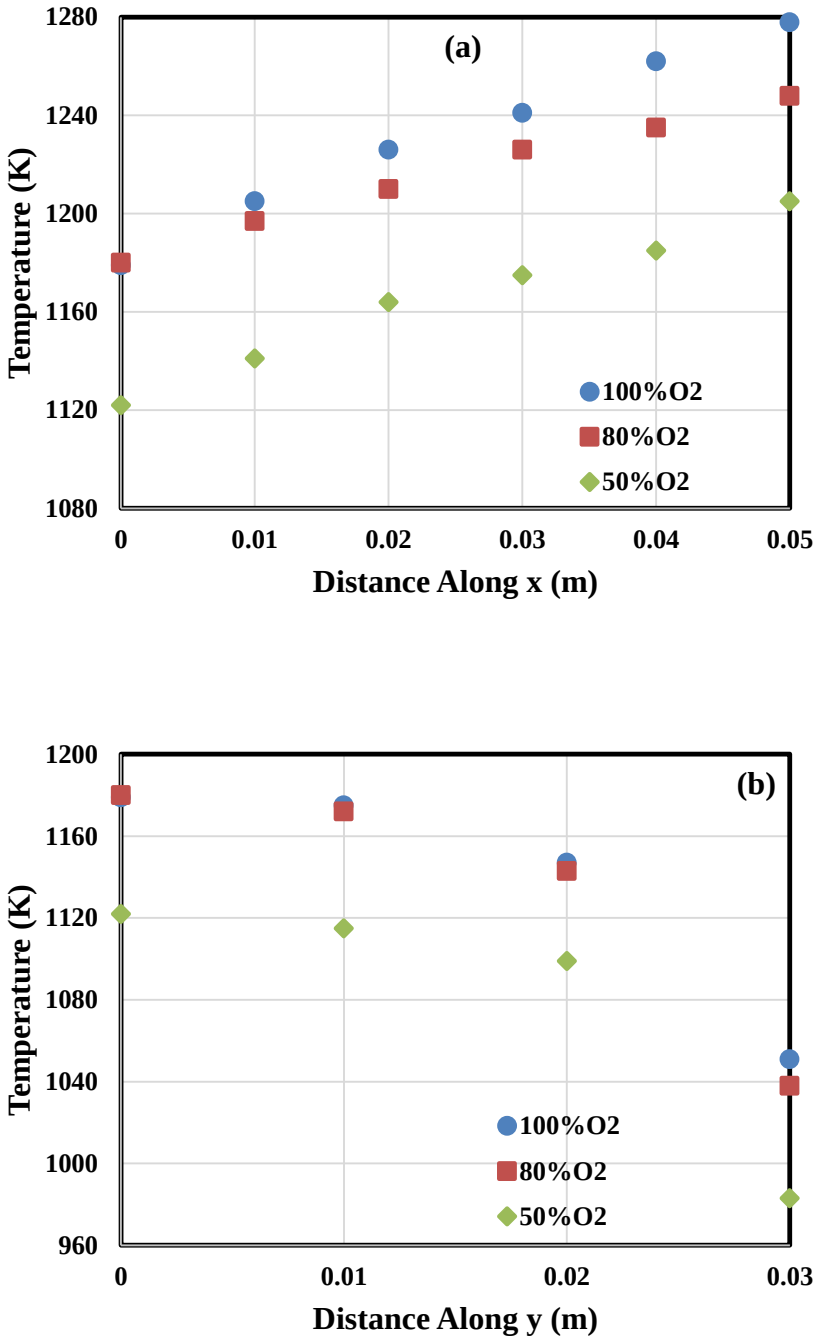

Figure 22: Effect of oxidizer mixtures composition on axial (a) and radial (at the exit plane) (b) temperature distributions at fixed fuel composition of 80%CH_4/20%H_2 and at an equivalence ratio of 0.65 for 55° swirl vane angle.

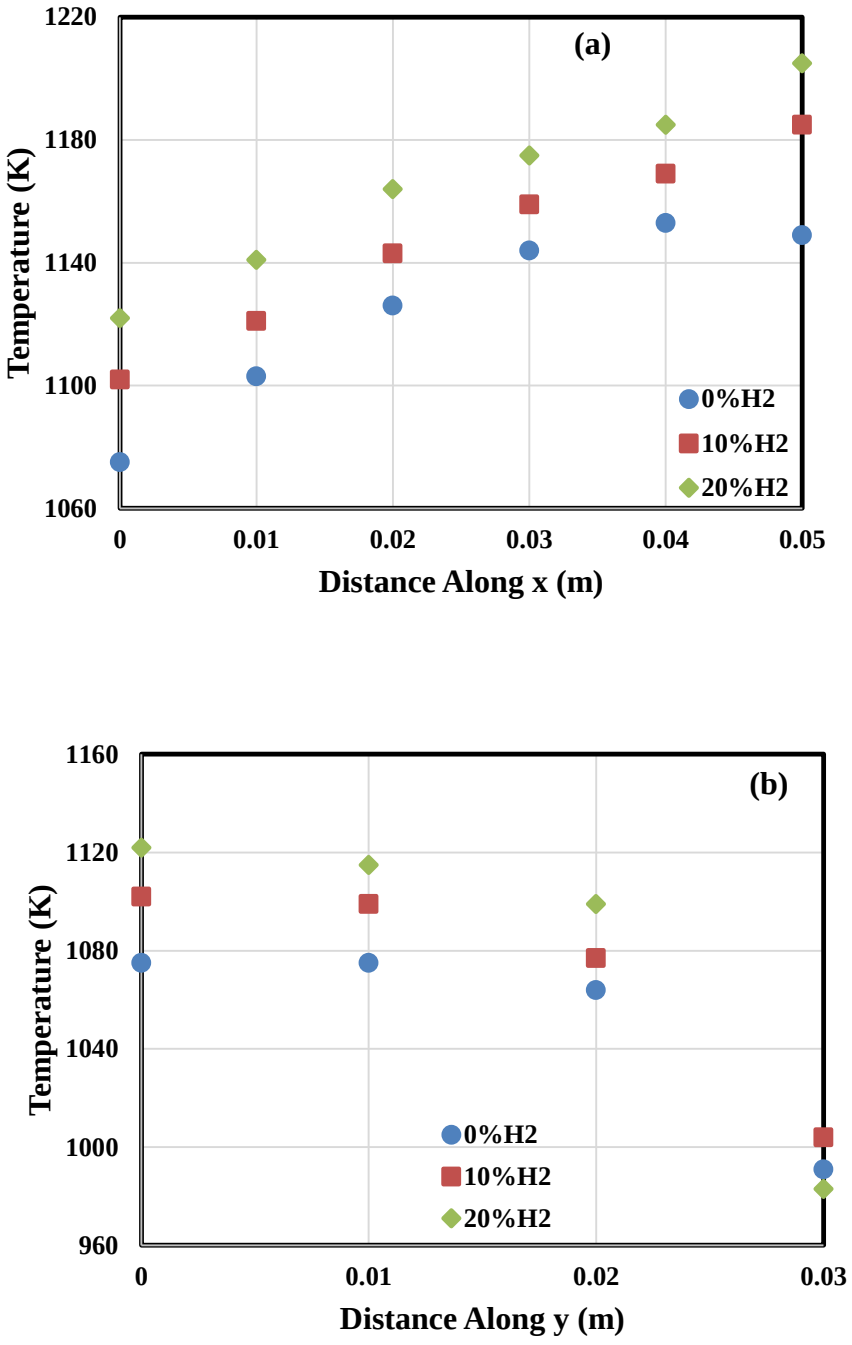

Figure 23: Effect of fuel composition on axial (a) and radial (at the exit plane) (b) temperature distributions at fixed oxidizer mixture composition of 50%O_2/50%CO_2 and at an equivalence ratio of 0.65 for 55° swirl vane angle.

4.3 Comparison of the Swirl Effect

The effect of the three swirlers discussed above on the flame stability and structure and temperature distributions over ranges of fuel and oxidizer compositions and equivalence ratio were compared in the following sections.

4.3.1 Effect of Swirl on Flame Stability and Structure

Figure 24 shows the blow-off limits at a given equivalence ratio of 0.65 and at fixed fuel and oxidizer mixture compositions for the three swirlers. As shown in Figure 24, the flame blows off at lower values of O_2 concentrations in the oxidizer mixture as the swirl vane angle increase. For 55^o swirl vane angle, the O_2 concentration in the oxidizer mixtures can go as low as 21.95 indicating wider stable operation range at higher swirl vane angles.

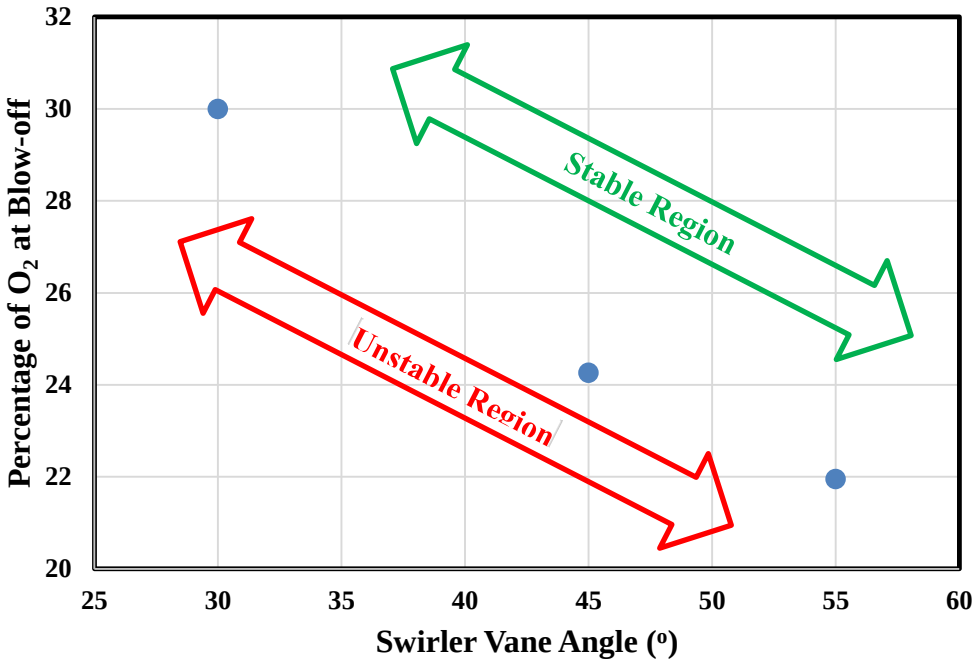

Figure 24: Effect of swirl vane angle on the stability limits of the flame at an equivalence ratio of 0.65 and at fixed fuel and oxidizer mixture compositions of 80%CH_4/20%H2 and 50%O_2/50%CO_2, respectively.

This is attributed to the increase of the flow momentum in the tangential direction which enhances the mixing within the flame core. Also, increasing the swirl vane angle enhances the sustainability of the created outer recirculation zone and, accordingly, the stability of the flame is enhanced.

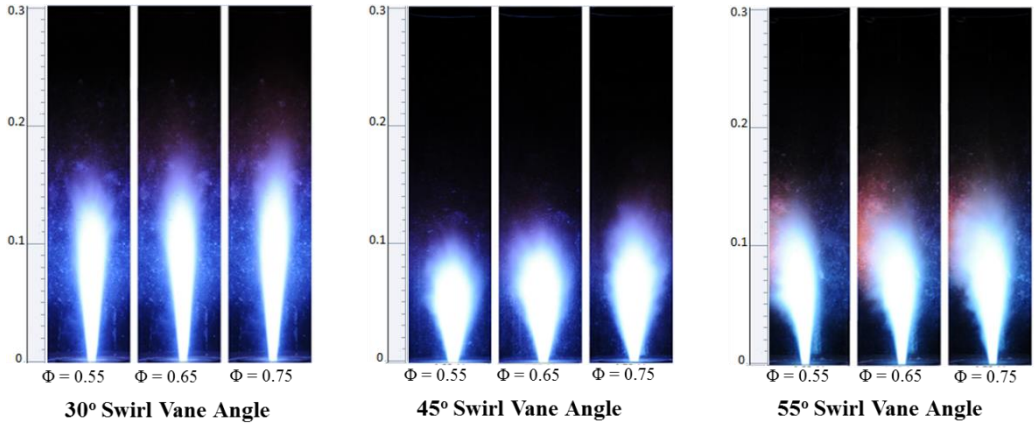

Figure 25: Effect of equivalence ratio on the flame structure for different swirl vane angles at fixed fuel and oxidizer mixture compositions of 80%CH_4/20%H_2 and 50%O_2/50%CO_2, respectively.

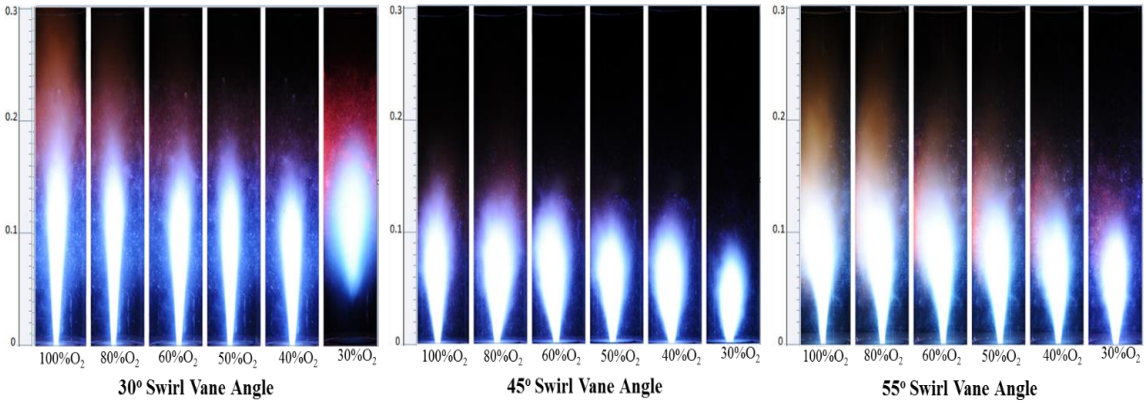

Figure 26: Effect of oxidizer mixture composition on the flame structure for different swirl vane angles at fixed fuel composition of 80%CH_4/20%H_2 and at an equivalence ratio of 0.65.

The dependence of flame structure on swirl number is investigated in Figure 25, Figure 26 and Figure 27 under the variation of equivalence ratio and fuel and oxidizer mixture compositions. As a matter of fact, increasing the swirl number (swirl vane angle) results in higher turbulence intensities and flame speed and shorter flame length. The swirler of 30^o swirl vane angle exhibits longest flame length in every case due to the lowest

turbulence intensity as most of the oxidizer flow to the combustor is supplied in the axial direction [3]. In contrast, the swirler with 55^{o} swirl vane angle is characterized by high turbulence intensity and high flame speed as shown in Figure 25, Figure 26 and Figure 27. In the three figures, the flame surface area is increased while increasing the swirl vane angle due to the improved mixing and turbulence. The flames obtained for the 55^{o} swirler are not erect like those in cases of 30^{o} and 45^{o} swirlers. This is attributed to the fact that tangential velocities (swirl velocities) are dominant at high swirl vane angles. Also, the flame length is increased in the case of the swirler with 55^{o} swirl vane angle as compared to the swirler with 45^{o} swirl vane angle. Effect of increasing the equivalence ratio on the flame structure is similar for all swirlers as presented in Figure 25. Increasing equivalence ratio at fixed fuel and oxidizer compositions resulted in elongated flames as shown in the figure. This is attributed to the decrease in oxygen concentration within the combustor. This situation forces the flame to extend its length so as to complete the combustion process. Figure 26 shows the influence of oxidizer mixture composition on the flame structure for the considered swirlers at fixed fuel composition and equivalence ratio.

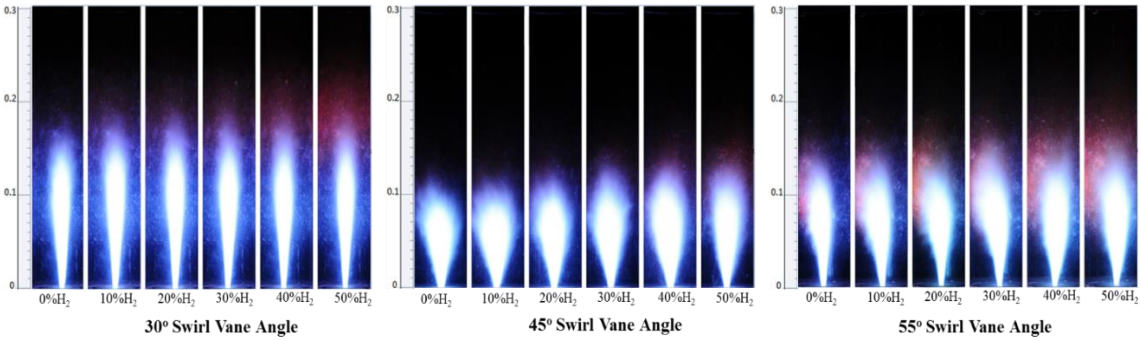

Figure 27: Effect of fuel composition on the flame structure for different swirl vane angles at fixed oxidizer mixture composition of 50%O_2/50%CO_2 and at an equivalence ratio of 0.65.

As the concentration of O_2 in the mixture decreases through the addition of CO_2, the flame length gradually became shorter for all the swirlers. Forcing most of the oxidizer flow in the axial direction (i.e. at higher Reynolds number) in the case of 30^{o} swirler

resulted in early flame lift-off at lower O_2 concentrations as compared to the other swirlers as shown in Figure 26. The lifted flame is highly characterized by a combustion noise as stated above. The flame surface area and flame speed were decreased while increasing CO_2 content of the mixtures. Unlike the case of swirler with 30^o swirl vane angle, the flame continued to be shorter until blow-off was reached, no lifted flame was observed, for the cases of swirlers with 45^o and 55^o swirl angles. The flame is characterized with a lot of wobbling due to the high turbulence intensities for the case of 55^o swirler. Similar effects of H_2 enrichment at fixed oxidizer composition and fixed equivalence ratio on the flame structure were observed for all swirlers as presented in Figure 27. Increasing the concentration of H_2 in the fuel resulted in stable and elongated flames for all swirlers.

4.3.2 Effect of Swirl on Temperature Distributions

In order to investigate the effect of swirl vane angles/swirl number on axial temperature distributions under various operating parameters, Figure 28Figure 29 and Figure 30 were plotted considering the three swirlers. The comparison is made in terms of temperature distribution at three axial points (x, y) along the center of the combustor including (0,0), (0.03,0) and (0.05,0). At all the considered locations close to the exit plane of the combustor and under all operating conditions, the swirler with 30^o swirl vane angle displayed maximum temperature distributions while minimum distributions were obtained from 45^o swirl vane angle as presented in Figure 28Figure 29 and Figure 30. It is obvious that the swirler with 30^o swirl vane angle showed maximum temperature distributions and this is due to the elongation of the flame while operating with the 30^o swirler in the axial direction due to low mixing ability as presented in Figure 25, Figure 26 and Figure 27. Although distributions obtained from 45^o and 55^o swirl vane angles were very close in most of the cases, the former exhibited lower

values of temperature as it could be seen from Figure 28Figure 29 and Figure 30. This is also attributed to the extended flame length in the case of 55^{o} swirl angle as compared to the case of 45^{o} swirl angle. Figure 28 shows the effect of swirl angle on the axial temperature distributions for a range of equivalence ratio at fixed fuel and oxidizer mixture composition. As shown in the figure and for all swirlers, the higher the equivalence ratio the higher the temperature due to the less amount of oxidizer as the equivalence ratio is increased. The temperature is increased towards the flame core in the axial direction.

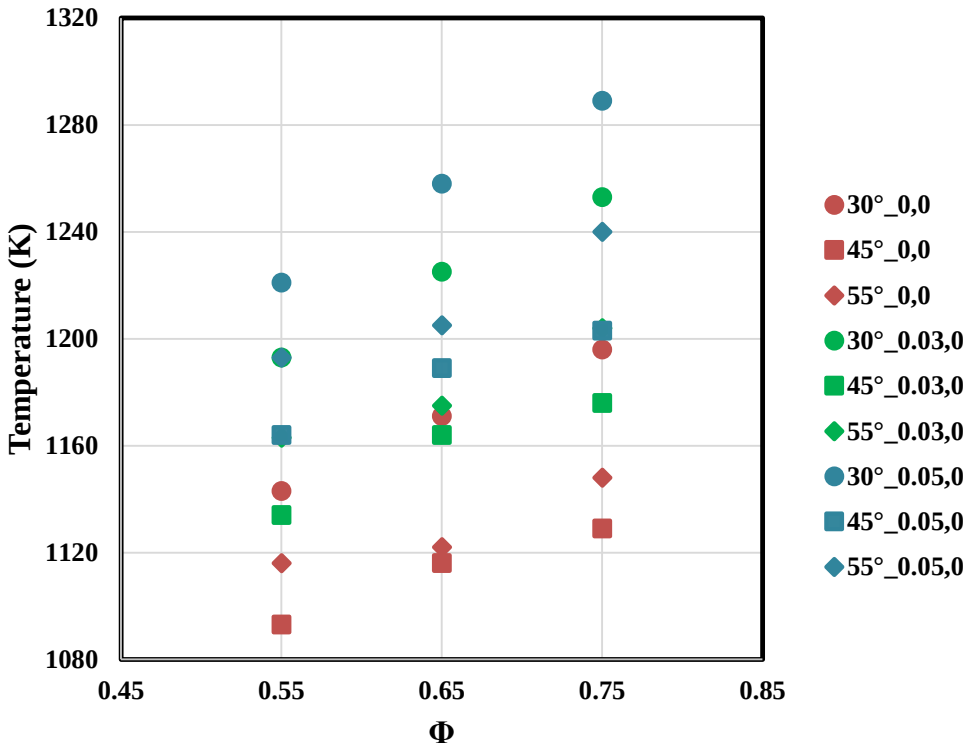

Figure 28: Effect of equivalence ratio on axial temperature distributions (at three axial points (x, y) including (0,0), (0.03,0) and (0.05,0)) for different swirl vane angles at fixed fuel and oxidizer mixture compositions of 80%CH_4/20%H_2 and 50%O_2/50%CO_2, respective.

Figure 29 presents the distributions of axial temperature for a range of oxidizer mixture compositions to investigate the effect of swirl on the distributions at fixed fuel composition and fixed equivalence ratio. For all the swirlers, the results showed that as the percentage of O_2 in the oxidizer mixtures is decreased, a decrease in the combustion

product temperature is encountered along the axis of the combustor as a result of the high heat capacity of the CO_2. The effect of swirl angle on axial temperature distribution is presented in Figure 30 for a range of H_2 enrichment concentrations at fixed equivalence ratio and oxidizer composition. The results showed improvement in the combustion temperature while increasing the enrichment level of H_2 in the fuel.

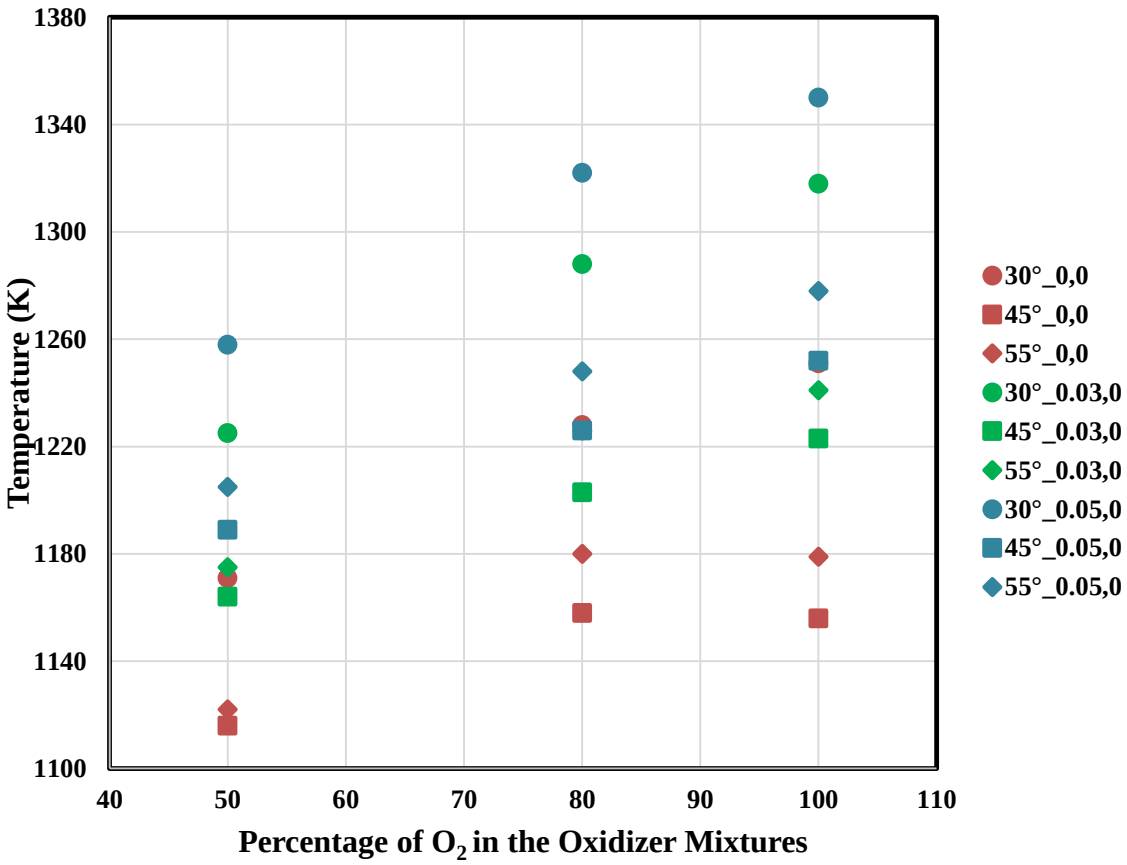

Figure 29: Effect of oxidizer mixture composition on axial temperature distributions (at three axial points (x, y) including (0,0), (0.03,0) and (0.05,0)) for different swirl vane angles at fixed fuel composition of 80%CH_4/20%H_2 and at an equivalence ratio of 0.65.

Due to keeping the input energy to the combustor fixed at a certain level, the 10%H_2 enrichment concentration resulted in insignificant improvement in the combustion temperature.

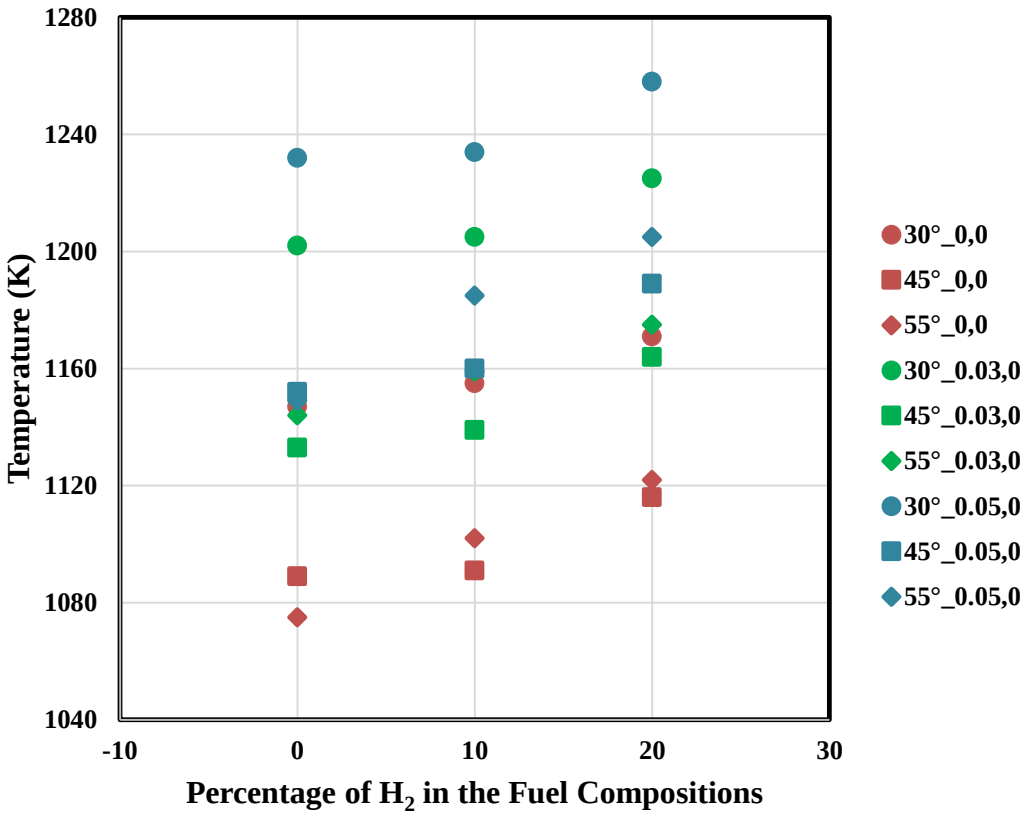

Figure 30: Effect of fuel composition on axial temperature distributions (at three axial points (x, y) including (0,0), (0.03,0) and (0.05,0)) for different swirl vane angles at fixed oxidizer mixture composition of 50%O_2/50%CO_2 and at an equivalence ratio of 0.65.

CHAPTER 5

NUMERICAL INVESTIGATION: RESULTS AND DISCUSSION

The experimental results indicated that 55^o swirl angle is more stable compared to the other swirl angles. Hence, the numerical investigation is carried out for 55^o swirl angle. The results obtained were validated with the experimental results obtained for 55^o swirl angle. These included flame visualization, temperature distribution, velocity field, species mass fraction, kinetic rate of reaction, equivalence ratio and swirl vane angle effects. All the numerical measurements were obtained with respect to the axis showed in Figure 4.

5.1 Flame Visualization and Temperature Distributions

Figure 31 shows the comparison between the experimental and computed flame structure at different percentages of O_2 in the oxidizer mixture at 0.65 equivalence ratio and 80%CH_4-20%H_2 fuel composition, while Figure 32 shows the comparison between the temperature fields of the computed flames at different percentages of O_2. Figure 31 indicated a good agreement between the structure of the flames obtained experimentally and numerically. Examining Figure 31 and Figure 32 carefully, it could be realized that a large amount of the oxidizer supplied escaped through the outer recirculation zone to the reactor walls due to sudden expansion which is created between the bluff body and the reactor. The model combustor was actually designed in a manner such that a large amount of fresh oxidizer or excess oxidizer can escape the burning zone through the

side walls and later mix-up with the combustion product downstream of the burner thereby; cooling the flue gasses along the reactor length.

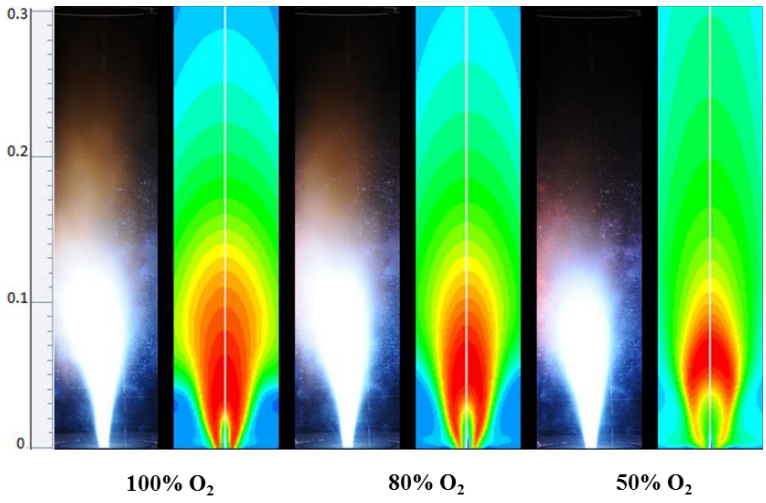

Figure 31: Experimental and numerical flame structure at different percentages of O_2, 0.65 equivalence ratio and fuel composition of 80%CH_4/20%H_2.

It could be seen that at 100%O_2 composition in the oxidizer, a maximum value of temperature is attained in the combustor at the burning zone (along the axis) while the minimum value of temperature is observed around the outer recirculation zone. But, as the percentage of O_2 in the oxidizer is being reduced due to the introduction of CO_2; the temperature in the outer recirculation zone gradually increased while the reduction in the values of temperature is experienced at the burning zone. Such situations were due to two major reasons (flame speed or burning velocity and Reynolds number) which also affect the stability of the flame. At a high O_2 concentration in the oxidizer, there exists high flame speed which eventually influence the combustion performance positively. Also, since O_2 has lower heat capacity as compared to CO_2 with poor radiative heat transfer properties hence, the combustor remained at a higher temperature. On the other hand, the introduction of CO_2 resulted in a reduction of O_2 percentage in the oxidizer and hence, increased the Reynolds number. Due to the physical (high molecular heat capacity, low thermal diffusivity etc.) and chemical

properties of the CO_2, the burning velocity is reduced and radiative heat transfer is modified thereby, resulting in temperature field modification. A large amount of heat is being absorbed by CO_2 and loses the same through radiative heat transfer. It is also noted that the flame decreases in length as the percentage of O_2 is decreased as a result of high Reynolds number.

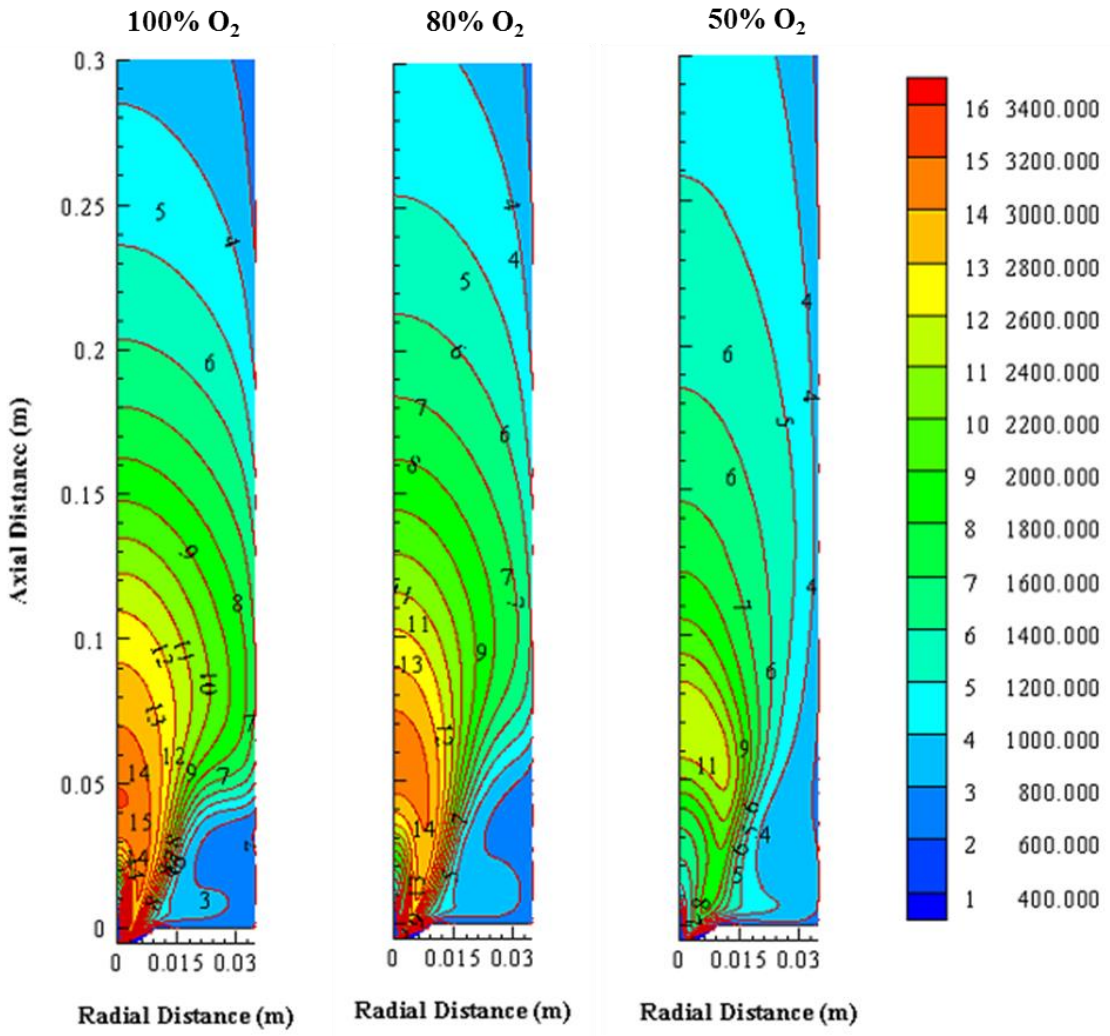

Figure 32: Temperature contours at different percentages of O_2, 0.65 equivalence ratio and fuel composition of 80%CH_4/20%H_2.

Therefore, stability is being affected by high Reynolds number which is experienced as the CO_2 percentage in the oxidizer is increased. Figure 33 shows the experimental and numerical temperature distribution along the axial and radial (at exit plane) direction (i.e. a & b respectively) while Figure 34 shows the computed axial and wall

temperatures of the combustor at 0.65 equivalence ratio and 80%CH_4/20%H_2 fuel composition. As it could be observed from Figure 33, there exist a good agreement between experimental and numerical results of temperature distributions except at the region close to the combustor wall. This deviation between experimental and numerical temperature distributions is attributed to the mixing of excess oxidizer with flue gasses and heat transfer through the wall by convection and radiation which emanated from outer recirculation zone. Figure 33-b shows that the maximum temperature occurred at the axis of the combustor while Figure 34 shows the exact location along the axis at which the overall maximum temperature occurs in the combustor. This location is attributed to the reaction rate and species consumption and formation as it will be explained later. Considering the wall temperature profile, it could be seen that there exists large recirculation of fresh (excess) oxidizer at the outer recirculation zone which causes a drop in wall temperature at this zone.

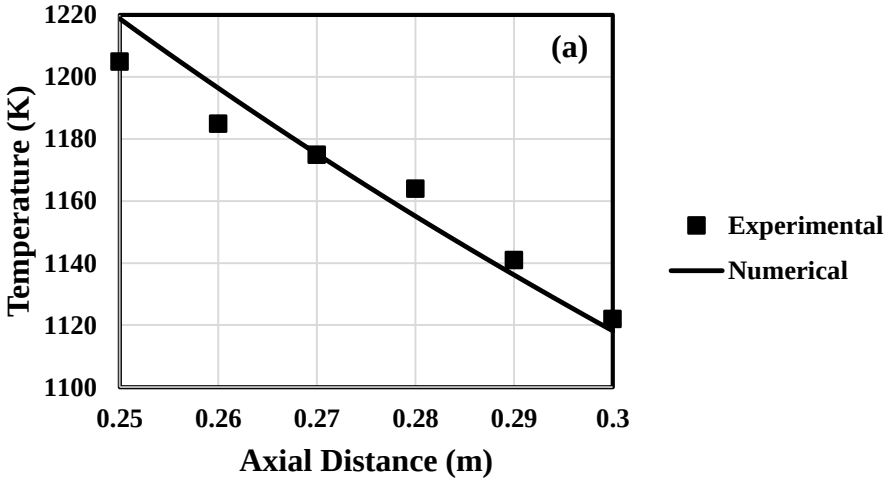

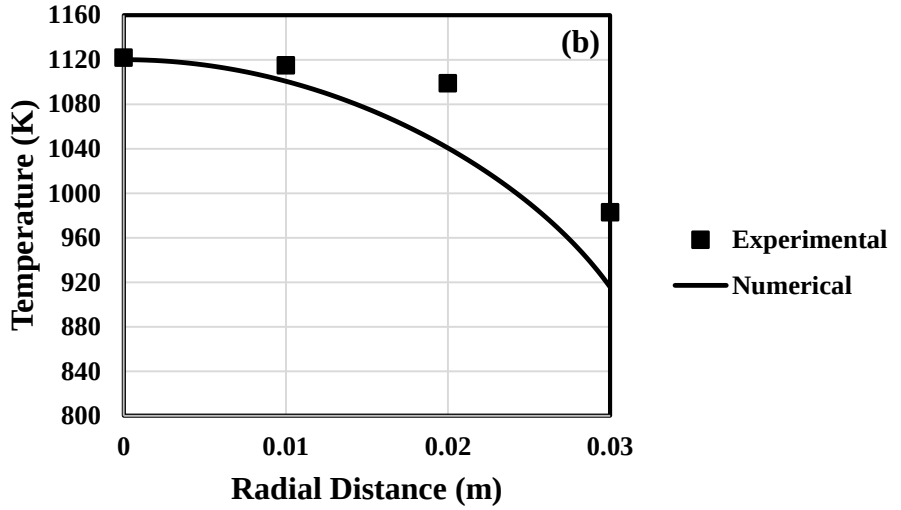

Figure 33: Experimental and numerical temperature distribution at 0.65 equivalence ratio, 80%CH_4/20%H_2 fuel composition and 50%O_2/50%CO_2 oxidizer mixture along axial (a) and radial (at the exit plane) (b) direction.

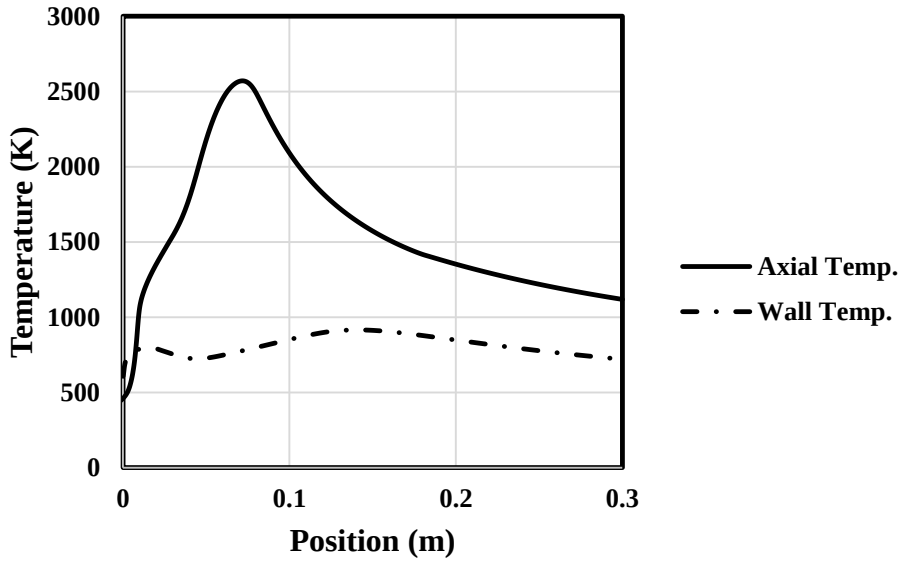

Figure 34: Temperature Distribution along the axis and side wall of the combustor at 0.65 equivalence ratio, 80%CH_4/20%H_2 fuel composition and 50%O_2/50%CO_2 oxidizer mixture.

5.2 Velocity Field

The developed numerical method is used in predicting and analyzing the flow field. Figure 35 shows the contour plots of radial and swirl velocity field while Figure 36 explains the velocity distributions along the axis of the combustor at an equivalence ratio of 0.65, 80%CH_4/20%H_2 fuel composition and 50%O_2/50%CO_2 oxidizer mixture. It could be observed from Figure 35 that there exist inner and outer recirculation zones downstream of the burner. These zones were characterized by negative radial velocity values. The inner recirculation appeared around the combustor axis and span between 0 to 0.02 m along the axis while the outer recirculation appeared around the reactor wall and span between 0.015 to 0.035 m length of the reactor. Recirculation is due to the sudden expansion of the swirling oxidizer mixture as it exits the bluff body into the reactor which leads to the rigorous backward pressure gradient and subsequently, the creation of the recirculation zones. Mixing of hot flue gasses with a cold fresh oxidizer is enhanced at the recirculation zones due to the existence of large turbulence intensities as a result of large fluctuations in velocity. The resulting effect of recirculation on temperature and stability have been explained in section 5.1.

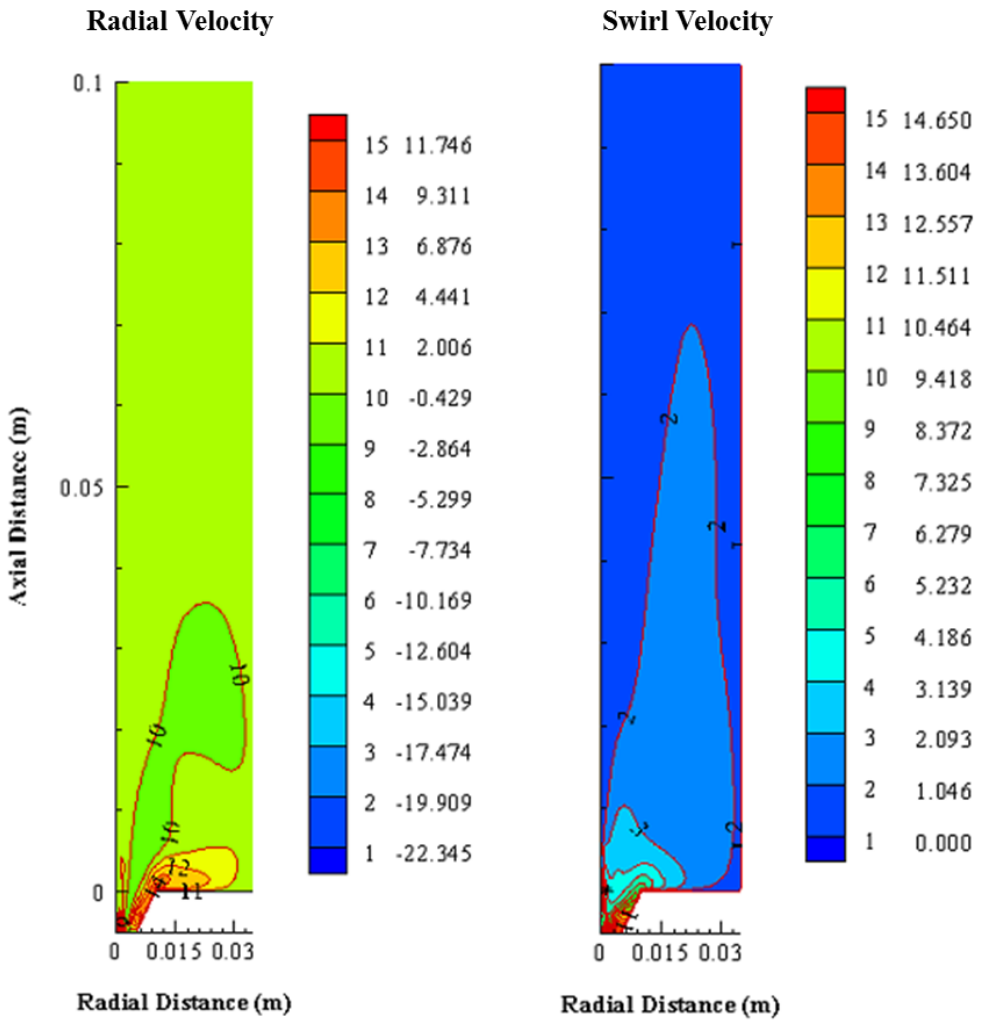

Figure 35: Contour plots showing velocity fields at 0.65 equivalence ratio, 80%CH_4/20%H_2 fuel composition, and 50%O_2/50%CO_2 oxidizer mixture.

The axial velocity is as a result of fuel supplied which degraded as the fuel is been consumed through chemical reaction process and finally approach zero at around 0.06 m along the combustor axis, the contour plots showing the kinetic rate of reaction (i.e. Figure 39) of fuels also testified to this scenario.

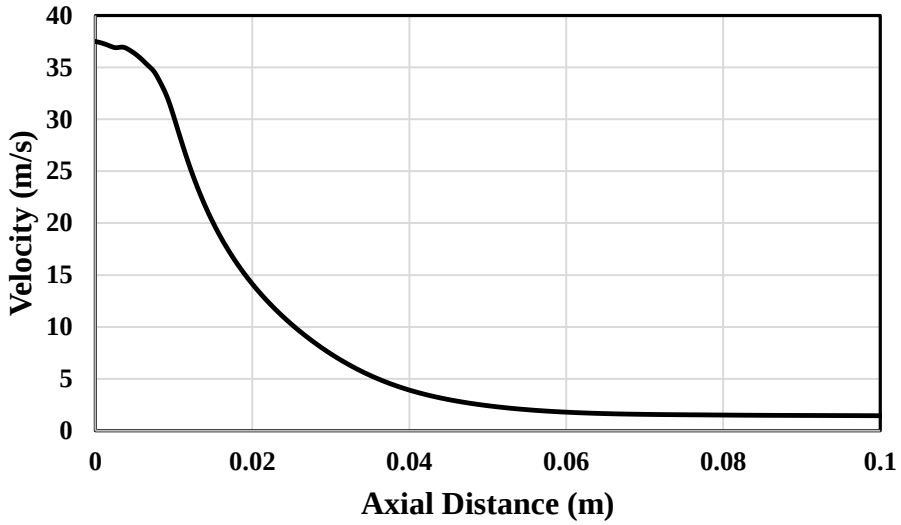

Figure 36: Velocity distribution along the axis of the combustor at 0.65 equivalence ratio, 80%CH_4/20%H_2 fuel composition and 50%O_2/50%CO_2 oxidizer mixture.

5.3 Species Mass Fraction

Figure 37 shows the contour plots of species mass fractions and Figure 38 shows the distributions of the species mass fractions and static temperature along the combustor axis at an equivalence ratio of 0.65, 80%CH_4/20%H_2 fuel composition and 50%O_2/50%CO_2 oxidizer mixture. Figure 37 indicates that the mass fraction of CO is high at the reaction zone and decreases in both axial and radial direction of the combustor. The high value of CO exhibited at the reaction zone is due to the fact that CO is an intermediary product when CH_4 react with O_2, while it disappearance down the reactor length and radius as a result of it further reaction with O_2 present in the oxidizer that escaped the reaction zone through outer recirculation zone due to sudden expansion and finally resulted in CO_2 production. The small fraction of CO at the exit plane is due to dissociation of CO_2 since there are enough O_2 to have a complete combustion process. Similarly, H_2O is having a high value of mass fraction at the reaction zone which confirmed that it is a product of combustion process, but this value

decreases as the process proceeds in both axial and radial direction. The decrease is due to a reduction in intensity of the reaction and increase in the amount of CO_2 in the reactor as a result of incoming fresh oxidizer. From Figure 38 it could be observed that H_2O formation increases as the reaction proceed and reached its maximum value around 0.06 m length of the reactor. At this point, the static temperature attains it peak value while the reaction driver (i.e. CH_4) approaches zero.

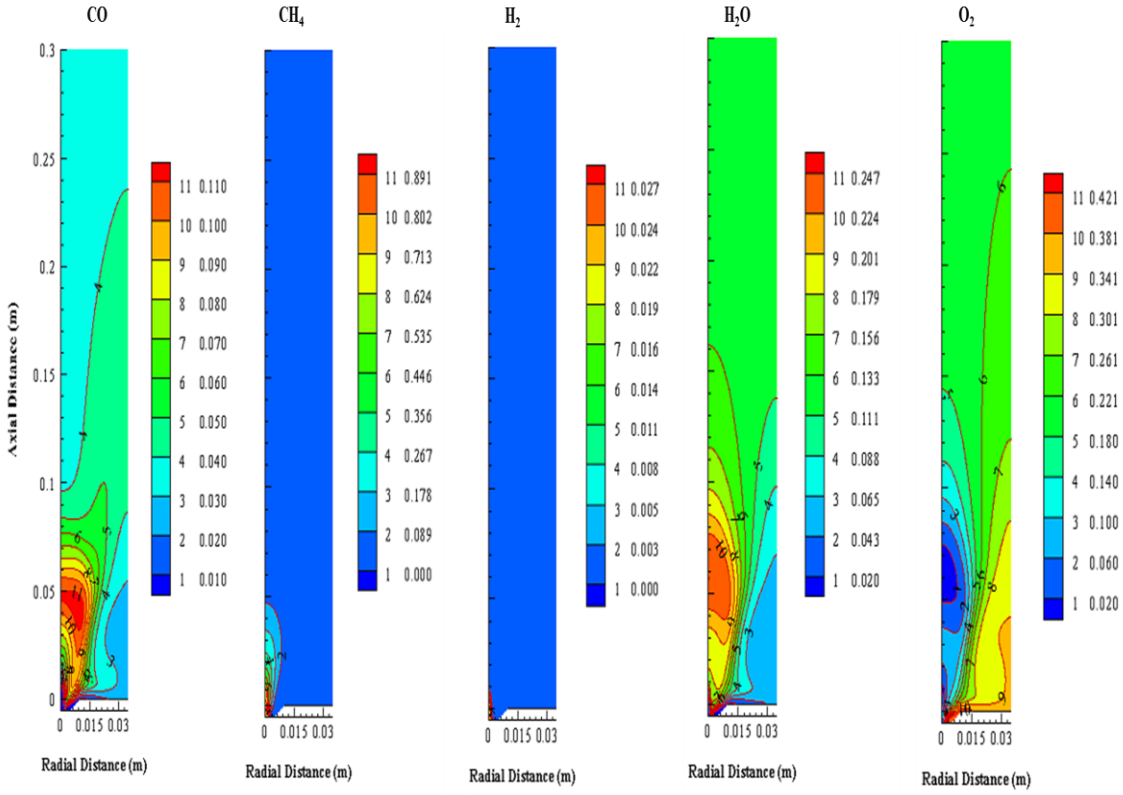

Figure 37: Contour plots showing species mass fraction at 0.65 equivalence ratio, 80%CH_4/20%H_2 fuel composition and 50%O_2/50%CO_2 oxidizer mixture.

Unlike CO and H_2O, O_2 attains its least value of the mass fraction at the burning zones while it attains its highest values around the inner and outer recirculation zones. The attainment of least value is due to the fact that O_2 is among the major requirements to initiate and sustain the combustion process, and is being consumed during the reaction process to generate the products. The attainment of highest value is as a result of the escape of a large amount of the supplied oxidizer during sudden expansion through outer recirculation zone. The reasons behind this have been explained in the sections

5.1 and 5.2. There was a further dilution of the fresh oxidizer with the burned gasses which enables the reaction of O_2 and CO as explained previously and also, reduces the static temperature. As expected, the mass fractions of CH_4 and H_2 were only high at the nozzle outlet and decrease downstream of the burner.

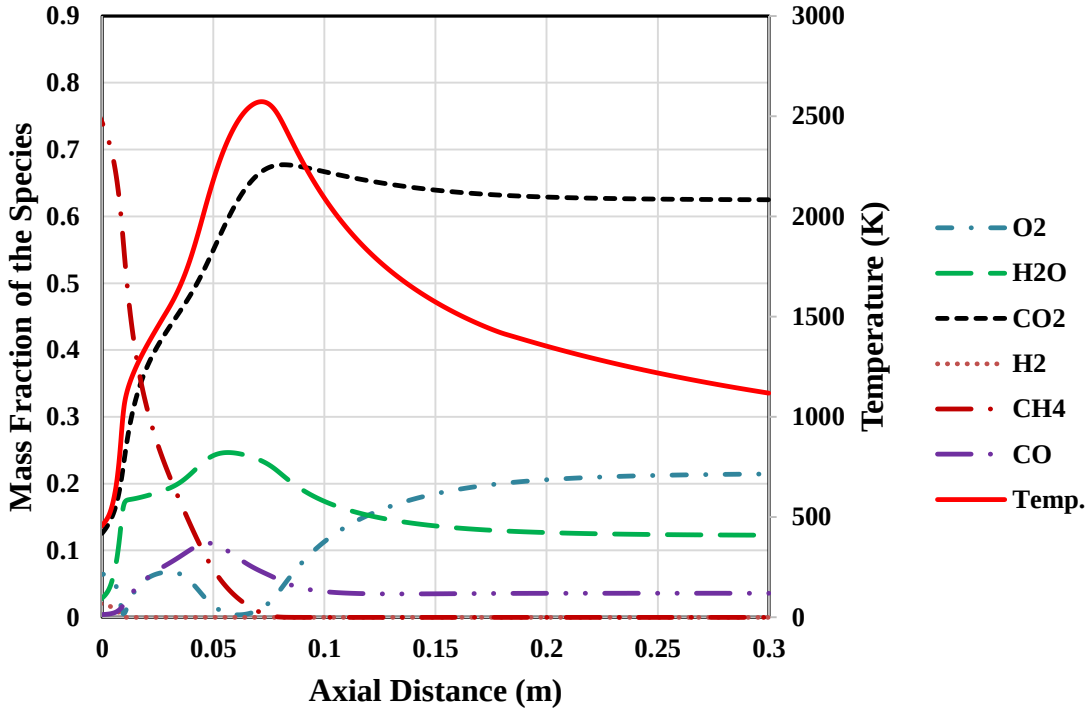

Figure 38: Species mass fraction and temperature distribution along the axis of the combustor at 0.65 equivalence ratio, 80%CH_4/20%H_2 fuel composition and 50%O_2/50%CO_2 oxidizer mixture.

Due to high flame speed and high reactivity nature of the H_2, it (i.e. H_2) only appeared between 0-0.01 m along the axis of the combustor and the effect could be seen in static temperature profile with a rapid increase in temperature around this range. Since the flame speed of CH_4 is low as compared to that of H_2, it took a while for the CH_4 to be completely consumed. The CH_4 mass fraction exists only between the axis and inner recirculation zone and from the inlet to 0.06 m along the axis of the combustor. The mass fraction is zero elsewhere indicating that there were no cases of unburned hydrocarbon.

5.4 Kinetic Rate of Reaction

Figure 39 shows the contour plots of kinetic rate of reaction (KRR) and Figure 40 shows the KRR along the combustor axis for two CH_4 reactions and H_2 reaction at 0.65 equivalence ratio, 80%CH_4/20%H_2 fuel composition, and 50%O_2/50%CO_2 oxidizer mixture. KRR_1 and KRR_2 represent the intermediate and complete reaction of CH_4 respectively while KRR_4 represents the reaction of H_2. It could be observed from Figure 40 that the peak value of KRR_1 corresponds to the peak value of CO presented in Figure 38, while the peak value of KRR_2 corresponds to the peak value of CO_2 presented in Figure 38. These show that the two reactions were actually responsible for the formation of the intermediate and final product. Furthermore, the contour plots show that the CH_4 reactions take place only between the axis of the combustor and inner recirculation zone. For the case of H_2, the reaction is so fast with a high rate of reaction as shown in the secondary axis of Figure 40, which is due to high reactivity nature of H_2. Also, the peak value of KRR_4 corresponds to the peak value of H_2 mass fraction presented in Figure 38.

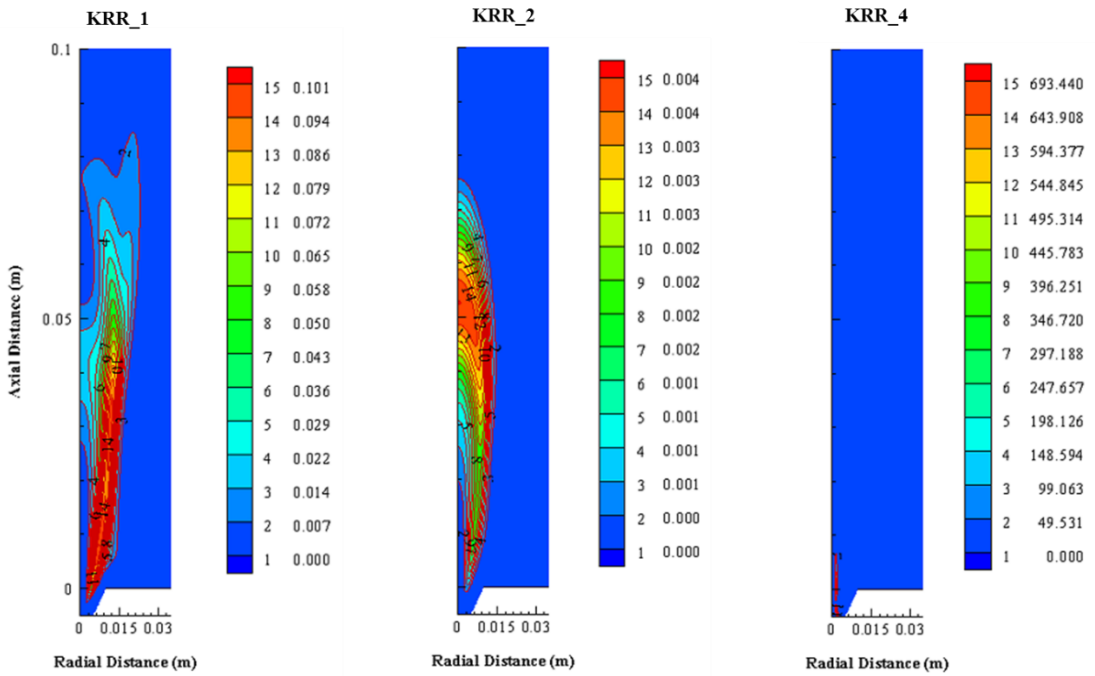

Figure 39: Contour plots showing kinetics rate of reaction (KRR) of CH_4 (1&2) and H_2 (4) reactions at 0.65 equivalence ratio, 80%CH_4/20%H_2 fuel composition, and 50%O_2/50%CO_2 oxidizer mixture.

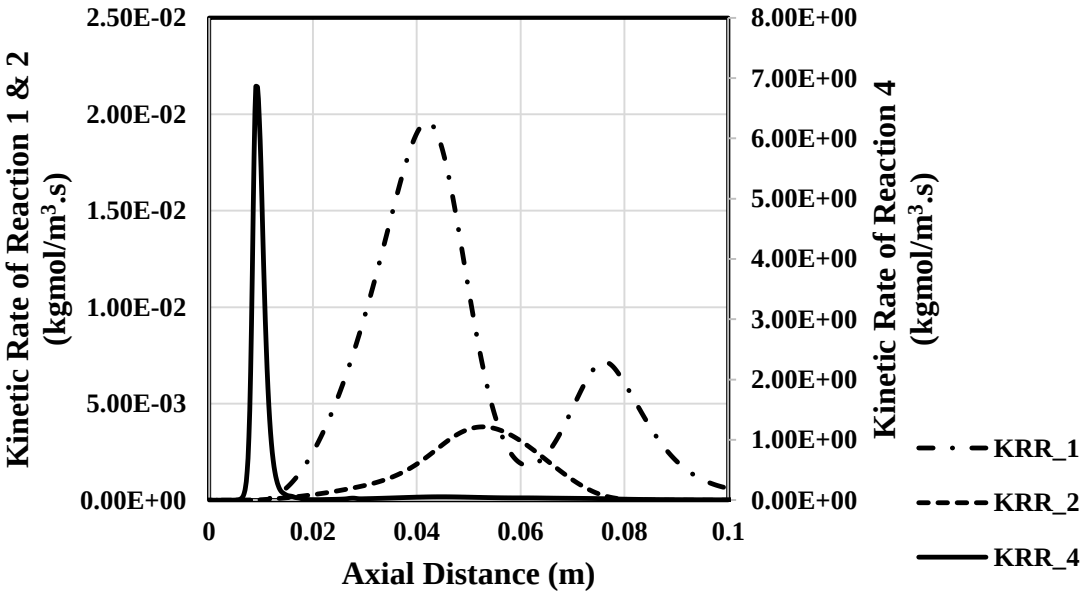

Figure 40: Kinetics rate of reaction (KRR) of CH_4 (1&2) and H_2 (4) reactions along the axis of the combustor at 0.65 equivalence ratio, 80%CH_4/20%H_2 fuel composition, and 50%O_2/50%CO_2 oxidizer mixture.

5.5 Effect of Equivalence Ratio on Stability, Temperature, and Velocity Fields

The effect of equivalence ratio on the stability of the flame, temperature and velocity fields were conducted at conditions that were stable (50%CH_4/50%H_2) so as to derive the appropriate equivalence ratio suitable for oxy-combustion of H_2-enriched-CH_4.

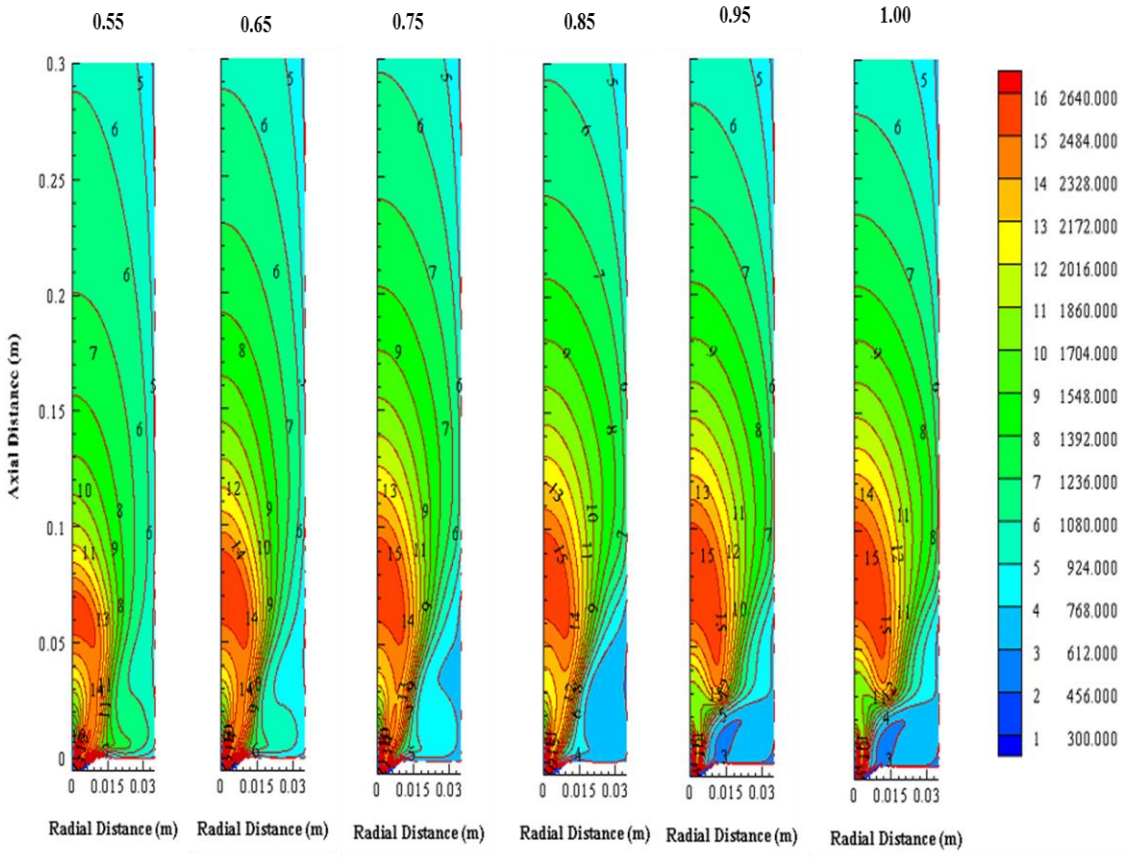

Figure 41: Contour plots showing the effect of equivalence ratio on flame stability and temperature distribution at 50%CH_4/50%H_2 fuel composition and 50%O_2/50%CO_2 oxidizer mixture.

Figure 41Figure 42 and Figure 43 show the temperature fields, axial temperature distribution and velocity fields for different equivalence ratios at 50%CH_4/50%H_2 fuel composition and 50%O_2/50%CO_2 oxidizer mixture. Figure 41 indicates that an increase

in equivalence ratio increases the flame length, because as the equivalence ratio is increased the amount of O_2 available for combustion process decreases and therefore, the flame extends its length to source for more O_2 to complete the combustion process. Further increase in equivalence ratio causes the flame (near and even at stoichiometric) to becomes completely unstable and lift-off the burner. This shows that oxy-combustion cannot be achieved at stoichiometric condition due to stability issues and, the understanding that oxy-combustion is achievable near stoichiometric condition is not true because it could be observed from Figure 41 that flame instability is observed at 0.95 equivalence ratio (i.e. near stoichiometric).

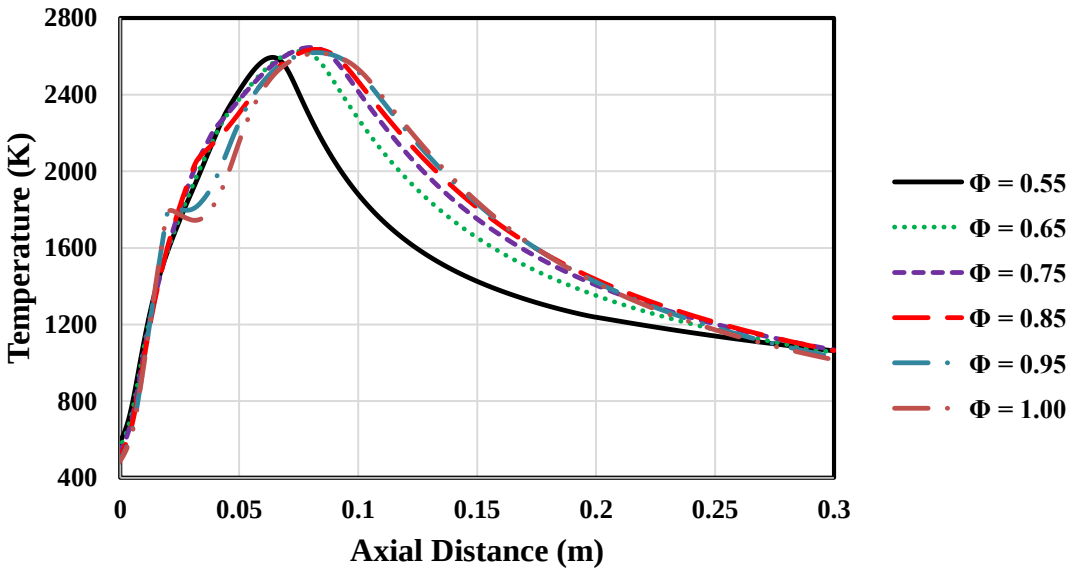

Figure 42: Temperature distributions along the axis of the combustor at 50%CH_4/50%H_2 fuel composition and 50%O_2/50%CO_2 oxidizer mixture.

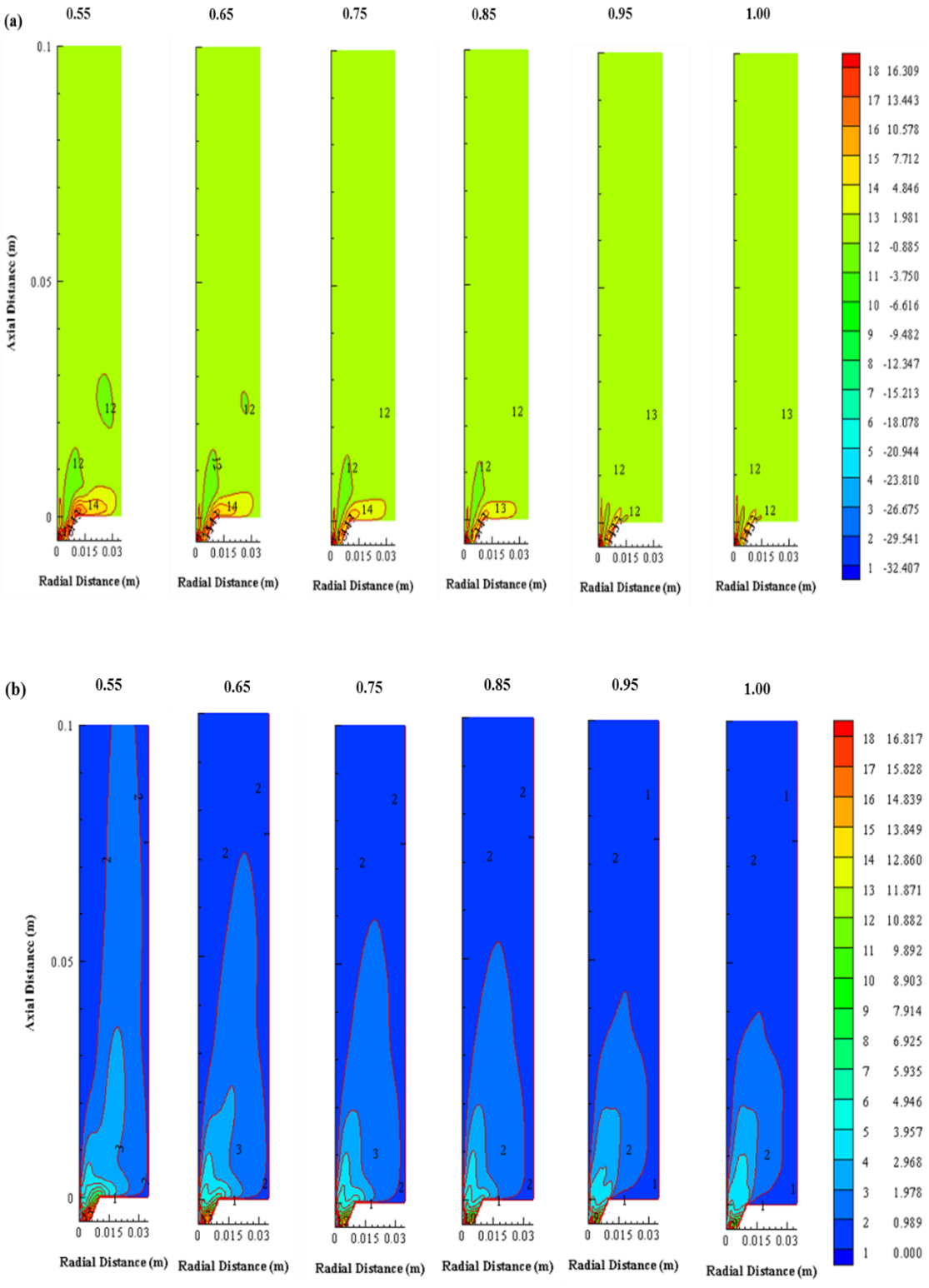

Figure 43: Contour plots showing radial (a) and swirl (b) velocity field at different equivalence ratios, 50%CH_4/50%H_2 fuel composition and 50%O_2/50%CO_2 oxidizer mixture.

Also, it is observed that the temperature increases with equivalence ratio in the region of stability (i.e. from 0.55 to 0.85 equivalence ratio) while it decreases with equivalence ratio when the flame becomes unstable. This is because at higher equivalence ratios there exists low O_2 concentration and due to the higher specific heat capacity of CO_2 the radiation heat loss becomes higher thereby, reducing the combustion temperature. Figure 43 shows that equivalence ratio affects the radial and swirl velocity field thereby, affecting the flame stability. As the equivalence ratio increases, both inner and outer recirculation zones decrease, and at a point in time outer recirculation zone completely disappears while inner recirculation zone drastically reduces near and at the stoichiometric condition. These indicate that inner recirculation zone is primarily responsible for flame stability.

5.6 Effect of Swirl Vane Angle on Temperature and Velocity Fields

Figure 44,Figure 45 and Figure 46 show the effect of swirl vane angle on temperature field, axial temperature distribution and velocity field respectively at 0.65 equivalence ratio, 50%CH_4/50%H_2 fuel composition, and 50%O_2/50%CO_2 oxidizer mixture. As the Swirl vane angle increases from 55^o to 75^o the flame temperature decreases. The increase in swirl vane angle actually enhances the rate of mixing of fresh cold oxidizer with burned gasses and as a result, the temperature of the combustion process is lowered. The optimum value could actually lie in the range of 55^o to 65^o or even 70^o as discussed by Linck et al [5] but not 75^o because as the swirl angle increases the interaction between the flow field and thermal field become stronger which eventually increase the thermo-acoustic level of the combustor beyond the acceptable limit. This can also be seen from the shape of the flame. Figure 46 indicates that the flame is stable at all the cases due to the presence of inner recirculation zone while Figure 47 shows

that the mixing rate is higher for 65° swirl vane angle since it exhibited a lower amount of CO at the exit plane.

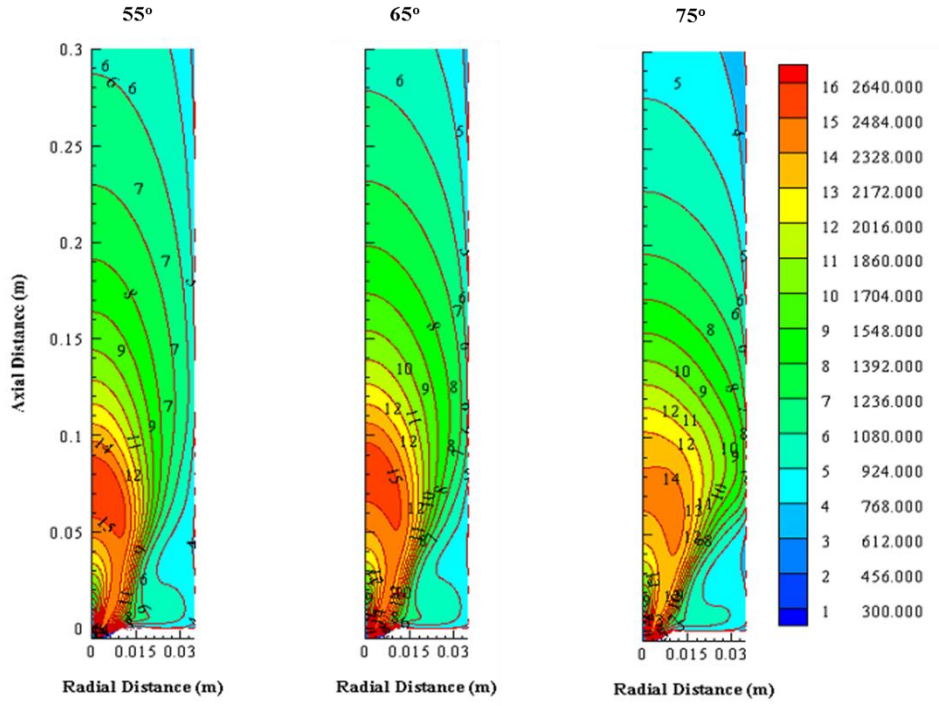

Figure 44: Contour plots showing the effect of swirl angle on flame stability and temperature distribution at 0.65 equivalence ratio, 50%CH_4/50%H_2 fuel composition, and 50%O_2/50%CO_2 oxidizer mixture.

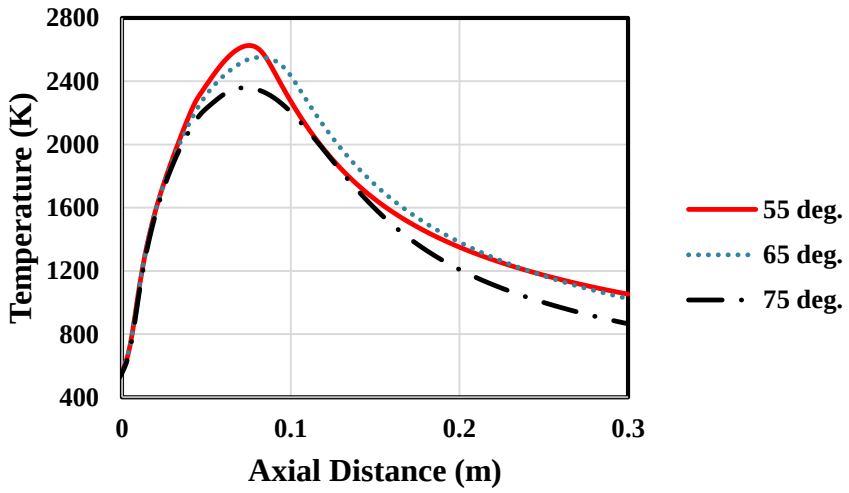

Figure 45: Temperature distributions along the axis of the combustor for different swirl vane angle at 0.65 equivalence ratio, 50%CH_4/50%H_2 fuel composition, and 50%O_2/50%CO_2 oxidizer mixture.

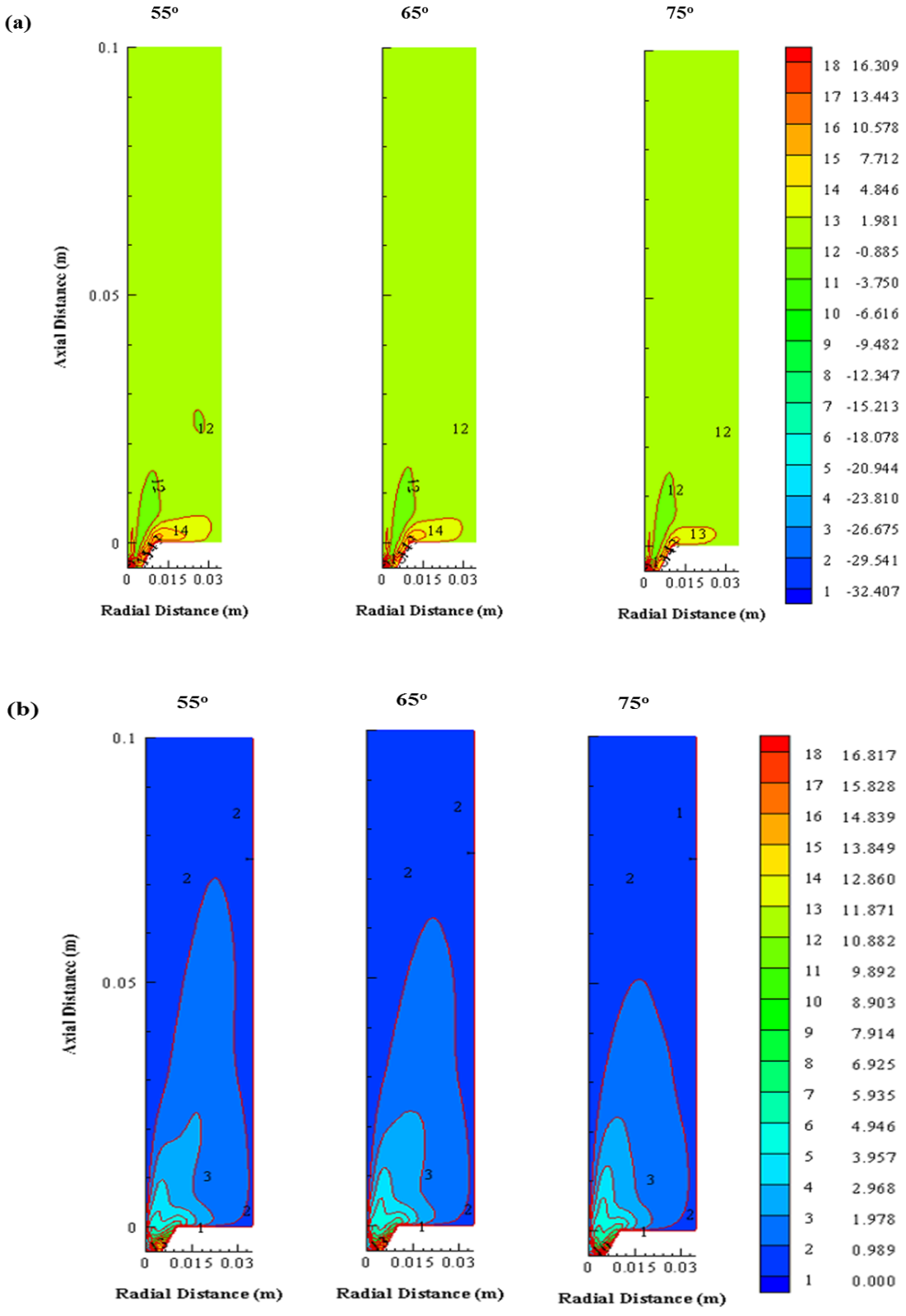

Figure 46: Contour plot showing radial (a) and swirl (b) velocity field for different swirl vane angle at 0.65 equivalence ratio, 50%CH_4/50%H_2 fuel composition, and 50%O_2/50%CO_2 oxidizer mixture.

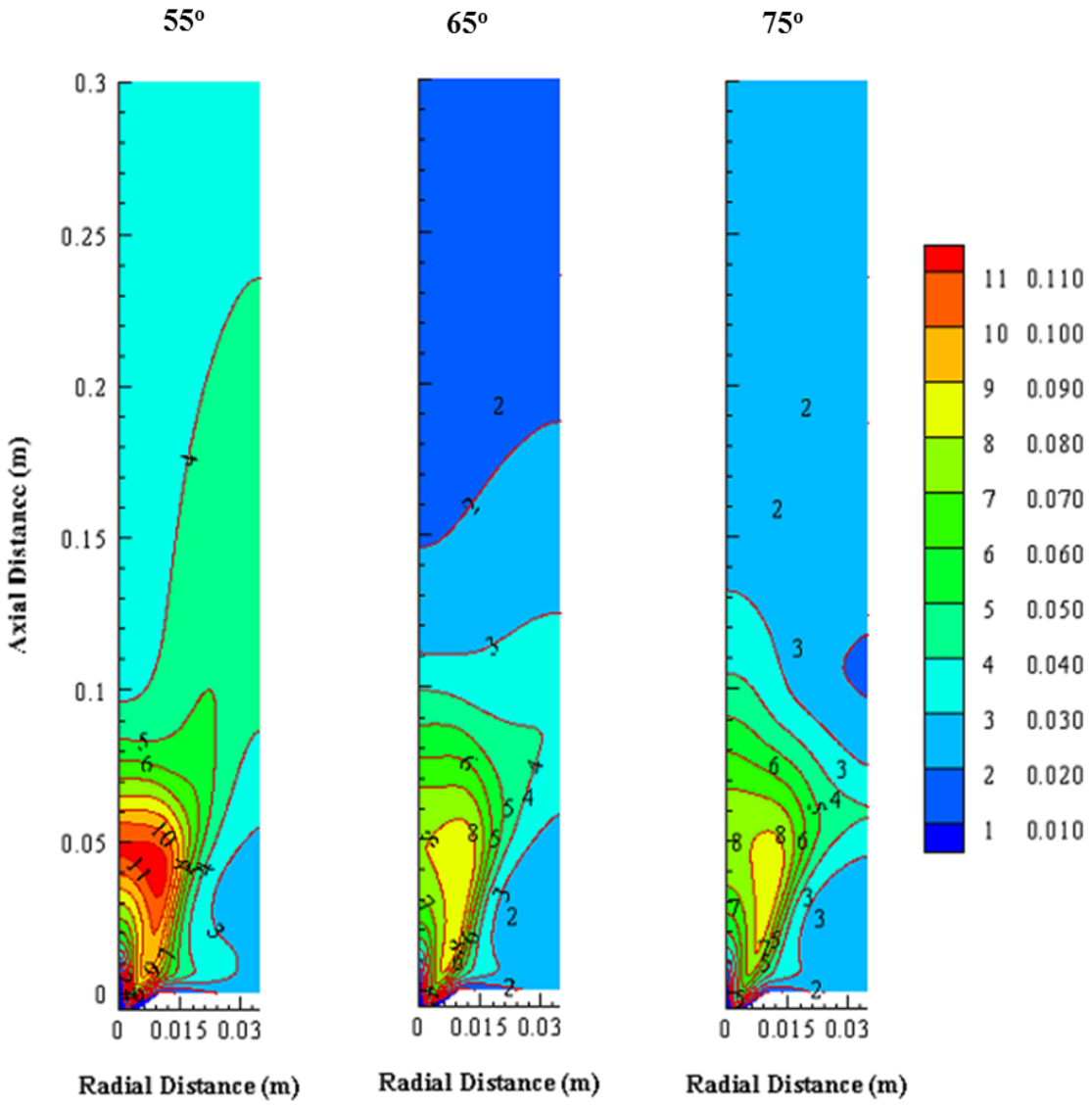

Figure 47: Contour plot showing CO mass fraction for different swirl vane angle at 0.65 equivalence ratio, 50%CH_4/50%H_2 fuel composition, and 50%O_2/50%CO_2 oxidizer mixture.

CHAPTER 6

CONCLUSIONS AND RECOMMENDATION

6.1 Conclusions

The present study covers experimental and numerical investigations of syngas oxy-combustion in gas turbine model combustor. The combustion characteristics of turbulent diffusion H_2-enriched-CH_4 oxy-combustion flames were investigated. The effect of swirl is studied over ranges of operating parameters including equivalence ratio, oxidizer mixture composition, and hydrogen enrichment level considering three swirlers with three swirl vane angles including 30º, 45º and 55º. The numerical study is achieved using Gambit for model/geometry development and ANSYS Fluent for computations. The models adopted for computations include; k-ε (standard), discrete ordinate (DO), and eddy-dissipation-concept (EDC) for turbulence, radiation, and species transport modeling respectively. The combustion chemistry is handled through the combination of appropriate oxy-fuel combustion reaction mechanism for CH_4 and H_2 reaction mechanism and imported into the ANSYS Fluent through CHEMKIN mechanism import. All the conservations, transports, and radiative transfer equations were accurately discretized and solutions were considered converged when the residuals were less than 10^{-3} for momentum equations and 10^{-6} for others. From the study, the following can be concluded:

- The flame blowout at very low oxygen concentrations in the oxidizer mixture, 20%O_2 or even less, at 50%H_2 enrichment level which indicates wide stable

flame operation range while utilizing H_2 for fuel (CH_4) enrichment in gas turbine combustor,

- From the experiment, swirler with 30^o swirl vane angle displays lowest level of stability with longest flame length and highest temperature under all operating conditions which indicates that utilization of such swirler is not good for gas turbine application,
- From the experiment as well, swirler with 55^o swirl vane angle exhibits the highest level of stability with moderate flame length and temperature levels which show that such swirler will enhance the performance of gas turbine combustor,
- There is a good agreement between experimental and numerical results,
- Numerical study shows that the optimum value of equivalence ratio for oxy-combustion of H_2-enriched-CH_4 in gas turbine combustor application lies around 0.85 because flame is completely unstable from equivalence ratio of 0.95 (i.e. near stoichiometric condition) therefore, it is not correct to say oxy-fuel combustion is achievable near stoichiometric condition,
- Stability is highly enhanced by formation of inner recirculation zone,
- Finally, the numerical study also shows that better performance of gas turbine combustor can be achieved by increasing the swirl vane angle up to 65^o or 70^o but not beyond these values because the flame achieved at 75^o appears not practicable.

6.2 Recommendation

The present study is conducted under atmospheric condition; it would be recommended that further study should be conducted at an elevated pressure and temperature

equivalent to what is attainable in a gas turbine. Since numerical results indicate that small fraction of CO exists at the exit plane of the model combustor, the analysis of species distribution within the reactor using laser system would be recommended for further study. Other turbulence models such as RSM and LES should be considered for numerical modeling. Finally, it would be recommended for a subsequent study to include thermodynamics (or exergy) analysis so as to obtain exact equivalence ratio that will be economic and safe for gas turbine application.

Nomenclature

d_h	:	Hub diameter (m)
$D_{i,m}$	:	Mass diffusion (m^2/s)
$D_{T,i}$	:	Thermal diffusion
d_o	:	Outside diameter (m)
G_k	:	Turbulence kinetic energy generation ($J/m^3.s$)
h_s	:	Sensible enthalpy (J/kg)
J_i	:	Species i diffusion flux ($mol/m^2.s$)
k_i	:	Coefficient of absorption
L	:	Gas layer thickness (m)
m_i	:	Species mass fraction
p	:	Fluid pressure (N/m^2)
P	:	Partial pressure (N/m^2)
Pr_{SGS}	:	Subgrid Prandtl number
$\vec{r}$	:	Position vector
$\vec{s}$	:	Direction vector
$\vec{s}'$	:	Scattering direction vector
S	:	Swirl number
S_ϕ	:	Source term
T	:	Temperature (K)
u_j	:	Constituent of velocity along the x_j direction (m/s)
ρ	:	fluid density (kg/m^3)
θ	:	Swirl vane angle (^{o})
ϕ_r	:	Averaged values of the Reynolds's reliant variable
φ_r	:	Fluctuating values of the Reynolds's reliant variable
Φ	:	Equivalence ratio

ϕ : Phase function

Γ_{φ} : Coefficient of diffusion

σ_{ij} : Stress tensor (N/m^2)

τ_{ij} : Subgrid-scale stress (N/m^2)

λ : Thermal conductivity (W/(m. K))

μ : Dynamics viscosity ($N.s/m^2$)

μ_{SGS} : Subgrid viscosity ($N.s/m^2$)

μ_t : Turbulence viscosity ($N.s/m^2$)

$a_{\varepsilon,i}$: Weighting factors of the emissivity for the grey gas i

R_e : Reynolds number of the oxidizer : $4\dot{m}/\pi(D_o - D_f)\mu_o$

$\dot{m}$ and μ_o respectively : Mass flow rate and dynamic viscosity of the oxidizer

D_o and D_f : Oxidizer and fuel tube diameter respectively

References

[1] D. Aaron and C. Tsouris, “Separation of CO2 from Flue Gas: A Review,” *Sep. Sci. Technol.*, vol. 40, no. 1, pp. 321–348, 2005.

[2] C. M. White, B. R. Strazisar, E. J. Granite, J. S. Hoffman, and H. W. Pennline, “Separation and Capture of CO2 from Large Stationary Sources and Sequestration in Geological Formations,” *EM Air Waste Manag. Assoc. Mag. Environ. Manag.*, vol. 2247, no. JUNE, pp. 29–34, 2003.

[3] E. B. Conference, “CFD SIMULATION OF A BURNER FOR SYNGAS CHARACTERIZATION: PRELIMINARY RESULTS AND EXPERIMENTAL VALIDATION,” *18th Eur. Biomass Conf. Exhib.*, vol. 3000, no. May, pp. 3–7, 2010.

[4] D. Singh, T. Nishiie, S. Tanvir, and L. Qiao, “An experimental and kinetic study of syngas/air combustion at elevated temperatures and the effect of water addition,” *Fuel*, vol. 94, pp. 448–456, 2012.

[5] E. Salzano, A. Basco, F. Cammarota, V. Di Sarli, and A. Di Benedetto, “Explosions of Syngas/CO2 Mixtures in Oxygen-Enriched Air Ernesto,” in *XXXV Meeting of the Italian Section of the Combustion Institute*, 2012, pp. 1–6.

[6] V. Silva, E. Monteiro, N. Couto, P. Brito, and A. Rouboa, “Analysis of Syngas Quality from Portuguese Biomasses: An Experimental and Numerical Study,” *Energy & Fuels*, vol. 28, no. 9, pp. 5766–5777, 2014.

[7] Y. Zhang, T. Yang, X. Liu, L. Tian, Z. Fu, and K. Zhang, “Reduction of emissions from a syngas flame using micromixing and dilution with CO2,” *Energy and Fuels*, vol. 26, no. 11, pp. 6595–6601, 2012.

[8] R. Siriwardane, J. Poston, K. Chaudhari, A. Zinn, T. Simonyi, and C. Robinson, “Chemical-Looping Combustion of Simulated Synthesis Gas Using Nickel Oxide Oxygen Carrier Supported on Bentonite.,” *Energy & Fuels*, vol. 21, no. 3, pp. 1582–1591, 2007.

[9] M. A. Habib, M. A. Nemitallah, P. Ahmed, M. H. Sharqawy, H. M. Badr, I. Muhammad, and M. Yaqub, “Experimental analysis of oxygen-methane combustion inside a gas turbine reactor under various operating conditions,” *Energy*, vol. 86, pp. 105–114, 2015.

[10] J. Gibbins and H. Chalmers, “Carbon capture and storage,” *Energy Policy*, vol. 36, no. 12, pp. 4317–4322, 2008.

[11] J. D. Figueroa, T. Fout, S. Plasynski, H. McIlvried, and R. D. Srivastava, “Advances in CO2 capture technology-The U.S. Department of Energy’s Carbon Sequestration Program,” *Int. J. Greenh. Gas Control*, vol. 2, no. 1, pp. 9–20, 2008.

[12] T. F. Wall, “Combustion processes for carbon capture,” *Proc. Combust. Inst.*, vol. 31 I, pp. 31–47, 2007.

[13] U. Desideri, L. Arcioni, and M. Tozzi, “Feasibility study for a carbon capture and storage project in northern Italy,” *Int. J. energy Res.*, vol. 32, no. 23 July 2008, pp. 1175–1183, 2008.

[14] K. Jordal, M. Anheden, J. Yan, and L. Strömberg, “Oxy-fuel combustion for coal-fired power generation with CO2 capture-Opportunities and challenges,” *Greenh. Gas Control Technol.*, no. February 2016, pp. 201–209, 2005.

[15] M. B. Toftegaard, J. Brix, P. A. Jensen, P. Glarborg, and A. D. Jensen, “Oxy-fuel combustion of solid fuels,” *Prog. Energy Combust. Sci.*, vol. 36, no. 5, pp. 581–625, 2010.

[16] C. Y. Liu, G. Chen, N. Sipöcz, M. Assadi, and X. S. Bai, “Characteristics of oxy-fuel combustion in gas turbines,” *Appl. Energy*, vol. 89, no. 1, pp. 387–394, 2012.

[17] M. Ditaranto and J. Hals, “Combustion instabilities in sudden expansion oxy-fuel flames,” *Combust. Flame*, vol. 146, no. 3, pp. 493–512, 2006.

[18] M. A. Habib, H. M. Badr, S. F. Ahmed, R. Ben-Mansour, K. Mezghani, S. Imashuku, G. J. Ia O’, Y. Shao-Horn, N. D. Mancini, A. Mitsos, P. Kirchen, and A. F. Ghoniem, “A review of recent developments in carbon capture utilizing oxy-fuel combustion in conventional and ion transport membrane systems,” *Int. J. energy Res.*, vol. 31, no. August 2007, pp. 135–147, 2007.

[19] A. P. Simpson and A. J. Simon, “Second law comparison of oxy-fuel combustion and post-combustion carbon dioxide separation,” *Energy Convers. Manag.*, vol. 48, no. 11, pp. 3034–3045, 2007.

[20] T. García-Armingol and J. Ballester, “Operational issues in premixed combustion of hydrogen-enriched and syngas fuels,” *Int. J. Hydrogen Energy*, vol. 40, no. 2, pp. 1229–1243, 2015.

[21] S. Daniele, P. Jansohn, and K. Boulouchos, “Experimental Investigation of Lean Premixed Syngas Combustion at Gas Turbine Relevant Conditions : Lean Blow Out Limits , Emissions and Turbulent Flame Speed,” in *Italian Section of the combustion institute: Combustion Colloquai*, 2009, pp. II–4, 1–11.

[22] D. E. Giles, S. Som, and S. K. Aggarwal, “NOx emission characteristics of counterflow syngas diffusion flames with airstream dilution,” *Fuel*, vol. 85, no. 12–13, pp. 1729–1742, 2006.

[23] V. Di Sarli, A. Basco, F. Cammarota, a Di Benedetto, E. Salzano, V. Diocleziano, I. Chimica, and N. Federico, “Flammability of Syngas / Co 2 Mixtures in Oxygen-Enriched Air,” in *XXXV Meeting of the Italian Section of the Combustion Institute*, 2012, pp. 1–6.

[24] S. R. Shabanian, M. Derudi, M. Rahimi, A. Frassoldati, A. Cuoci, and T. Faravelli, “Experimental and numerical analysis of syngas MILD combustion,” in *XXXIV Meeting of the Italian Section of the Combustion Institute*, pp. 1–7.

[25] P. Kutne, R. Sadanandan, and W. Meier, “Experimental Analysis of the Combustion Behaviour of Syngas Mixtures in a Gas Turbine Model Combustor

Under Elevated Pressure," in *Proceedings of the European Combustion Meeting 2009*, 2009.

[26] Q. Fan, S. Hui, Q. Zhou, Q. Zhao, and T. Xu, "Experimental investigations on combustion characteristics of syngas composed of CH4, CO, and H2," *Front. Chem. Eng. China*, vol. 4, no. 4, pp. 404–410, 2010.

[27] M. Zhang, J. Wang, J. Wu, Z. Wei, Z. Huang, and H. Kobayashi, "Flame front structure of turbulent premixed flames of syngas oxy-fuel mixtures," *Int. J. Hydrogen Energy*, vol. 39, no. 10, pp. 5176–5185, 2014.

[28] B. K. Dam, N. D. Love, and A. R. Choudhuri, "Flame stability of methane and syngas oxy-fuel steam flames," *Energy and Fuels*, vol. 27, no. 1, pp. 523–529, 2013.

[29] V. Ratna Kishore, M. R. Ravi, and A. Ray, "Effect of Hydrogen Content and Dilution on Laminar Burning Velocity and Stability Characteristics of Producer Gas-Air Mixtures," *Int. J. React. Syst.*, vol. 2008, pp. 1–8, 2008.

[30] S. G. Davis, A. V. Joshi, H. Wang, and F. Egolfopoulos, "An optimized kinetic model of H2/CO combustion," *Proc. Combust. Inst.*, vol. 30, no. 1, pp. 1283–1291, 2005.

[31] M. C. Lee, S. Bin Seo, J. Yoon, M. Kim, and Y. Yoon, "Experimental study on the effect of N2, CO2, and steam dilution on the combustion performance of H2 and CO synthetic gas in an industrial gas turbine," *Fuel*, vol. 102, pp. 431–438, 2012.

[32] M. C. Lee, S. Bin Seo, J. H. Chung, S. M. Kim, Y. J. Joo, and D. H. Ahn, "Gas turbine combustion performance test of hydrogen and carbon monoxide synthetic gas," *Fuel*, vol. 89, no. 7, pp. 1485–1491, 2010.

[33] Z. Huang, J. Wang, E. Hu, C. Tang, and Y. Zhang, "Prgress in hydrogen enriched hydrocarbons combustion and engine applications," *Front. Energy*, vol. 8, no. 1, pp. 73–80, 2014.

[34] K. Zeng, Z. Huang, B. Liu, L. Liu, D. Jiang, Y. Ren, and J. Wang, "Combustion characteristics of a direct-injection natural gas engine under various fuel injection timings," *Appl. Therm. Eng.*, vol. 26, no. 8–9, pp. 806–813, 2006.

[35] Z. . Huang, S. . Shiga, T. . Ueda, H. . Nakamura, T. . Ishima, T. . Obokata, M. . Tsue, and M. . Kono, "Correlation of ignitability with injection timing for direct injection combustion fuelled with compressed natural gas and gasoline," *Proc. Inst. Mech. Eng. Part D J. Automob. Eng.*, vol. 217, no. 6, pp. 499–506, 2003.

[36] E. Hu, Z. Huang, B. Liu, J. Zheng, X. Gu, and B. Huang, "Experimental investigation on performance and emissions of a spark-ignition engine fuelled with natural gas–hydrogen blends combined with EGR," *Int. J. Hydrogen Energy*, vol. 34, no. 11–12, pp. 528–539, 2009.

[37] H. Miao, L. Lu, and Z. Huang, "Flammability limits of hydrogen-enriched

natural gas," *Int. J. Hydrogen Energy*, vol. 36, no. 11, pp. 6937–6947, 2011.

[38] E. Hu, Z. Huang, J. He, C. Jin, and J. Zheng, "Experimental and numerical study on laminar burning characteristics of premixed methane-hydrogen-air flames," *Int. J. Hydrogen Energy*, vol. 34, no. 11, pp. 4876–4888, 2009.

[39] J. Wang, Z. Huang, Y. Fang, B. Liu, K. Zeng, H. Miao, and J. Deming, "Combustion behaviors of a direct-injection engine operating on various fractions of natural gas–hydrogen blends," *Int. J. Hydrogen Energy*, vol. 32, no. 15 SPEC. ISS., pp. 3555–3564, 2007.

[40] D. Fritsche, M. Füri, and K. Boulouchos, "An experimental investigation of thermoacoustic instabilities in a premixed swirl-stabilized flame," *Combust. Flame*, vol. 151, no. 1–2, pp. 29–36, 2007.

[41] D. W. Davis, P. L. Therkelsen, D. Littlejohn, and R. K. Cheng, "Effects of hydrogen on the thermo-acoustics coupling mechanisms of low-swirl injector flames in a model gas turbine combustor," *Proc. Combust. Inst.*, vol. 34, no. 2, pp. 3135–3143, 2013.

[42] K. Kashinath, M. P. Juniper, and S. Hemchandra, "Nonlinear Phenomena in Thermoacoustics : a Comparison between Singe-Mode and Multi- Mode Methods," in *19th International Congress on Sound and Vibration, Icsv19*, 2012, pp. 953–960.

[43] A. M. Steinberg, I. Boxx, M. Stöhr, C. D. Carter, and W. Meier, "Flow-flame interactions causing acoustically coupled heat release fluctuations in a thermo-acoustically unstable gas turbine model combustor," *Combust. Flame*, vol. 157, no. 12, pp. 2250–2266, 2010.

[44] C. Tang, J. He, Z. Huang, C. Jin, J. Wang, X. Wang, and H. Miao, "Measurements of laminar burning velocities and Markstein lengths of propane-hydrogen-air mixtures at elevated pressures and temperatures," *Int. J. Hydrogen Energy*, vol. 33, no. 23, pp. 7274–7285, 2008.

[45] M. C. Lee, J. Yoon, S. Joo, J. Kim, J. Hwang, and Y. Yoon, "Investigation into the cause of high multi-mode combustion instability of H2/CO/CH4 syngas in a partially premixed gas turbine model combustor," *Proc. Combust. Inst.*, vol. 35, no. 3, pp. 3263–3271, 2015.

[46] C. Y. Liu, G. Chen, N. Sipöcz, M. Assadi, and X. S. Bai, "Characteristics of oxy-fuel combustion in gas turbines," *Appl. Energy*, vol. 89, no. 1, pp. 387–394, 2012.

[47] P. Heil, D. Toporov, H. Stadler, S. Tschunko, M. Förster, and R. Kneer, "Development of an oxycoal swirl burner operating at low O2 concentrations," *Fuel*, vol. 88, no. 7, pp. 1269–1274, 2009.

[48] P. L. Therkelsen, J. E. Portillo, D. Littlejohn, S. M. Martin, and R. K. Cheng, "Self-induced unstable behaviors of CH4 and H2/CH4 flames in a model combustor with a low-swirl injector," *Combust. Flame*, vol. 160, no. 2, pp. 307–321, 2013.

[49] S. Kadowaki, “The effects of heat loss on the burning velocity of cellular premixed flames generated by hydrodynamic and diffusive-thermal instabilities,” *Combust. Flame*, vol. 143, no. 3, pp. 174–182, 2005.

[50] J. Wang, Z. Huang, H. Kobayashi, and Y. Ogami, “Laminar burning velocities and flame characteristics of CO–H2–CO2–O2 mixtures,” *Int. J. Hydrogen Energy*, vol. 37, no. 24, pp. 19158–19167, 2012.

[51] M. Subramanya and A. Choudhuri, “Investigation of combustion instability effects on the flame characteristics of fuel blends,” *5th Int. Energy Convers. Eng. Conf. June 25, 2007 - June 28, 2007*, vol. 2, no. June, pp. 817–830, 2007.

[52] T. Lieuwen, V. McDonell, D. Santavicca, and T. Sattelmayer, “Burner Development and Operability Issues Associated with Steady Flowing Syngas Fired Combustors,” *Combust. Sci. Technol.*, vol. 180, no. 6, pp. 1169–1192, 2008.

[53] T. Lieuwen, V. McDonell, E. Petersen, and D. Santavicca, “Fuel Flexibility Influences on Premixed Combustor Blowout, Flashback, Autoignition, and Stability,” *J. Eng. Gas Turbines Power*, vol. 130, no. 1, p. 011506, 2008.

[54] D. R. Noble, Q. Zhang, and T. Lieuwen, “Hydrogen Effects Upon Flashback and Blowout,” in *Proceedings of ICEPAG2006*, 2006.

[55] Q. Zhang, D. R. Noble, A. Meyers, K. Xu, and T. Lieuwen, “Characterization of Fuel Composition Effects in H2/CO/CH4 Mixtures Upon Lean Blowout,” in *ASME/IGTI Turbo Expo*, 2005, pp. 1–13.

[56] J. P. Longwell, E. E. Frost, and M. a. Weiss, “Flame Stability in Bluff Body Recirculation Zones,” *Ind. Eng. Chem.*, vol. 45, no. 8, pp. 1629–1633, 1953.

[57] Q. Zhang, D. R. Noble, and T. Lieuwen, “Blowout Measurements in a Syngas-Fired Gas Turbine Combustor,” in *The 22nd Annual International Pittsburgh Coal Conference*, 2005, pp. 1–6.

[58] D. D. R. Noble, Q. Zhang, A. Shareef, J. Tootle, A. Meyers, and T. Lieuwen, “Syngas mixture composition effects upon flashback and blowout,” *ASME Conf. Proc.*, vol. 2006, no. 42363, pp. 357–368, 2006.

[59] M. Abdulsada, N. Syred, P. Bowen, T. O’Doherty, A. Griffiths, R. Marsh, and A. Crayford, “Reprint of ‘effect of exhaust confinement and fuel type upon the blowoff limits and fuel switching ability of swirl combustors,’” *Appl. Therm. Eng.*, vol. 53, no. 2, pp. 348–357, 2013.

[60] P. Palies, D. Durox, T. Schuller, and S. Candel, “Experimental Study on the Effect of Swirler Geometry and Swirl Number on Flame Describing Functions,” *Combust. Sci. Technol.*, vol. 183, no. 7, pp. 704–717, 2011.

[61] Y. Huang and V. Yang, “Dynamics and stability of lean-premixed swirl-stabilized combustion,” *Prog. Energy Combust. Sci.*, vol. 35, no. 4, pp. 293–364, 2009.

[62] J. Wan, A. Fan, Y. Liu, H. Yao, W. Liu, X. Gou, and D. Zhao, “Experimental investigation and numerical analysis on flame stabilization of CH4/air mixture

in a mesoscale channel with wall cavities," *Combust. Flame*, vol. 162, no. 4, pp. 1035–1045, 2015.

[63] Y. Huang and V. Yang, "Effect of swirl on combustion dynamics in a lean-premixed swirl-stabilized combustor," *Proc. Combust. Inst.*, vol. 30 II, no. 2, pp. 1775–1782, 2005.

[64] C. Külsheimer and H. Büchner, "Combustion dynamics of turbulent swirling flames," *Combust. Flame*, vol. 131, no. 1–2, pp. 70–84, 2002.

[65] M. B. Linck, A. K. Gupta, G. Bourhis, and K. Yu, "Combustion Characteristics of Pressurized Swirling Spray Flame and Unsteady Two-Phase Exhaust Jet," in *American Institute of Aeronautics and Astronautics*, 2006, no. January, pp. 1–15.

[66] D. Fanaca, P. R. Alemela, C. Hirsch, and T. Sattelmayer, "Comparison of the Flow Field of a Swirl Stabilized Premixed Burner in an Annular and a Single Burner Combustion Chamber," *J. Eng. Gas Turbines Power*, vol. 132, no. 7, p. 071502, 2010.

[67] B. Dam, N. Love, and A. Choudhuri, "Flashback propensity of syngas fuels," *Fuel*, vol. 90, no. 2, pp. 618–625, 2011.

[68] P. Strakey, T. Sidwell, and J. Ontko, "Investigation of the effects of hydrogen addition on lean extinction in a swirl stabilized combustor," *Proc. Combust. Inst.*, vol. 31 II, pp. 3173–3180, 2007.

[69] R. W. Schefer, D. M. Wicksall, and A. K. Agrawal, "Combustion of hydrogen-enriched methane in a lean premixed swirl-stabilized burner," *Proc. Combust. Inst.*, vol. 29, no. 1, pp. 843–851, 2002.

[70] R. W. Schefer, "Hydrogen enrichment for improved lean flame stability," *Int. J. Hydrogen Energy*, vol. 28, pp. 1131–1141, 2003.

[71] P. M. Allison, J. F. Driscoll, and M. Ihme, "Acoustic characterization of a partially-premixed gas turbine model combustor: Syngas and hydrocarbon fuel comparisons," *Proc. Combust. Inst.*, vol. 34, no. 2, pp. 3145–3153, 2013.

[72] S. K. Alavandi and A. K. Agrawal, "Experimental study of combustion of hydrogen-syngas/methane fuel mixtures in a porous burner," *Int. J. Hydrogen Energy*, vol. 33, no. 4, pp. 1407–1415, 2008.

[73] A. Amato, B. Hudak, P. D'Carlo, D. Noble, D. Scarborough, J. Seitzman, and T. Lieuwen, "Methane oxycombustion for low CO2 cycles: Blowoff measurements and analysis," *J. Eng. Gas Turbines Power*, vol. 133, no. 6, p. -–, 2011.

[74] F. Liu, H. Guo, and G. J. Smallwood, "The chemical effect of CO2 replacement of N2 in air on the burning velocity of CH4 and H2 premixed flames," *Combust. Flame*, vol. 133, no. 4, pp. 495–497, 2003.

[75] S. De Persis, F. Foucher, L. Pillier, V. Osorio, and I. G??kalp, "Effects of O2 enrichment and CO2 dilution on laminar methane flames," *Energy*, vol. 55, pp. 1055–1066, 2013.

[76] S. Seepana and S. Jayanti, “Experimental studies of flame extinction in a swirl-stabilized oxy-fuel burner,” *Fuel*, vol. 93, pp. 75–81, 2012.

[77] T. Fujimori and T. Yamada, “Realization of oxyfuel combustion for near zero emission power generation,” *Proc. Combust. Inst.*, vol. 34, no. 2, pp. 2111–2130, 2013.

[78] P. Kutne, B. K. Kapadia, W. Meier, and M. Aigner, “Experimental analysis of the combustion behaviour of oxy-fuel flames in a gas turbine model combustor,” *Proc. Combust. Inst.*, vol. 33, no. 2, pp. 3383–3390, 2011.

[79] Y. Xie, J. Wang, M. Zhang, J. Gong, W. Jin, and Z. Huang, “Experimental and numerical study on laminar flame characteristics of methane oxy-fuel mixtures highly diluted with CO2,” *Energy and Fuels*, vol. 27, no. 10, pp. 6231–6237, 2013.

[80] C. Ghenai, “Combustion of Syngas Fuel in Gas Turbine Can Combustor,” *Adv. Mech. Eng.*, vol. 2010, pp. 1–13, 2010.

[81] M. de la Torre, N. Love, and A. Choudhuri, “Effect of diluents, firing input, and hydrogen content on premixed oxy-syngas flames,” *11th Int. Energy Convers. Eng. Conf.*, pp. 1–8, 2013.

[82] E. . Keramida, H. . Liakos, M. . Founti, A. . Boudouvis, and N. . Markatos, “Radiative heat transfer in natural gas-fired furnaces,” *Int. J. Heat Mass Transf.*, vol. 43, no. 10, pp. 1801–1809, 2000.

[83] M. Safer, F. Tabet, A. Ouadha, and K. Safer, “A numerical investigation of structure and emissions of oxygen-enriched syngas flame in counter-flow configuration,” *Int. J. Hydrogen Energy*, vol. 40, no. 6, pp. 2890–2898, 2015.

[84] C. V. da Silva, H. A. Vielmo, and F. H. R. Franca, “Numerical Simulation of the Combustion of Methane and Air in a Cylindrical Chamber,” *Therm. Eng.*, vol. 5, no. 1, pp. 13–21, 2006.

[85] A. F. Tabatabaei and M. A. Soroudi, “A Kinetic Study of Syngas Combustion Characteristics for Gas Turbine Applications,” in *Chia Laguna, Cagliari, Sardinia, Italy*, 2011, pp. 1–16.

[86] C. E. Arrieta and A. A. Amell, “Combustion analysis of an equimolar mixture of methane and syngas in a surface-stabilized combustion burner for household appliances,” *Fuel*, vol. 137, pp. 11–20, 2014.

[87] S. Kumaresh and M. Y. Kim, “Combustion and Emission Characteristics in a Can-type Combustion Chamber,” *Int. J. Mech. Aerospace, Ind. Mechatron. Manuf. Eng.*, vol. 8, no. 7, pp. 1304–1307, 2014.

[88] G. C. Krieger, a. P. V. Campos, M. D. B. Takehara, F. Alfaia da Cunha, and C. a. Gurgel Veras, “Numerical simulation of oxy-fuel combustion for gas turbine applications,” *Appl. Therm. Eng.*, vol. 78, pp. 471–481, 2015.

[89] A. Cuoci, A. Frassoldati, T. Faravelli, and E. Ranzi, “Accuracy and Flexibility of Simplified Kinetic Models for CFD applications,” in *Italian Section of the combustion institute: Combustion Colloquai*, 2009, pp. 1–6.

[90] M. Ilbas, I. Yilmaz, T. N. Veziroglu, and Y. Kaplan, “Hydrogen as burner fuel: Modelling of hydrogen-hydrocarbon composite fuel combustion and NOx formation in a small burner,” *Int. J. Energy Res.*, vol. 29, no. 11, pp. 973–990, 2005.

[91] A. De and S. Acharya, “Parametric study of upstream flame propagation in hydrogen-enriched premixed combustion: Effects of swirl, geometry and premixedness,” *Int. J. Hydrogen Energy*, vol. 37, no. 19, pp. 14649–14668, 2012.

[92] A. De and S. Acharya, “Dynamics of upstream flame propagation in a hydrogen-enriched premixed flam,” *Int. J. Hydrogen Energy*, vol. 37, no. 19, pp. 17294–17309, 2012.

[93] N. M. Marinov, C. K. Westbrook, and W. J. Pitz, “Transport phenomena in combustion,” *Eighth International Symposium on Transport Processes*, vol. 8. pp. 118–141.

[94] A. Frassoldati, A. Cuoci, and T. Faravelli, “Simplified kinetic schemes for oxy-fuel combustion,” *Sustain. Foss.*, pp. 1–14, 2009.

[95] J. Andersen, C. L. Rasmussen, T. Giselsson, and P. Glarborg, “Global combustion mechanisms for use in CFD modeling under oxy-fuel conditions,” *Energy and Fuels*, vol. 23, no. 3, pp. 1379–1389, 2009.

[96] L. Chen and A. F. Ghoniem, “Simulation of oxy-coal combustion in a 100 kW th test facility using RANS and LES: A validation study,” *Energy and Fuels*, vol. 26, no. 8, pp. 4783–4798, 2012.

[97] M. a. Nemitallah and M. a. Habib, “Experimental and numerical investigations of an atmospheric diffusion oxy-combustion flame in a gas turbine model combustor,” *Appl. Energy*, vol. 111, pp. 401–415, 2013.

[98] I. Ansys, *ANSYS Fluent Theory Guide*, vol. 15, no. November. 2013.

[99] S. A. Hashemi, A. Fattahi, G. A. Sheikhzadeh, and M. A. Mehrabian, “Investigation of the effect of air turbulence intensity on NOx emission in non-premixed hydrogen and hydrogen-hydrocarbon composite fuel combustion,” *Int. J. Hydrogen Energy*, vol. 36, no. 16, pp. 10159–10168, 2011.

[100] T. H. Shih, W. W. Liou, A. Shabbir, Z. Yang, and J. Zhu, “A New K-epsilon Eddy Viscosity Model for High Reynolds Number Turbulent Flows: Model Development and Validation,” *Comput. \& Fluids*, vol. 24, no. August, pp. 227–238, 1995.

[101] M. A. Rajhi, R. Ben-Mansour, M. A. Habib, M. A. Nemitallah, and K. Andersson, “Evaluation of gas radiation models in CFD modeling of oxy-combustion,” *Energy Convers. Manag.*, vol. 81, pp. 83–97, 2014.

[102] I. R. Gran and B. F. Magnussen, “A numerical study of a bluff-body stabilized diffusion flame. Part 2. Influence of combustion modeling and finite-rate chemistry,” *Combust. Sci. Technol.*, vol. 119, no. 1–6, pp. 191–217, 1996.

Vitae

Name	: Mansur Aliyu
Nationality	: Nigerian
Date of Birth	: 9/11/1985
Email	: mnsraliyu@gmail.com
Address	: 21, Kamal-deen street, Okekere, Ilorin, Kwara state, Nigeria
Academic Background	: Master of Science (MS), Mechanical Engineering, King Fahd University of Petroleum and Minerals, Dhahran, Kingdom of Saudi Arabia. Bachelor of Engineering (B. Eng.) Mechanical/Production Engineering, Abubakar Tafawa Balewa University, Bauchi, Nigeria.